YEDITEPE UNIVERSITY
GRADUATE SCHOOL OF NATURAL AND APPLIED SCIENCES

INVESTIGATING THE FACTORS AFFECTING THE SPECIFIC ABSORPTION RATE (SAR) OF MAGNETIC NANOPARTICLES FOR MAGNETIC HYPERTHERMIA

A Thesis Submitted
by
Beyza Abişoğlu

In Partial Fulfillment
of the Requirements for the Degree of
Master of Science
in
Chemical Engineering

Supervisor
Assist. Prof. Dr. Cem Levent Altan

Istanbul-2024

INVESTIGATING THE FACTORS AFFECTING THE SPECIFIC ABSORPTION RATE (SAR) OF MAGNETIC NANOPARTICLES FOR MAGNETIC HYPERTHERMIA

by

Beyza Abişoğlu

Approved by:

Assist. Prof. Dr. Cem Levent Altan
(Yeditepe University) .....
(Thesis Supervisor)

Assoc. Prof. Dr. Murat Oluş Özbek
(Gebze Technical University) .....

Assist. Prof. Dr. Semin Funda Oğuz
(Yeditepe University) .....

DATE OF APPROVAL: ..../..../20...

DECLARATION OF ORIGINALITY

I hereby declare that this thesis is my own work and that all information in this thesis has been obtained and presented following academic rules and ethical conduct. I have fully cited and referenced all material and results as required by these rules and conduct, and this thesis study does not contain any plagiarism. The necessary permissions have been obtained if any material used in the thesis requires copyright. No material from this thesis has been used to award of another degree.

To the best of my knowledge and belief, it contains no material previously published or written by another person nor material accepted for the award of any other degree except where due acknowledgement has been made in the text.

I accept all kinds of legal liability that may arise in case contrary to these situations.

Beyza Abişoğlu

Signature

ABSTRACT

INVESTIGATING THE FACTORS AFFECTING THE SPECIFIC ABSORPTION RATE (SAR) OF MAGNETIC NANOPARTICLES FOR MAGNETIC HYPERTHERMIA

Hyperthermia is an alternative treatment method based on disrupting the structure of proteins associated with cancer cells and stimulating immune response by raising the temperature locally above 40-43 ^{o}C at the tumor site. The application of magnetic nanoparticles in hyperthermia is called magnetic hyperthermia and nanoparticles have the ability to locally enhance the temperature by converting externally applied electromagnetic energy into heat energy through different mechanisms. The efficiency of nanoparticles in magnetic hyperthermia applications is quantified by specific absorption rate (SAR) which depends on size, magnetic properties, concentration, and colloidal stability of nanoparticles and frequency and intensity of the magnetic field. In the literature, the effects of these variables on SAR have mostly been studied separately, whereas this study aims to investigate the SAR values of superparamagnetic and comparably larger magnetite nanoparticles depending on these factors in a holistic manner. According to the results obtained, nanoparticles have been successfully synthesized and modified by co-precipitation and partial oxidation methods. The necessity of using pure water data as a base while obtaining the heating curves of these structures has also been revealed. It has been determined that the temperature enhancements and SAR values increase by raising the frequency and field intensity for all nanoparticles under the influence of an externally applied magnetic field, whereas it may decrease due to colloidal stability in bare nanoparticles as the size changes. It has been further determined that the temperature changes increase with increasing concentration at all frequencies and field strength intensities, while the SAR values exhibited complex and diverse patterns. Finally, it has been revealed that superparamagnetic particles with colloidal stability may not provide sufficient temperature variation under low frequencies while larger particles are highly affected by magnetic field strength as opposed to frequency. Additionally, the temperature enhancement and SAR value especially for modified superparamagnetic nanoparticles have been decreased as compared to bare nanoparticles, potentially due to the deterioration of magnetic properties.

ÖZET

INVESTIGATING THE FACTORS AFFECTING THE SPECIFIC ABSORPTION RATE (SAR) OF MAGNETIC NANOPARTICLES FOR MAGNETIC HYPERTHERMIA

Hipertermi, tümör bölgesinde lokal olarak sıcaklığın 40-43 ^{o}C üzerine çıkartılarak kanser hücrelerine ait proteinlerin yapılarının bozulmasına ve bağışıklığın duyarlı hale getirilmesine dayanan alternatif bir tedavi yöntemidir. Hipertermi uygulamalarında manyetik nanoparçacıkların kullanımına manyetik hipertermi denmektedir ve nanoparçacıklar dışarıdan uygulanan elektromanyetik enerjiyi farklı mekanizmalar ile ısı enerjisine dönüştürerek lokal olarak sıcaklığı arttırmaktadır. Manyetik hipertermi uygulamalarında nanoparçacıkların verimlilikleri, spesifik absorpsiyon hızı (SAR) ile ölçülmektedir ve manyetik nanoparçacıkların boyutuna, manyetik özelliklerine, konsantrasyonuna, koloidal stabilitelerine, manyetik alanın frekansına ve şiddetine bağlı olarak değişmektedir. Literatürde bu değişkenlerin SAR üzerindeki etkileri çoğunlukla ayrı olarak incelenmiş, bu çalışmada ise, süperparamanyetik ve göreceli daha büyük magnetit nanoparçacıklarına ait SAR değerlerinin bu etkenlere bağlı ve bir bütün olarak incelenmesi hedeflenmiştir. Elde edilen sonuçlar, birlikte çöktürme ve kısmi oksitlenme yöntemleriyle nanoparçacıkların başarılı bir şekilde elde edildiğini ve modifiye edilebildiklerini ortaya koymuştur. Bu yapılara ait ısınma eğrileri elde edilirken saf suya ait verinin de baz olarak kullanım gerekliliği ortaya konmuştur. Manyetik alan etkisi altında tüm nanoparçacıklarda frekansın ve alan şiddetinin artması ile sıcaklık değişimlerinin ve SAR değerlerinin arttığı, boyut değişimiyle de yalın nanoparçacıklarda stabiliteye bağlı azalabildiği belirlenmiştir. Konsantrasyon artışıyla tüm frekans ve alan şiddeti değerlerinde sıcaklık değişimleri artarken, SAR değerlerinde kompleks ve farklı davranışlar elde edilmiştir. Son olarak, koloidal stabiliteye sahip nanoparçacıkların düşük frekans ve manyetik alan şiddeti altında yeterli sıcaklık değişimi sağlayamadıkları ve daha büyük parçacıkların manyetik alan şiddetinden, frekansa oranla daha çok etkilendikleri ortaya konmuştur. Ayrıca, sıcaklık artışı ve SAR değeri özellikle modifiye edilmiş süperparamanyetik nanoparçacıklarda potansiyel olarak manyetik özelliklerin azalmasından ötürü yalın nanoparçacıklara kıyasla düşüş göstermiştir.

ACKNOWLEDGEMENTS

First of all, I would like to thank my advisor Assist. Prof. Cem Levent Altan for his endless knowledge, guidance, motivation, belief, sincerity and especially his patience throughout the master's thesis stage. I was proud to work with him and his group at every step starting from my undergraduate education. I was able to complete this path because he answered every question I had, changed my perspective with his advice, lifted me up every time I fell, showed me that every problem can be solved, and especially because he always made me feel that he was always behind me in all circumstances. I am very lucky to be his student and I will always be grateful to him for being one of the reasons that became the person I am today.

I would also like to thank Dr. Melis Çağdaş, whose door is always open and who is always by my side. From the moment I met her, she impressed me with her stance and personality. I am grateful to her for making my life easier during my master's degree process, for being one of my biggest sources of motivation, and for making me stronger in every situation I face. Thank you very much for being one of my biggest supporters at every event.

I would also like to thank Sibel S. Erdem, Nihan Verimli and İrem Goralı for their contributions in this project.

I am very grateful to all my friends, but especially to Ezgi Uslu, Katia Haviters, Berk Alarcin, Kemal Düzkar, Özlem Yaka, Damla Işık, Zeynep Yükseloğlu, Miray Şenkal,Doğa Özenli and İrem Yüklü with whom I have crossed paths at different times over the years. I have achieved this success thanks to the support and help you all have given me under all circumstances. You make my life more bearable.

Finally, I would like to thank my mother, father and sister for all their hard work, endless support and efforts. I could never do anything without their support, patience and encouragement. Thanks to you, I know that I can overcome anything. I hope I can always make you happy and I am very lucky to have this family.

TABLE OF CONTENTS

LIST OF FIGURES

LIST OF TABLES

LIST OF ABBREVIATIONS

γ-Fe_2O_3	Maghemite
ρ	Density
φ	Concentration
C	Heat capacity
f	Frequency
H	Magnetic field strength
AMF	Alternating magnetic field
COP	Co-precipitation
DC	Direct current
DNA	Deoxyribonucleic acid
DW	Distilled water
EPR	Enhanced permeability and pretention
Fe	Iron
Fe_2O_3	Iron (III) oxide
Fe_3O_4	Magnetite
FeO	Iron (II) oxide
FTIR	Fourier Transform Infrared Spectroscope
GA- Fe_3O_4	Glutamic acid coated nanoparticles
HRTEM	High-resolution transmission electron microscopy
MNP	Magnetic nanoparticles
NP	Nanoparticles
PEG	Polyethylene glycol
PEI	Polyethyleneimine
POX	Partial oxidation
RPM	Revolutions per minute
SAR	Specific absorption rate
SLP	Specific loss power
SPA	Specific power absorption
TEM	Transmission electron microscopy

UV-Vis	Ultraviolet visible
VSM	Vibrating sample magnetometer
XRD	X-ray diffraction

1. INTRODUCTION

Cancer occurs when the cells that make up any of the organs or tissues in the body differentiate and proliferate in an uncontrolled manner by going beyond their inherited or genetically natural behavior. After circulatory system diseases, cancer is the second leading cause of death as of today [1]. Cancer may develop due to environmental and hereditary factors such as alcohol, obesity, smoking and diet, either alone or in combination, while 5% to 10% may develop due to genetic defects [2]. Cancer cells can form masses called tumors in the tissue or organ where they originate, or they can spread to different tissues or organs by the lymphatic or blood circulation through a process called metastasis [3]. As a consequence of the symptoms, cancer can be diagnosed using blood and urine tests, ultrasonography, computed tomography, magnetic resonance imaging, positron emission tomography, antigens and pathological examinations.

The most commonly utilized traditional methods for the treatment of cancer are surgery, chemotherapy and radiotherapy. Although the main goal is to reduce and eliminate the tumor mass, alternative treatment approaches such as stem cell, immunotherapy and hormone therapy have been developed due to the side effects and relatively low efficiency of these traditional approaches [4]. Hyperthermia is also one of the alternative treatment techniques being studied for cancer treatment. The essential aim of hyperthermia is to activate the immune system by increasing the temperature of the cancerous body tissue or organ to between 39 and 42 ^{o}C. Local hyperthermia can further reach up to 44 ^{o}C, which disrupts the structure of proteins in cancer cells and damages tumor vessels. In addition, cancer cells can become more sensitive and responsive to radiotherapy after hyperthermia treatment which implies that the method itself becomes more efficient when applied in combination with other traditional techniques [5].

The application of magnetic nanoparticles as heating agents in hyperthermia treatments is called as magnetic hyperthermia [6]. Magnetic nanoparticles are frequently employed in biomedical applications due to their unique physical and magnetic properties as well as their non-toxicity and sufficient biological interactions [7]. Since they can be directly targeted locally to tumor sites by applying an external magnetic field, they are also being studied as drug delivery agents. [8]. There are several methods to synthesize magnetic nanoparticles

and the most widely applied method is co-precipitation, which allows the production of superparamagnetic nanoparticles due to its simplicity [9]. On the other hand, the partial oxidation method, which allows the formation of nanoparticles with relatively larger, is not preferred due to the difficulty in maintaining the colloidal stability of the nanoparticles [10]. Magnetic nanoparticles, which possess magnetic properties, are able to convert externally applied electromagnetic energy into heat by different mechanisms and thus locally reach the temperatures required for hyperthermia [6].

The efficiency of magnetic nanoparticles in hyperthermia applications directly depends on many factors such as their size, magnetic properties, colloidal stability, concentration, frequency and intensity of the applied alternating magnetic field [11]. The effect of these factors and the heating efficiency of magnetic nanoparticles is generally expressed in terms of specific absorption rate (SAR) which can be defined as the rate of energy converted into heat per unit mass of magnetic nanoparticles. The effects of the above-mentioned factors on SAR have been evaluated in numerous studies in the literature [6,11]. However, while frequency and magnetic field strength are generally examined in almost all studies, some other factors have not been fully incorporated. On the other hand, since nanoparticles possessing coercivity and remanence with colloidal stability are difficult to obtain, those have not been generally preferred for comparison in studies. Therefore, the aim of this study is to investigate the effects of size, concentration, surface modification, frequency of externally applied magnetic field and magnetic field intensity on temperature enhancement and SAR values of magnetic nanoparticles that are synthesized by co-precipitation and partial oxidation methods.

2. THEORETICAL BACKGROUND

2.1. CANCER

Cancer is a major disease that occurs when tissues divide in an uncontrolled manner and grow irregularly. Cancer is the leading cause of death worldwide. About 10 million people lost their lives by reason of cancer in 2020, according to World Health Organization (WHO) [12]. Trillions of cells, which have the ability to divide a limited number of times, must grow, divide, and produce new cells in order to form a healthy and properly functioning body. Apoptosis, also known as programmed cell death, is a controlled process in which healthy cells undergoes self-elimination after completing a certain number of division cycles. Morphological and biochemical changes such as rounding and fragmentation of the genome into smaller pieces are observed in cells undergoing apoptosis. Following these morphological and biological changes, phagocytes are stimulated, which can detect and subsequently clear unwanted cells [13].

Dysregulation of the cell cycle can lead cells to divide in an uncontrolled manner and lead to the formation of masses of excessive cells. This genetic error interferes with crucial cellular functions and contributes to the formation of tumors which can be classified as either benign or malignant, as shown in Figure 2.1.

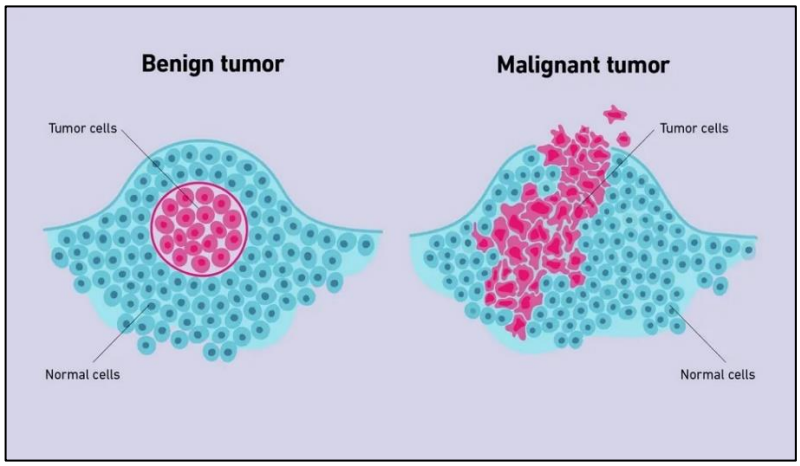

Figure 2.1. Benign tumor vs Malignant tumor [14]

Benign tumor cells do not spread to nearby normal tissues or other parts of the body, while malignant tumor cells have the ability to migrate throughout the body via the bloodstream or lymphatic system by a process called metastasis. While surgical intervention is a simple method that can be applied in the treatment of benign tumors, the spread of malignant or metastasized tumors to various parts of the body makes this method ineffective [15].

In order to understand how cancer spreads, it is necessary to distinguish the differences between normal cells and cancer cells. Normal cells avoid damaging their environment by constantly sending signals to each other to prevent proliferation when they reach a certain threshold, while cancer cells ignore these signals and continue to grow. Another fundamental difference that distinguishes cancer cells and normal cells is that healthy cells adhere to each other due to the molecules they secrete and stay in specific locations while cancer cells can move throughout and invade the body. The immune system has the capability to discern whether the cells are normal or abnormal and effectively eliminate abnormal cells. On the other hand cancer cells have developed strategies to deceive or evade the immune system as they develop resistance to avoid destruction and maintain continous reproduction [13].

As a consequence when cell proliferation becomes independent of growth factors, a massive masses of cells called tumors are formed. Atypical cells, which are different from normal cells and do not turn into cancer as a whole, begin to proliferate in a limited area and form benign tumors as a result of abnormalities in cell growth. In the advanced stage, the tumor gains the ability to metastasize and begins to spread to nearby tissues and various parts of the body through the circulation system and such tumors are called as malignant [16].

Cancer can start in a vital organ and spread to other body parts, blood vessels and nerves, disrupting their normal functions and causes death. For instance, a tumor may obstruct a portion of the lung and organ failure might occur from insufficient oxygen absorption. Bleeding and reduced oxygen flow occurs when blood vessels are damaged and these complications can be fatal. Calcium is released into the bloodstream when bones are affected from cancer. An imbalance of calcium in the body can significantly impact heart and muscle function, ultimately leading in organ failure and death [17].

2.1.1. Cancer Treatment Methods

There are various methods that can be applied to treat cancer. These methods can be implemented solely or in combination by considering the type of the cancer, the location and size of the tumor and the phase of cancer progression. In general, chemotherapy, radiotherapy, and surgery are the most widely applied traditional methods. The inadequate and ineffectual results of these methods have led to significant improvements for modern treatment methods such as immunotherapy, drug delivery, gene therapy, hyperthermia etc.

2.1.1.1. Traditional Treatment Methods

Chemotherapy

Chemotherapy is a term used to refer to a treatment of a disease using chemicals and was first introduced by Paul Ehrlich, who was working on aniline dyes and alkylating agents for the treatment of cancer [18]. In a healthy body, damaged cells are removed by the body to balance cell proliferation, and subsequently new cells are formed. However for cancerous cells proliferation ratio is much higher than the death rate. Chemotherapy ceases the progression of the tumor by depriving the cells' ability to divide by damaging genes inside the nucleus of cells which control the division and force the cells to apoptosis [16]. This treatment method is also used to prevent the spread of cancer, alleviate symptoms, and shrink the tumor for complementary treatments like surgery or radiotheraphy. Although treatment can be achieved with chemotherapy up to a certain level, this method also has disadvantages. While the drugs designed for chemotherapy highly affect cancer cells, due to lack of selectivity they also damage and affect healthy cells which consequently arise side effects such as hair loss, vomiting, fatigue, weight changes, kidney problems, and nerve problems [19].

Radiotherapy

X-rays which are high energy bearing electromagnetic radiation were discovered by Willhelm Röntgen in 1895, and in the same year the first cancer patient was treated with radiotheraphy [20]. In radiotheraphy, ionizing radiation which consists of gamma, X-rays, and subatomic particles that have adequate energy is used. In this treatment, energy accumulation is observed due to the generation of high energy photons in the cells through

which the radiation passes. This high energy damages the DNA of cancer cells,thereby causing cell death. The beams are targeted directly to the tumor site in order to prevent damaging the surrounding healthy cells rather than the tumor cells. Although radiotherapy is mainly used to destroy cancer cells, it is also applied to control the growth of tumor. While it can be applied individually, it can also be preferred synergistically before surgery and chemotherapy to increase the efficiency of subsequent treatment method by shrinking the tumor. Radiotherapy is also used to prevent cancer from recurring after traditional treatment methods. While local tumors can generally be treated with this method, it cannot be used for tumors caused by cancer cells which have metastasized and spread to different regions, due to the nature of the method. While less radiation can be given for tumors located in areas close to the surface of the body, much more intense radiation must be given for lower and hard-to-reach areas. However, as with every treatment method, radiotherapy has side effects including diarrhoea, fatigue, sore skin and hair loss. While these side effects may occur during treatment, they may be permanent in survivors [21].

Surgery

The use of surgery to treat cancer dates back approximately 5000 years, and the first document regarding the surgical removal of the tumor causing breast cancer is the Edwin Smith papyrus from 1600 BC [22]. Surgery is a method used to remove the tumor formed by cancer cells from the area where it is located. In this method, a certain section of surrounding healthy tissue is also removed in addition to the tumor in order to prevent the cancer from recurring. Surgery plays a leading role in treating of most cancer types and in certain cases is highly required to improve quality of life and alleviate symptoms or side effects. Immediately before surgery for cancer treatment, a biopsy is performed to determine whether the cells under examination carry a risk of cancer and to take the necessary precautions [16]. Although surgery is a preventive and therapeutic method, it can also cause immune response and lead to the formation of metastases. This phenomena along with the long process required for wound healing, and the weakened immune system leading to vulnerability are generally seen as the disadvantages of surgery for cancer treatment [23].

2.1.1.2. Modern Treatment Methods

Immunotherapy

Compared to the traditional treatment methods mentioned in the previous sections, immunotherapy has provided significant improvements in patients' quality of life and survival rate. It has emerged as a promising treatment method to effectively treat various cancer types such as breast cancer and pancreatic cancer. In 1891, first immunotherapy treatment was performed by William B. Coley who injected inactivated mixture of bacteria which became to known as Coley's Toxin into a patient to produce an infection to activate the immune system that would regress the growth and reproduction of cancer cells [24].

Immunotherapy is essentially the use of the immune system in the fight against cancer, just like infections and other diseases. The immune system detects and removes abnormal cells from the system, and in some cases, they also concentrate in the tumor area. These tumor-infiltrating cells are called lymphocytes. The presence of much higher levels of lymphocytes in the tumor area negatively affects the progression of cancer in patients. However, cancer cells can evade the growth-inhibiting and slowing effects of the immune system by undergoing genetic changes. For this reason, it becomes necessary to apply immunotherapy in different approaches (Figure 2.2). For example, by using immune checkpoint inhibitors, immune cells are enabled to respond to cancer cells much more strongly. In another application, immune cells concentrated in the tumor area are taken from the tumor site, enhanced to high concentrations in the laboratory environment, and then injected into the tumor area for a much more effective defense [25]. Although it is not as widely used as surgery, chemotherapy and radiotherapy at this stage, immunotherapy can be applied solely or synergistically for many types of cancer. As with all other methods, immunotherapy has side effects such as attacking healthy cells simultaneously with cancer cells, headache, nausea, weakness, shortness of breath, low blood pressure, behavioral changes and distraction [26].

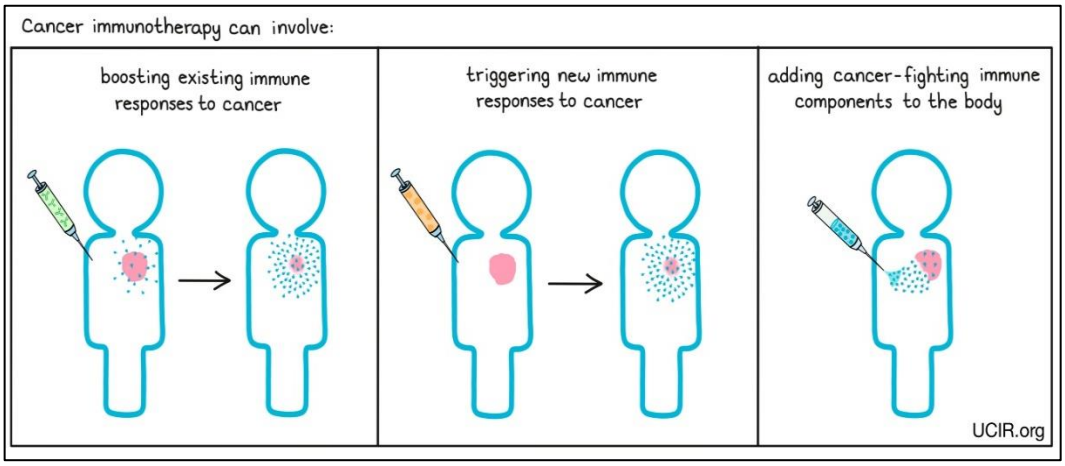

Figure 2.2. Cancer immunotherapy approaches [27]

Gene Therapy

Gene therapy for cancer treatment is based on the principle of changing the genetic functions and DNA of immune and cancer cells. Gene therapy, which was first tried clinically in 1990, can be considered a relatively new approach to cancer treatment. The purpose of this method is to prevent the progression of cancer by fixing the genes of cancer cells that have undergone mutation and alteration. More than one approach can be followed for the application of gene therapy. In gene editing, the faulty gene is removed thus the DNA of cancer cells is directly affected. In gene replacement, the faulty or non-functioning gene is replaced with a healthy and working copy. The insertion of new genetic codes into immune cells that are fighting cancer cells is called gene insertion. Finally, gene blocking aims to terminate all functions of the faulty gene, thus destroying itself or preventing it from possessing cancerous characteristics [28]. All these approaches mentioned above can be applied in vivo and ex vivo. While in vivo gene therapy is based on directing genetic material prepared in a laboratory environment directly to an organ or tissue through a vector, ex vivo gene therapy is the removal of faulty cells from the patient and transplanting them to the patient after genetically modifying them (Figure 2.3) [29]. However, there are some side effects of gene therapy such as infection, fever, undesired immune system response, targeting the wrong cells, lack of effectiveness, and uncontrolled cell division [30].

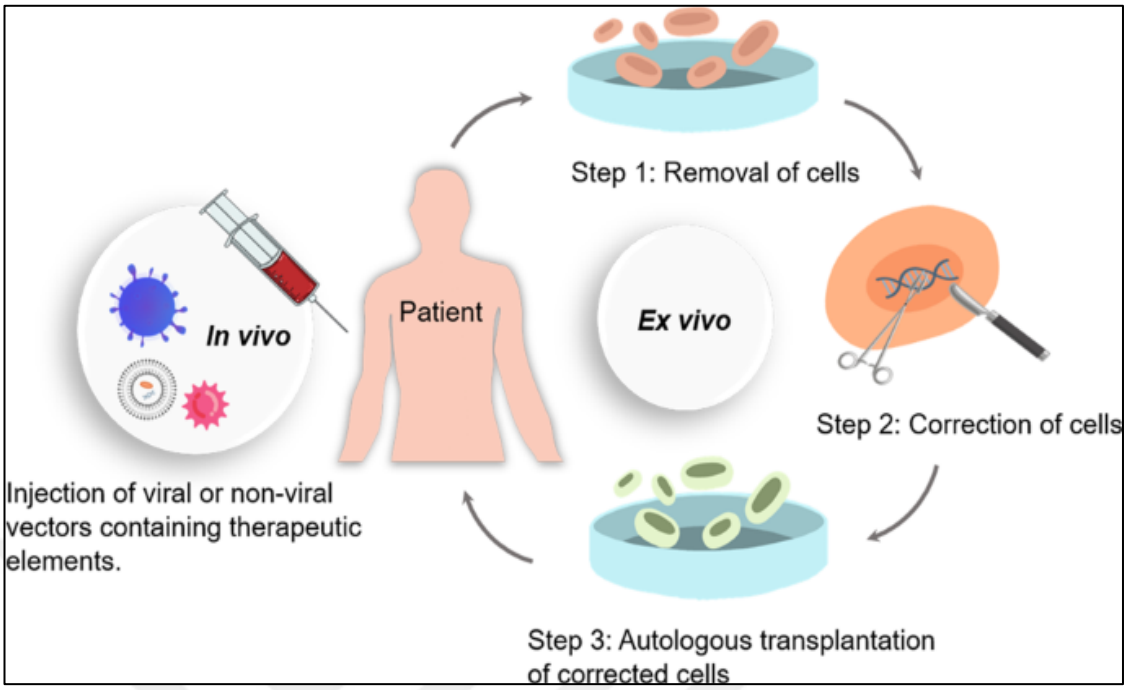

Figure 2.3. In vivo and ex vivo approaches for gene therapy [31]

2.1.1.3. Nanotechnology-Based Therapies

Chemotherapy, surgery, and radiotherapy are still the mostly applied traditional methods for the treatment of cancer. Although technological advances have been made for these treatments, which already have some advantages, treatment methods with high effectiveness and low side effects cannot be fully applied due to their corresponding drawbacks. For instance, for chemotherapy, the common obstacles are insufficient drug concentration that reaches the tumor site, intolerable cytotoxicity, and the emergence of resistance to multiple drugs. The use of high concentrations of chemotherapy drugs, which are intended to reach the tumor area, causes damage to healthy cells while trying to directly affect cancer cells as these traditional chemotherapy drugs solely cannot selectively distinguish cancer cells or living cells within the body. In addition, since these drugs are rapidly eliminated from the body, high doses are required to reach the desired concentration at the tumor site. Consequently, the necessity of using high doses of drugs arises in order to obtain an efficient treatment which is both uneconomical and in some cases a constraint due to maximum allowable dosages are exceeded [19,32].

For these reasons, studies are being carried out to integrate different agents into drug systems so that chemotherapy drugs can be selectively directed to the targeted tumor site in order to decrease the applied dose thus associated side effects.

Nanotechnology allows for the creation of high surface/volume ratio bearing nanoparticles with incomparable physical and chemical properties which can be tuned mostly by control of their size and morphology. These nano-sized particles can be produced by a variety of synthesis methods, and can be organic or inorganic. For application purposes, these obtained nanoparticles are further modified with different substances to ensure colloidal stability in base fluids and attain surface functionalization to interact with specific molecules. For this purpose, nanoparticles are functionalized with surfactants, polymers, lipids or dendrimers either in a single step during synthesis or in two steps afterwards [33,34]. Considering biomedical applications and especially cancer treatment, these surface modifications enable nanoparticles to be targeted to the site of tumor by providing biochemical interactions with specific receptors found on the surface of target cells. In this way, especially chemotherapy drugs can be selectively targeted to the tumor site with functionalized nanoparticles, avoiding the high doses of drugs needed in conventional administration by reducing the toxicity and associated side effects. This method of application also enhances the efficiency of the application as it increases the amount of cancer cells that can be affected. While it is possible to integrate multiple drugs with therapeutic properties into the nano-sized materials that make up drug delivery systems, it is also possible to ensure that these active substances avoid drug resistance and are released in a controlled manner at the tumor site. Drug delivery systems can basically be directed to the target site as active and passive targeting as shown in Figure 2.4 [35].

Passive targeting exploits the specific properties of tumor vessels to concentrate drug delivery systems in targeted tumor tissues. Vessels in tumors are irregularly distributed with numerous pores, resulting in large spaces between cells and defective lymphatic drainage. As a result, macromolecules of small size, such as nanoparticles, can be transported to the tumor site through the leaky vasculature of tumor tissue, and the high concentration of the drug delivery system at the tumor site can be achieved through enhanced permeability and retention (EPR) effect induced by poor lymphatic drainage and specific features of the tumor vasculature. However, the passive targeting method has several limitations, such as

unorganized and non-uniform tumor vessels, lack of EPR in various tumor types, and insufficient drug diffusion at the tumor site [36].

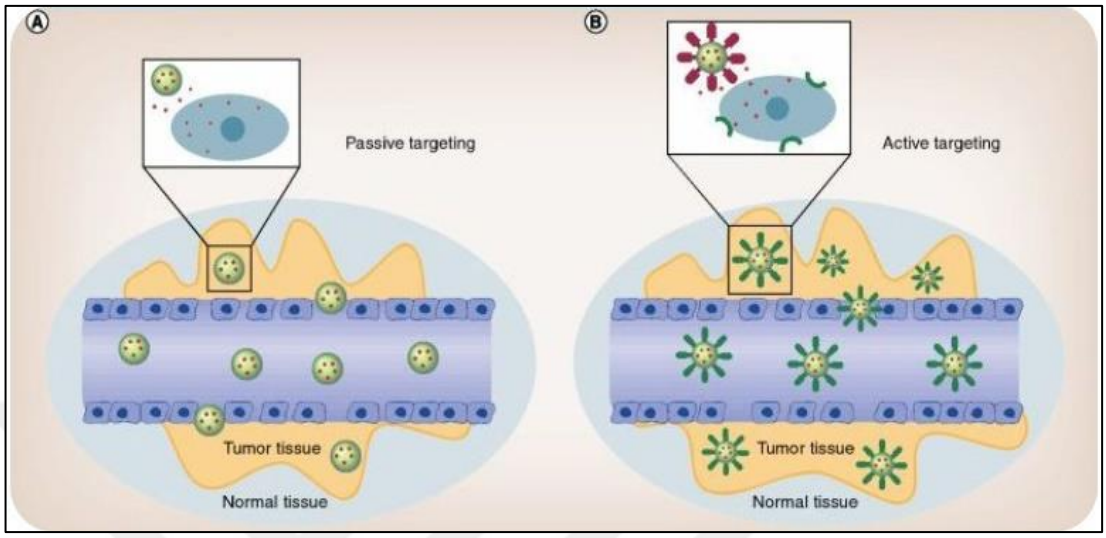

Figure 2.4. Active and passive drug delivery mechanism [35]

In active targeting, the drug carrier system is conjugated with selective agents and becomes capable of interacting directly with cancer cells without the need for a passive transport process. For this purpose, agents including antibodies, peptides or small targeting molecules are conjugated to the surface of drug carrier nanoparticles to interact with specific ligands or receptors uniquely expressed on the cells of target tissues. The ligands and receptors selection is crucial for the design of the targeted drug delivery system. First of all, it is required for determination of the receptors expressed in cancer cells in order to prevent the therapy agent from being targeted to healthy tissue and to ensure homogeneous distribution. Then, internalization of the targeted conjugate system after binding to target cells via receptor-mediated endocytosis must occur with adequate diffusion. Finally and essentially, the choice of ligand to be integrated into the nanoparticle carrier system is of great importance as it solely determines the selectivity. Considering the design of the drug delivery system, relatively smaller sized nanoparticles with a ratio of high surface area to volume can achieve much higher ligand density on their surfaces. In this way, these nanoparticles can achieve enhanced interaction with the targeted cells and be internalized more effectively [32,37].

Active targeting drug delivery systems generally use nanoparticles to transport the therapeutic agent, and structures including micelles, liposomes, nanospheres, nanocapsules and dendrimers are also used for this purpose. The most common active targeting ligands integrated into these nano-sized carriers include antibodies, folates, aptamers, transferrin and peptides. Since these ligands integrated into the systems will directly determine the efficiency of the drug delivery system, a specific selection must be made depending on the application and target. While antibodies can bind to the target precisely and at a high rate, they can also create immune resistance. On the other hand, although folate receptors are found very densely in some cancer cells and provide adequate targeting, they are not present in the same density in other types. Similarly, while aptamers can also bind to a wide spectrum of targets, there are purification complications and difficulty in high-scale production [38].

2.1.1.4. Hyperthermia

Hyperthermia is a relatively novel and alternative method for cancer treatment as compared to traditional approaches. This treatment method is essentially based on the principle of raising the temperature in the tumor area formed by cancer cells to approximately 40-45°C locally with minimal impact on surrounding healthy cells [39]. In the normal circulatory system, veins, capillaries and arterioles have an organized structure. However, in tumors, these structures assemble into a complex network. Since this vascular abnormality in tumors causes difficulties in heat distribution, a mild enhancement in local temperature causes cell death by denaturation and coagulation of cellular proteins in cancer cells, whereas healthy cells can easily preserve normal body temperature at the same condition. At the same time, this phenomenon can cause physiological responses such as low oxygen levels, i.e. hypoxia and vasodilation, which can directly lead to the destruction of cancer cells. In addition, these high temperatures reached locally can induce structural changes in the cell membrane and inhibit the growth and metastatic potential of the cancer cells that comprise the tumor [40]. Hyperthermia has three different application modes: local, regional and whole body, depending upon the cancer stage, the targeted organ and the depth of the tumor area. Local hyperthermia is applied to small accessible tumors located in body cavities such as the rectum, vagina and esophagus or near the skin surface. On the other hand, tumors that are spread over a larger area, such as an organ, are treated using regional hyperthermia, which can be accomplished by heating the blood or irrigating body cavities. Finally, the whole body hyperthermia treatment method is usually applied for metastatic types of cancer and at

advanced stages using heat blankets or infrared chambers. Although positive therapeutic results have been achieved in hyperthermia applications, due to the presence of potential side effects such as burns, bleeding and swelling may occur, it is necessary to precisely determine the heating area, i.e. the tumor location, for an effective, selective and damage-minimized application. Therefore, for the most efficient and effective application of hyperthermia, the heat source must be located or targeted directly at the tumor site [41].

2.2. MAGNETITE

Magnetite (Fe_3O_4) is a common type of iron oxide, which has inverse cubic spinel crystal structure at ambient conditions with mixed tetrahedral-octahedral sites. Natural magnetite generally occurs as octahedral crystals bound with [111] planes and contains both ferric and ferrous ions in its chemical structure ($FeO.Fe_2O_3$) as shown in Figure 2.5.

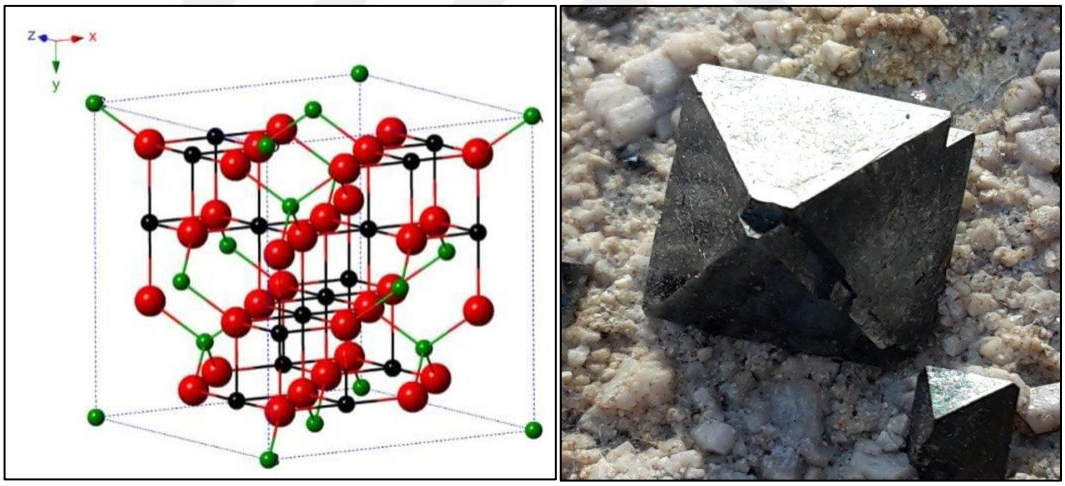

Figure 2.5. The structure of magnetite in that green balls are ferric, red are oxygen, and black are ferrous ions (a) [42], naturally occurring magnetite minerals (b) [43]

Magnetite exhibits unique electrical and magnetic properties due to the electron transfer between iron (II) ions present at octahedral and iron (III) ions occupying both octahedral and tetrahedral sites [42].

Magnetite particles can basically contain single or multiple magnetic domains. When the particle size is below the critical diameter value, the particles have a single-domain structure, and when this threshold is exceeded, they have a multi-domain structure. (Figure 2.6) It is

known that magnetite nanoparticles exhibit superparamagnetic properties when the particle size is decreased in the region below the critical size, and exhibit different magnetic behavior as the particle size increases. This transition leads to a significant change in the magnetic properties as saturation magnetization, the remaining magnetization when an externally applied magnetic field is removed (remanence) and the opposite field required to reduce the magnetization back to zero (coercivity) are highly affected [44].

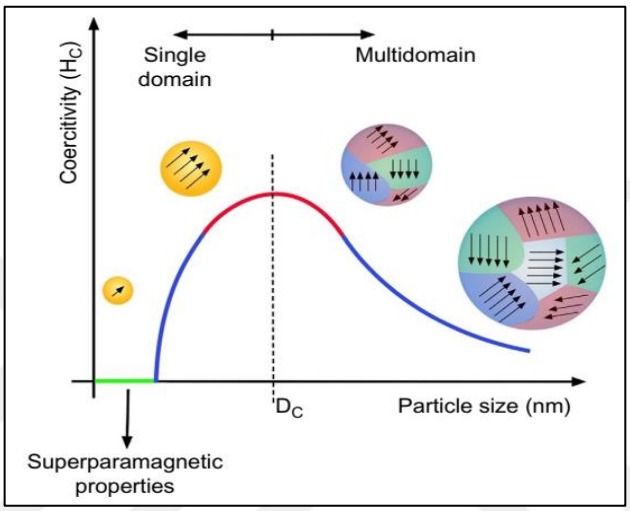

Figure 2.6. Magnetic properties of magnetic nanoparticles in relation to particle size [44]

Basically, magnetite nanoparticles with dimensions below 20 nm exhibit superparamagnetic properties, showing magnetic behavior only under the influence of an external magnetic field. These particles align themselves according to the direction of the externally applied magnetic field. However, when the field is removed, they do not have any remaining magnetization (Figure 2.7). Chemical co-precipitation and thermal decomposition method in which supersaturation levels aid the formation of relatively smaller nanoparticles are generally used to synthesize superparamagnetic magnetite nanoparticles. Therebesides, when magnetite nanoparticles are larger than roughly 20 nm, these particles exhibit ferrimagnetic or ferromagnetic properties. Unlike their superparamagnetic counterparts, these particles, once magnetized, have a residual magnetization (remanence) even in the absence of an externally applied magnetic field. [45,46].

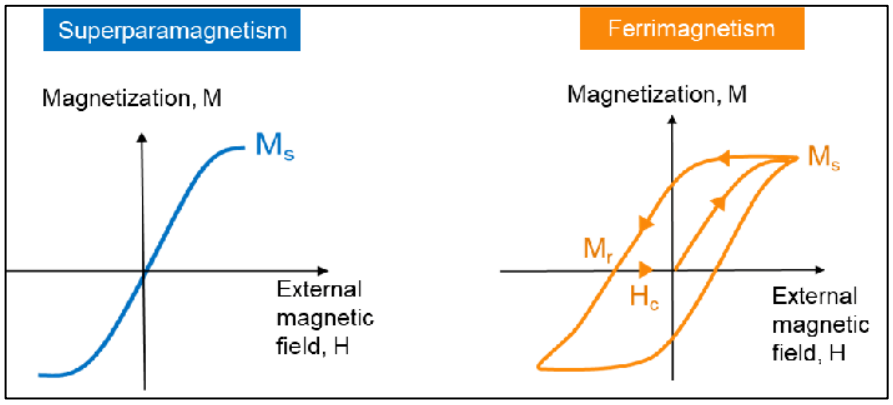

Figure 2.7. Hysteresis curves for superparamagnetic and ferrimagnetic nanoparticles [45]

2.2.1. Synthesis Methods of Magnetic Nanoparticles

There are various organic solvent-based and water-based chemical synthesis methods to synthesize magnetite nanoparticles (MNP). While phase-pure magnetite nanoparticles can be obtained following the application of these synthesis methods, particle related properties such as average size, size distribution, magnetic behavior and morphology varies. Since the adequacy of nanoparticles in a particular application is directly related to their particle size, size distribution and magnetic properties, the choice of synthesis method is crucial for the efficiency of the application. The most commonly used techniques to prepare magnetite nanoparticles are co-precipitation, partial oxidation, thermal decomposition and microemulsion. While these methods offer different advantages, depending on the application, the particles obtained using these methods may be adequate or unsuitable depending on their physical and magnetic properties.

2.2.1.1. Co-precipitation

Chemical co-precipitation is unarguably the simplest and the most widely preferred pathway to synthesize magnetite nanoparticles. This method is based on the simultaneous precipitation of ferrous (Fe^{+2}) and ferric (Fe^{+3}) salts at the stoichiometric ratio required to form the magnetite phase (1:2) at elevated pH values as described by the following reaction pathway.

$$Fe^{+2} + 2Fe^{+3} + 8OH^{-} \rightarrow Fe_3O_4 \qquad (2.1)$$

The magnetic particles with superparamagnetic properties with relatively small particle sizes around 5 to 20 nm (Figure 2.8) can produce in high yield and high purity by using this method. Therefore, this method is used for many different applications as it can also be scaled up without any complications.

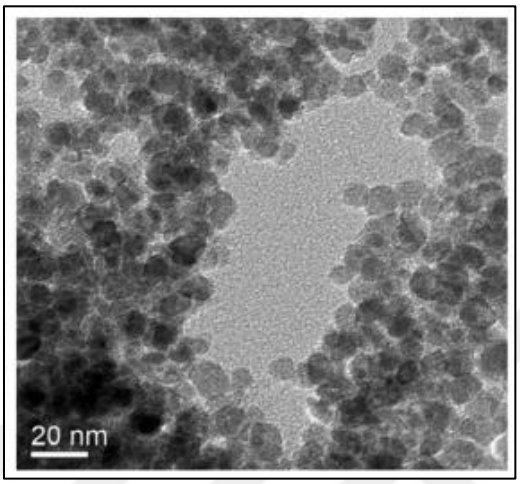

Figure 2.8. Transmission Electron Microscopy image of magnetite nanoparticles synthesized via co-precipitation method

In this method, reaction parameters including the applied temperature of reaction, the type of salt used, pH and ionic strength can slightly change the size and shape of the particles. However, when the reaction kinetics are taken into account, the nucleation rate of the particles overrides the growth rate since very high supersaturation values are reached. Thus, since the nucleation occurs rapidly, the resulting particles are relatively small in size and the variation of the reaction parameters cannot have a radical effect on the particle size (Figure 2.9). Another advantage of this method is that the surfaces of the magnetite nanoparticles obtained can be easily modified with different surface active agents and polymers in order to provide both colloidal stabilization and functionalization on an application basis [46,47].

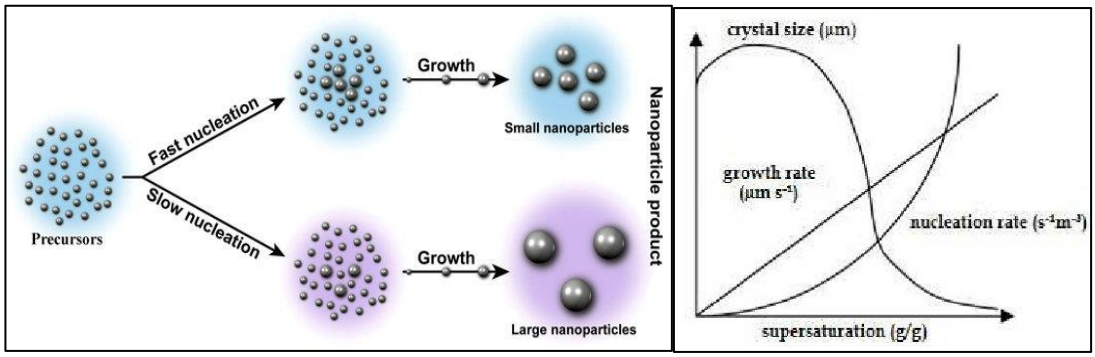

Figure 2.9. Schematic illustration of nucleation and growth process of nanoparticles [47]

2.2.1.2. Partial Oxidation

The partial oxidation method is a less commonly used water-based chemical method for synthesizing mangetite nanoparticles. Unlike superparamagnetic nanoparticles obtained by co-precipitation, magnetic nanoparticles with ferrimagnetic properties can be synthesized by the partial oxidation method. This method contains only ferrous ions originally, and these ions are slowly converted into ferric ions by a mild oxidant at high pH. The fact that ferric ions, which are necessary for the formation of magnetite, are formed gradually, causes lower supersaturation values in the reaction medium, and therefore the growth rate exceeds the nucleation rate, resulting in nanoparticles of larger sizes such as 20-50 nm (Figure 2.10) [46,48].

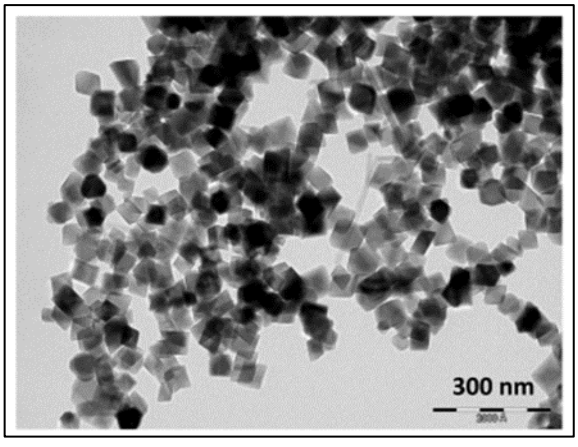

Figure 2.10. Transmission Electron Microscopy image of magnetite nanoparticles synthesized via partial oxidation method

Since many different iron oxide types such as maghemite and goethite can be produced with this method, reaction conditions such as temperature, time, reactor volume, and even mixing speed must be controlled and the reaction must be carried out in an inert atmosphere for the formation of pure magnetite nanoparticles. Due to strong magnetic interactions, ferrimagnetic particles with larger sizes tend to agglomerate more than superparamagnetic particles of small sizes, so it is difficult to achieve colloidal stabilization, which is indispensable for biomedical applications. Therefore, in order for larger nanoparticles to be used efficiently in applications, polymers or surfactants should be used for surface modification to increase stability, surface functionality and prevent oxidation that deteriorates magnetic properties [49].

2.2.1.3. Thermal Decomposition

One of the methods used to produce monodispersed magnetic nanoparticles is the thermal decomposition method, which is based on breaking the chemical bonds in the compound with heat. The process involves produce the nanopartickes by the decomposition of metal precursors in organic solvents in the presence of stabilizing surfactants such as triocytlamine at high temperature and pressure.. This method has major advantages such as allow to control over size, morphologies, properties of magnetic nanoparticles and produce the desired iron oxide particles. Reaction time, boiling point of solvent and molecule length of surfactant are the main parameters for composition and size of obtained particles [50,51].

2.2.1.4. Microemulsion

The microemulsions system consists of two immiscible liquids forms thermodynamically stable isotropic dispersion in the presence of surfactant and cosurfactant. In this method, water microdroplets stabilized by surfactants is dispersed in oil medium which is the continuous phase. Microdroplets will collide, unite and break until the precipitation forms. The precipitate can be collected via filtration or centrifugation with the usage of a solvent such as ethanol or acetone. The essential advantage of this method is that the nanoparticles have uniform average size and morphology with a narrow size distribution, as water microdroplets act as nanoreactors. On the other hand, the inability to synthesize large amounts of nanoparticles and the relative complexity of the synthesis can be stated as disadvantages [52].

2.3. MAGNETIC HYPERTHERMIA

The application of magnetic nanoparticles at the tumor site as heating agents in the hyperthermia method, which is an alternative and relatively novel treatment method for cancer, is called as magnetic hyperthermia. In magnetic hyperthermia treatment, the local temperature of the tumor area is increased by the heat generated when an alternative magnetic field is applied to magnetic nanoparticles. As a very general explanation, in this application, magnetic nanoparticles are delivered to the tumor area either using direct injection or targeting agents, and the local temperature of the tumor area is increased with the heat generated under the effect of an externally applied magnetic field (Figure 2.11) [53]. Thus, cancer cells are destroyed by damaging the cell membrane without damaging healthy cells. This method was first proposed and employed by Gilchrist et. al. by the usage of maghemite nanoparticles to destroy cancer cells by heating them to a temperature of 43°C and 46°C without damaging healthy cells in 1957 [54]. The magnetic hyperthermia application is basically relying on energy conversion to heat by processes called as hysteresis losses and Neel and Brownian relaxations under an alternating magnetic field (AMF) as shown in Figure 2.12.

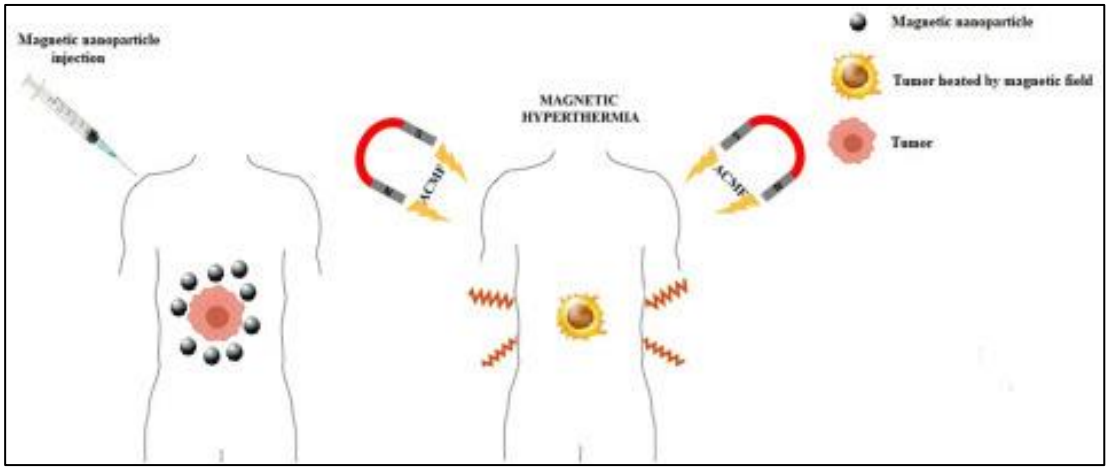

Figure 2.11. The application of magnetic hyperthermia by magnetic nanoparticles [53]

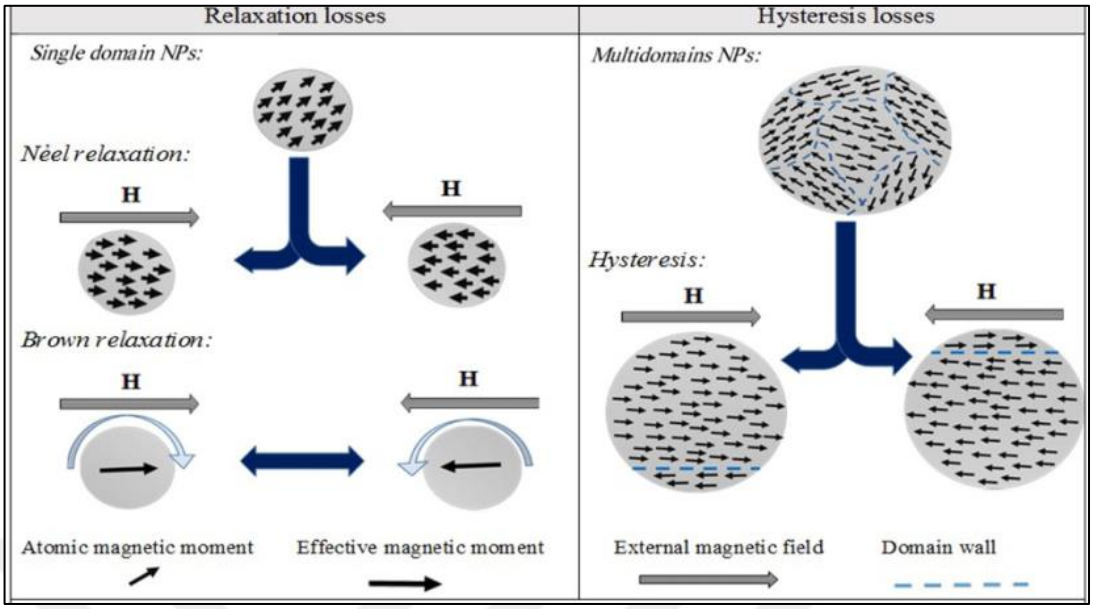

Figure 2.12. The heating mechanism representation of magnetic nanoparticles [55]

The hysteresis losses observed in multidomain nanoparticles are based on the phenomenon of domain wall displacement. When an external magnetic field is applied to magnetic nanoparticles, their magnetic moments align in the direction of the applied magnetic field, or vice versa. When magnetic moments are parallel to to externally applied magnetic field, the domains grow until covering all volume which is the point of saturation, , the domains have opposite direction moments to the external field diminish.Whereas, the Neel relaxation is the reorientation of the magnetic moments within particle while Brownian relaxation is the rotation of the whole particle in the carrier liquid including its magnetic moments [23,55].

The heating performance of magnetic nanoparticles in hyperthermia applications is specified by the specific sorption rate (SAR), which is the power generated into heat per unit mass of magnetic nanoparticles. In order to determine the SAR values of magnetic nanoparticles intended to be used in hyperthermia application, the time-dependent temperature change of a nanofluid with a certain concentration is examined under the influence of an externally applied alternative magnetic field for which the corresponding magnetic field and frequency are kept constant [56].

$$SAR\left(\frac{W}{g_{Fe_3O_4}}\right) = \frac{C.\rho}{\varphi}.\frac{\Delta T}{\Delta t} \quad (2.2)$$

The SAR values of magnetic nanofluids then can be calculated by the heating curve obtained and using Equation 2.2, where *C* (J/g.^{o}C) and ρ (g/ml) are the specific heat capacity of base fluid and density of the fluid in which magnetic nanoparticles dispersed, φ is the concentration of magnetite-based nanofluids in g/mL, ΔT/Δt represents the temperature derivative over time on the corresponding heating curve.

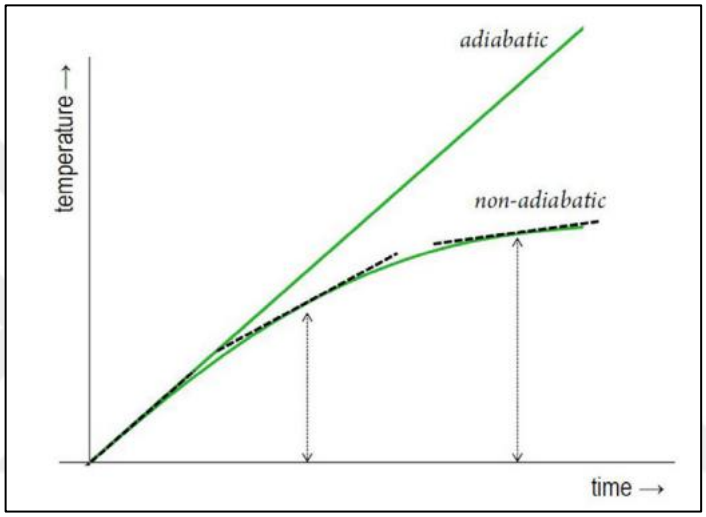

Figure 2.13. Comparison of taken temperature data depend on time with an adiabatic and a non-adiabatic setup [57]

The SAR parameter is a measure of the power dissipation determined by calorimetric measurements, which are most accurate and efficient under adiabatic conditions in the absence of heat loss. Figure 2.13. shows the heating curves of time-dependent temperature change in nanofluids under the influence of an externally applied AMF for adiabatic and non-adiabatic conditions in calorimetric measurements. Although heat losses do occur in non-adiabatic systems, adiabatic systems are difficult to construct and the measurements themselves require considerable time, which is why almost all research on magnetic hyperthermia is carried out under non-adiabatic conditions [56,58–60]. The slope value, which expresses the time-dependent change of the temperature required for the calculation of the SAR value for nanofluids, is therefore placed in Equation 2.2 by finding the maximum value obtained at the initial stage of the heating curve in non-adiabatic systems. Since this slope is similar to the value expected to be obtained in an adiabatic system, it ensures that

the calculated SAR value is also comparable to the value likely to be obtained in the adiabatic case [57].

2.3.1. Factors Affecting Magnetic Hyperthermia

The utilization capacities and heating efficiency of magnetic nanoparticles in hyperthermia applications depend on several factors such as particle size, morphology, magnetic anisotropy and saturation magnetization, which directly affect the relaxation mechanism. In addition to these factors, SAR also depends on the strength and frequency of the externally applied alternating magnetic field, the concentration of the nanofluid and the surface modification of the nanoparticles, which have a significant impact on particle interaction and colloidal stability. Therefore, the effects of all these fundamentally different factors individually on SAR values, which express the efficiency of MNP in hyperthermia application, have been frequently investigated in the literature.

2.3.1.1. Effect of Frequency and Amplitude of The Applied Magnetic Field

The effect of frequency and applied magnetic field strength on the heating efficiency of magnetic nanoparticles has been investigated extensively for decades. Numerous studies have agreed that increasing the frequency and amplitude of the AMF to an increase in SAR values. However, the range of frequency and magnetic field strength for safe clinical application is constrained by the fact that both frequency and magnetic field enhances the generation of unwanted eddy currents that can adversely affect healthy tissues. Hence, the Atkinson-Brezovich limit is used as the safe upper limit at which eddy current effects can be tolerated, and according to this limit the product of frequency and amplitude must be smaller than $Hxf < 9.46 \times 109\ Am^{-1}s^{-1}$[61].

Narayanaswamy et al. investigated the magneto-thermal efficiency of 10 nm sized MNP synthesized via chemical co-precipitation method. The effect of frequency ranging between 166-765.8 kHz under constant 350 G magnetic field strength. The effect of magnetic field strength ranging between 100 and 300 G at constant frequency of 765.8 kHz were investigated. The temperature versus time plots at constant field strength and constant frequency are shown in Figure 2.14 for a sample concentration of approximately 10 mg/ml. The results show that, without exception, both the temperature difference and corresponding

SAR values increase with increasing magnetic field strength at constant frequency and with increasing frequency under constant magnetic field strength. The results also indicate a non-linear enhancement in SAR values with the change in magnetic field strength at constant frequency, while the change in frequency at constant magnetic field strength exhibit roughly a linear increase (Figure 2.15) [58].

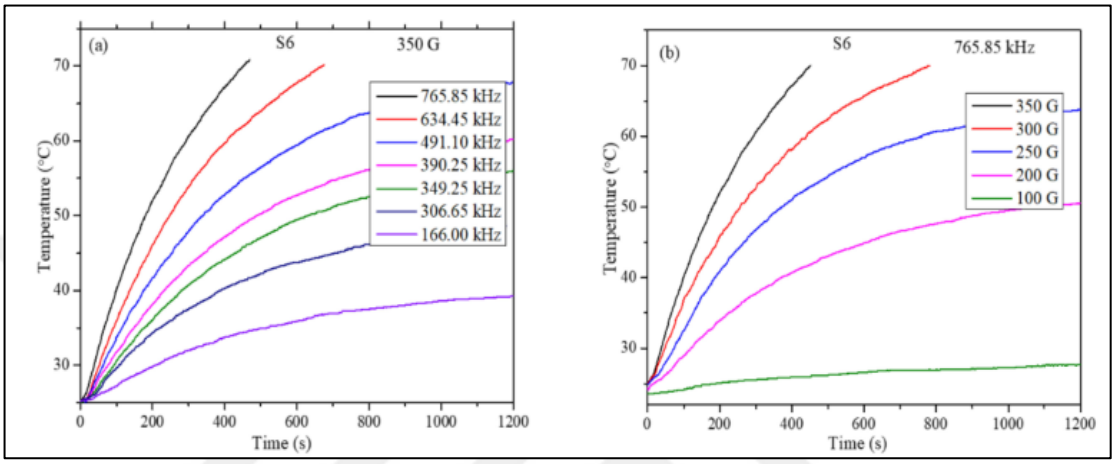

Figure 2.14. Heating curves at concentration 10 mg/ml (a) at fixed 350 G field strength, (b) at fixed frequency 765.85 kHz [58]

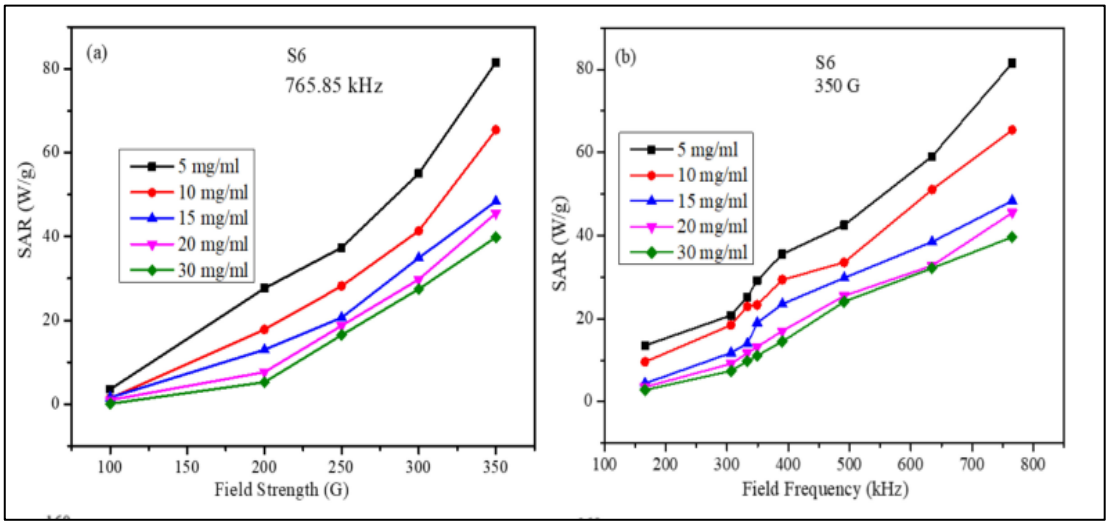

Figure 2.15. Specific absorption rate values with differs concentration (a) with respect to the field strength at a fixed frequency, (b) with respect to frequency at fixed strength [58]

Another study was conducted by Shah et al. to studied the effect of alternating magnetic field intensity and frequency on the SAR values of MNPs for a concentration of 20 mg/ml. The nanoparticles were exposed to a magnetic field strength varying between 15.1 and 47.7 kA/m at 194 kHz, and it was observed that as the field strength was altered with SAR increasing from 3.7W/g to 43.3W/g with altered field intensity. Moreover, at a constant magnetic field strength of 38.2 kA/m, the frequency was varied between 123 and 430 kHz, and the directly proportional correlation between the SAR value and the frequency was clearly demonstrated with SAR values ranging from 10.9 to 76.4 W/g (Table 2.1) [56].

Table 2.1. SAR values at fixed field strength (38.2 kA/m) and frequency (194 kHz) [56]

Field strength H (kA/m)	Frequency f (kHz)	SAR (W/g NP)	Field strength H (kA/m)	Frequency F (kHz)	SAR (W/g NP)
15.1	194	2.7±0.9	38.2	123	10.9±1.5
22.8	194	11.1±2.1	38.2	143	16.7±2.0
35.8	194	19.4±2.1	38.2	194	21.6±0.7
38.2	194	21.6±0.7	38.2	430	76.4±3.6
47.7	194	31.3±3.2			

Xu and Pan studied the effect of the magnetic field frequency and strength on the heating efficiencies of magneto ferritin nanoparticles with a core size 4.3 nm. The effect of applied frequency and magnetic field strength can be seen in Figure 2.16 that showed the time-dependent temperature change of magnetic nanoparticles with 4.3 nm core size. Magnetic field frequency was varied from 274.5 kHz to 805.5 kHz whereas magnetic field amplitude was kept constant at 19.5 kA/m. It is clearly evident that temperature increased with increasing of frequency and SAR values were also increased from 7.9 to 56.3 W/g. In addition, the effect of applied magnetic field strength ranging between 11.9-19.5 kA/m at

constant frequency of 805.5 kHz was investigated. This results demonstrated that when amplitude of the AMF increased, temperature increased and expected SAR values increased from 35.6 to 56.3 W/g [62].

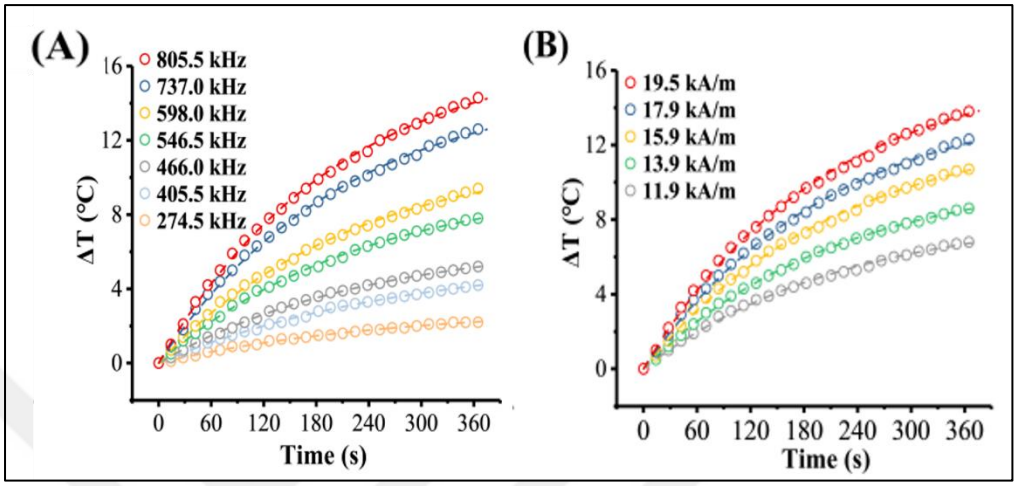

Figure 2.16. The curves of temperature versus time for magnetic nanoparticle with 4.3 nm core size at different a) frequencies, b) field strengths [62]

2.3.1.2. The Effect of Concentration

Another factor affecting the SAR values of magnetic nanoparticles is the concentration, which directly affects the dipolar interactions between magnetic nanoparticles and the relaxation mechanism. Although many studies have been conducted to investigate the effect of concentration on SAR values, inconsistent results have been obtained. While many experimental studies show that SAR values decrease with increasing nanoparticle concentration, there are also studies with contrary results indicating that concentration and SAR values are directly proportional. In addition to all these results, there are also studies showing that SAR values are independent of concentration and remain constant without being affected.

Xu and Pal investigated the effect of Fe concentration on the specific loss power (SLP) values of magneto-ferritin which is a potential nanomaterial with a tunable nanosized inner core and good biocompatibility by applying the frequency and magnetic field amplitude of 805.5 kHz and 19.5 kA/m. SLP values were found to be 51.3 W/g at 1.5 mg Fe/mL concentration and 67.7 W/g at 5 mg Fe/mL concentration for magnetic nanoparticles with 4.8 nm core size. According to these results, it was determined that SLP values increased by

the increase in Fe concentration, and this was attributed to the enhancement of dipolar interaction resulting from the increment in concentration. On the other hand, in the same study, although an increase in SLP values was obtained for smaller particles with increasing Fe concentration, a tendency to decrease in SLP was observed for larger particles [62].

Linch et. al. studied the effect of concentration over the heating abilities of magnetic nanofluids containing starch-coated superparamagnetic magnetite nanoparticles of 15-17 nm size by altering the concentration from 3 mg/mL to 15 mg/mL under an AMF of 184 kHz and 12 kA/m. As can be seen in Figure 2.17 which shows the time dependent heating curves of nanofluids with varies concentration, temperature rising rate is strongly dependent with the concentration of the particles in the nanofluids. Higher temperature rising rate is obtained by increment of the concentration of the particles in the nanofluids [60].

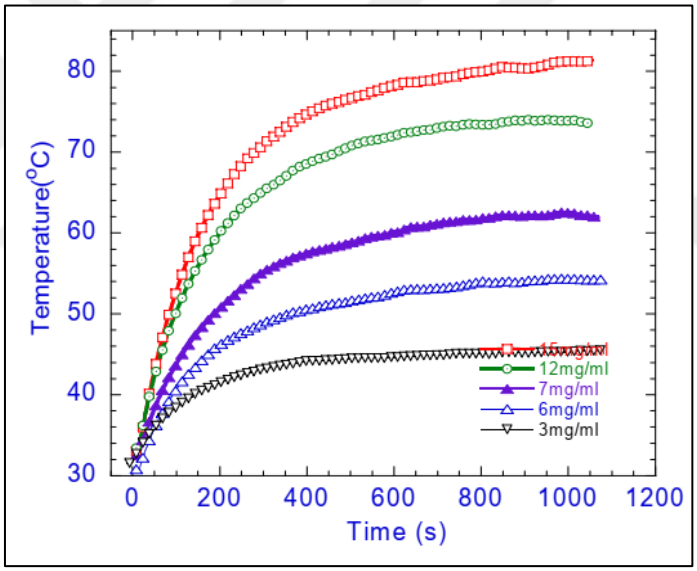

Figure 2.17. Time-dependent heating curves for magnetic nanofluid varying concentrations [60]

Considering the values given in Table 2.2, it was seen that the highest SAR value, 129 W/g, was attained at the lowest iron oxide concentration and SLP values of MNP were inversely proportional to concentration. Essentially, it is known that the heat losses caused by relatively small sized superparamagnetic nanoparticles occur through Neel and Brownian relaxations, which are directly affected by the interactions between particles. Therefore, an increase in magnetic particle concentration causes a decrease in the distance between

particles, which may affect the interaction between particles, and leads to a decrement in SLP values [60].

Table 2.2. Initial heating rate and specific loss power values at varies concentrations [60]

Concentration of particles (mg/mL)	dT/dt (°C/s)	SLP values(W/g)
3	0.092	129
6	0.141	97
7	0.159	94
12	0.240	83
15	0.310	86

These studies have demonstrated that SAR values show a correlation, either with increasing or decreasing with Fe or nanoparticle concentration. Despite all these results, Shah et al. measured the SAR values of 8-9 nm sized superparamagnetic magnetite nanoparticles coated with starch at concentrations of 4.3, 6.4 and 8.6 mg/mL, and showed that although more concentrated nanoparticle dispersions were observed to heat faster, the SAR values were not affected by the nanoparticle concentration. This finding is consistent with the SAR calculation, which is normalized by the mass of the nanoparticles and allows comparison of magnetic heating experiments with varying concentrations [56].

Table 2.3. The effect of nanoparticle concentration over SAR [56]

Magnetite concentration (mg/mL)	SAR (W/g Fe)	SAR (W/g NP)
4.3	45.5 ± 6.4	32.9 ± 4.6
6.4	43.9 ± 3.2	31.8 ± 2.3
8.6	43.3 ± 4.4	31.3 ± 3.2

2.3.1.3. Effect of Particle Size and Morphology

The effects of size and morphology on the heating efficiency of magnetic nanoparticles for hyperthermia applications have also been experimentally investigated. The heating mechanism of magnetic nanoparticles is related to relaxation mechanisms such as Neel relaxation, Brownian relaxation and hysteresis losses as mentioned earlier. While hysteresis losses are dominant for nanoparticles with multi-domain structures and relatively larger sizes, the dominant mechanisms for single-domain superparamagnetic nanoparticles with smaller sizes are Neel and Brownian losses. In a consequence of the contribution of these mechanisms, which vary in nanoparticles with multi-domain or single-domain regions, the studies on the effect of particle size on SAR have yielded different results and no clear consensus has been reached [63].

The morphology of magnetic nanoparticles, which can be differentiated by the chosen synthesis and surface modification, has also been shown to have an effect on the heating efficiency. In these studies, it was revealed that magnetic nanoparticles with spherical, cubic, octahedral or octopod morphology have different SAR values and consequently different heating efficiencies due to the variation of their magnetic properties such as relaxation mechanism and saturation magnetization [64].

Mai et al. studied magnetic particles with different sizes ranging from 7.5 to 416 nm in a magnetic field of 80 kHz and 32.5 kA/m and according to the results shown in Figure 2.18, which expresses the time-dependent temperature change of the particles under the influence of an externally applied AMF, it is evident that the calculated SAR values are highly size-

dependent. For magnetic particles with diameters between 46 and 416 nm, SAR values were found to increase with decreasing size due to the contribution of hysteresis losses. On the other hand, SAR values were found to be 15.6 W/g for 7.5 nm particles and 39.4 W/g for 13 nm particles which have superparamagnetic properties. For these particles, Neel and Brownian losses are dominant and the resulting improvement can be attributed to the enhancement of saturation magnetization of corresponding nanoparticles [65].

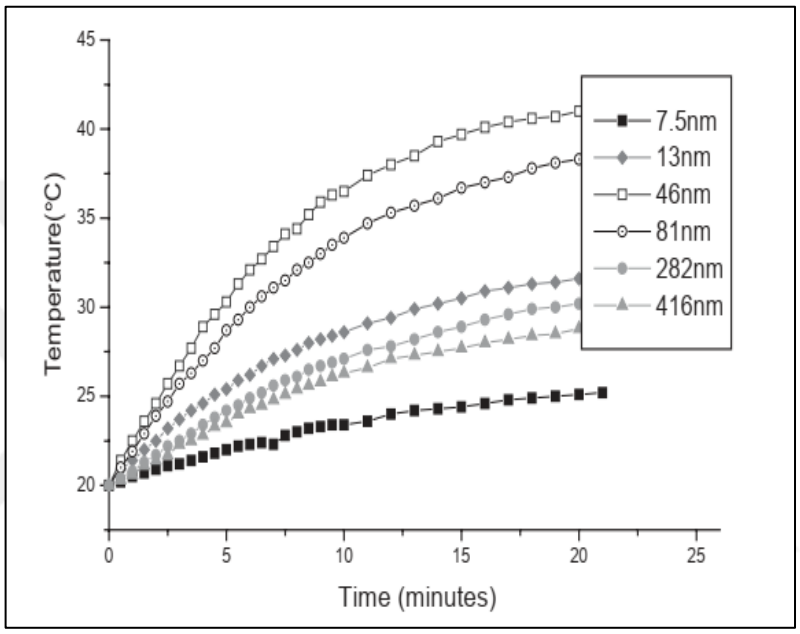

Figure 2.18. Heating curves for magnetic particles having different sizes in a magnetic field of 80 kHz and 32.5 kA/m [65]

Presa et al. studied the effect of size over the specific absorption rate of γ-Fe_2O_3 nanoparticles synthesized via co-precipitation method with average particles sizes of 6,8,11,13 nm. Figure 2.19 illustrates that increasing the size of particle from 8 nm to 11 nm leads to an enhancement in SAR values from 10 W/g to 40 W/g, but this dramatic change is not observed when the particle size is further increased from 11 nm to 13 nm. This variation in the enhancement has been attributed to the fact that the nanoparticle size proportionally changes the SAR values at a cubic rate, but it is basically shown that the SAR values increase with increasing particle size [66].

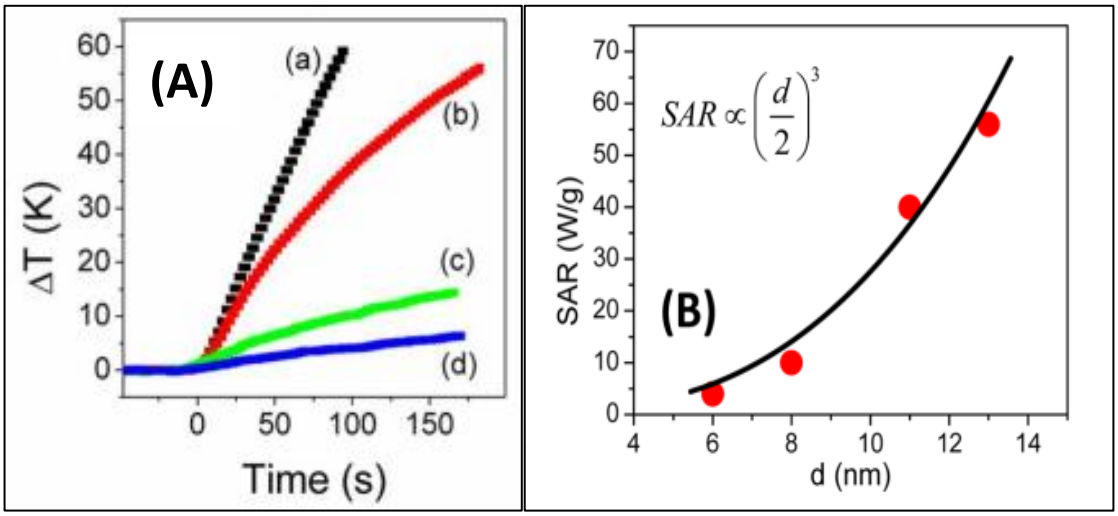

Figure 2.19. The variation of temperature for different sizes of nanoparticles (A), size dependent specific absorption rate values (B) [66]

Gonzalez-Fernandez et al. analyzed the effects of particle size by measuring the specific power absorption (SPA) of uncoated magnetite nanoparticles between 5 and 110 nm in size range at 260 kHz and 16 mT. According to Figure 2.20, the maximum value was observed for nanoparticles with an average size of 24 nm and the values decreased significantly for all particles above and below this size threshold due to the transition from single domain to multi-domain regions [67].

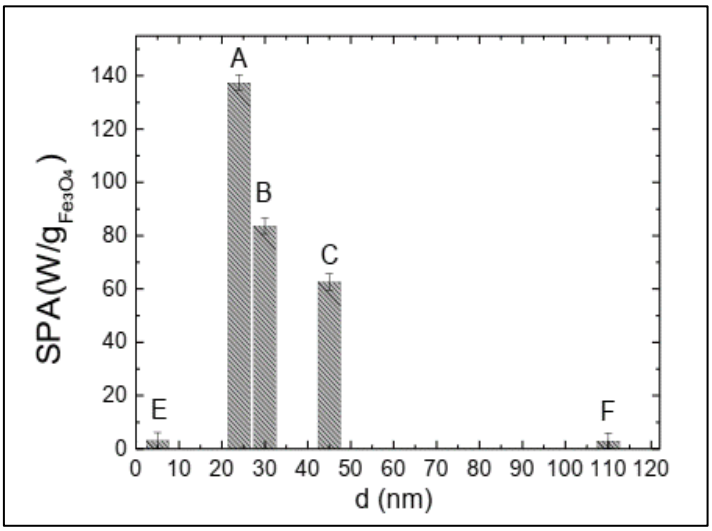

Figure 2.20. Specific Power Absorption values for different sizes of bare nanoparticles [67]

Khurshid et al. studied nanoparticles with different morphologies and investigated their heating efficiency by exposing all particles under the influence of a magnetic field of 310 kHz and 400 to 800 Oe. As can be seen in Figure 2.21, the heating rate of cubic magnetic nanoparticles with an average size of 20 nm was found to be higher than that of spherical magnetic nanoparticles in every magnetic field examined. With the variation of this heating rate, the SAR values of the cubic and spherical particles under 600 Oe and 310 kHz magnetic fields were calculated as 200 W/g and 135 W/g, respectively. Considering the magnetic properties of the investigated nanoparticles, it was observed that the anisotropy was larger for cubic particles, whereas the saturation magnetization was larger for spherical nanoparticles, which exhibited lower enhancement. This suggests that saturation magnetization is not a key and influential factor in terms of enhancement, as SAR values and temperature heating rates are higher for cubic nanoparticles [68].

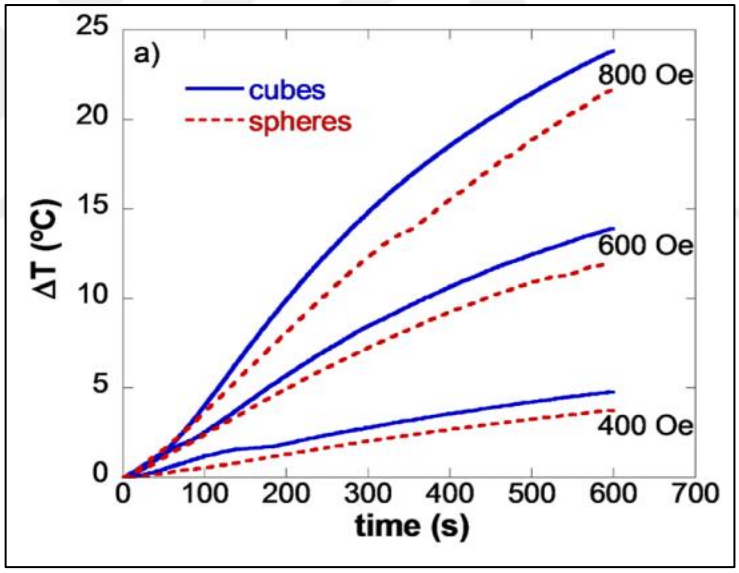

Figure 2.21. Temperature versus time data for the spherical and cubic magnetic nanoparticles at 310 kHz and different magnetic field strengths [68]

Mohapatra et al. synthesized magnetite nanoparticles with different morphologies and studied the effect of geometry on heating characteristics under a fixed frequency of 265 kHz and a field strength of 39 kA/m. Figure 2.22 shows the time-dependent temperature change for nanoparticles of different morphologies and the results revealed that at approximately 300 s, the local temperature increased for all samples regardless of the type of morphology as nanowires with a length of 80 nm and a diameter of 15 nm have the highest SAR values

of 846 W/g in comparison to other nanoparticles. This indicates the importance of the anisotropy of the particles on the heating rate due to the high shape anisotropy of the nanowires. The results also show that particles with cubic morphology have a higher heating rate than spherical particles, as stated in the previous study [69].

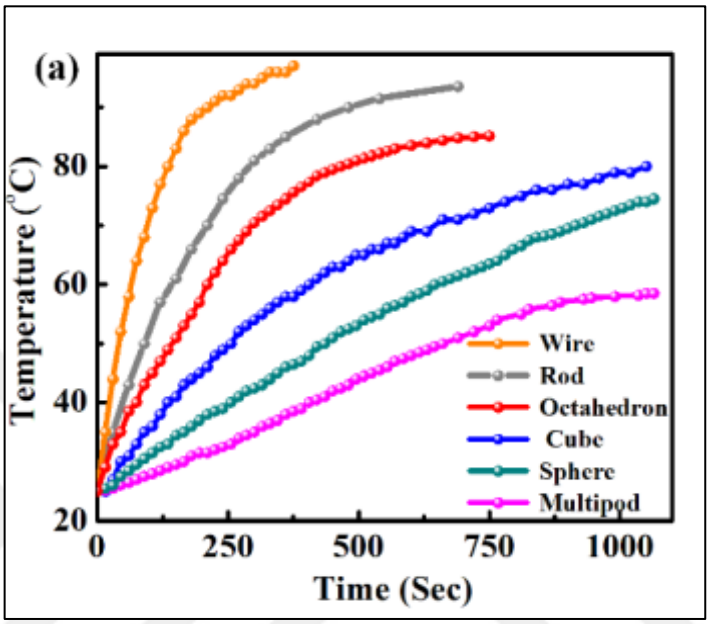

Figure 2.22. Time-dependent temperature variation of samples with different morphologies [69]

2.3.1.4. Effect of Surface Modification

Surface modification of magnetic nanoparticles plays a critical role in biocompatibility, functionality and colloidal stability. In order to effectively utilize magnetic nanoparticles in hyperthermia applications, surface modification with polymers and/or surfactants is essential to ensure that the particles remain suspended in suspension and do not precipitate over time. Various studies have also been conducted on the effect of surface modification on SAR values of magnetic nanoparticles, but the results are generally inconsistent. In principle, the surface coating can alter the viscosity of the nanofluids and inhibit the relaxation process of the particles. Moreover, since surface modification agents create a non-magnetic layer around the particles, thus reduce the saturation magnetization and cause SAR values to decrease [70].

Rajan et al. investigated the effect of surface modification of magnetic nanoparticles on the heating ability for magnetic hyperthermia using biocompatible surfactants and polymers such as polyethylene glycol, citric acid and ethylene diamine to achieve colloidal stability by electrostatic and steric repulsive interactions. The results of the study showed that the highest SAR value was found to be 115 W/g for glutamic acid coated nanoparticles (GA-Fe_3O_4), which have higher magnetic anisotropy and also faster relaxation time. In contrast, although Citric acid-coated particles have the highest saturation magnetization value, the relaxation time is slower than that obtained for GA-Fe_3O_4 NPs, so the relatively higher SAR value could not be achieved with this nanoparticle system [63].

In another study by Jamir et al., the heating efficiencies of Fe_3O_4 nanoclusters modified with chitosan and dextran were investigated and the effect of surface modification on SAR was analyzed. At a fixed concentration of 1 mg/ml, the SAR value of the dextran modified nanoclusters was found to be 40% higher than that of the bare nanoclusters and a decrease in SAR values was obtained with increasing concentration (Figure 2.23). The increase in SAR value as a result of both concentration decrease and surface modification was attributed to the dipolar interaction between the particles [70].

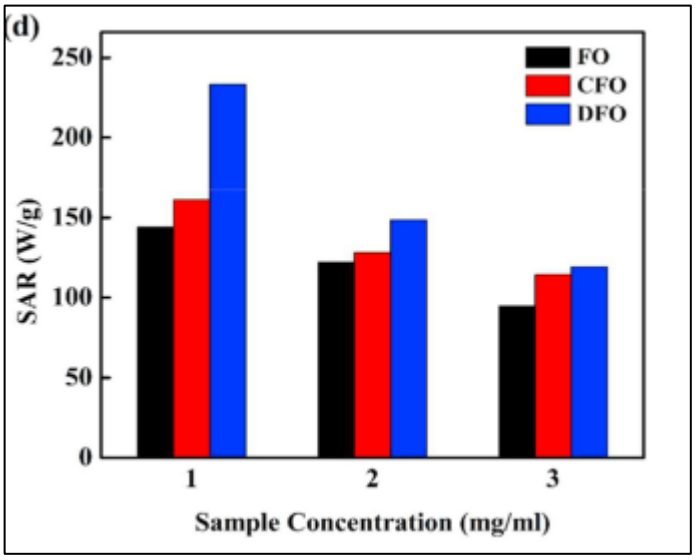

Figure 2.23. The variation of SAR dependence of concentration for bare (FO), chitosan modified (CFO) and dextran modified (DFO) nanoclusters [70]

Majeed et al. measured SAR values of core-shell Silica and magnetite nanoparticles under the influence of an externally applied AMF (265 kHz and 400 A). According to the results obtained, the temperature enhancement was higher in modified nanoparticles than that of bare nanoparticles and the SAR value decreased with the increase in the shell thickness around the particle. However, according to the results given in Figure 2.24, the initial slope obtained in bare nanoparticles appears to be higher than that of all samples and the relatively lower SAR value calculated and shown in the inset is not clearly addressed [71].

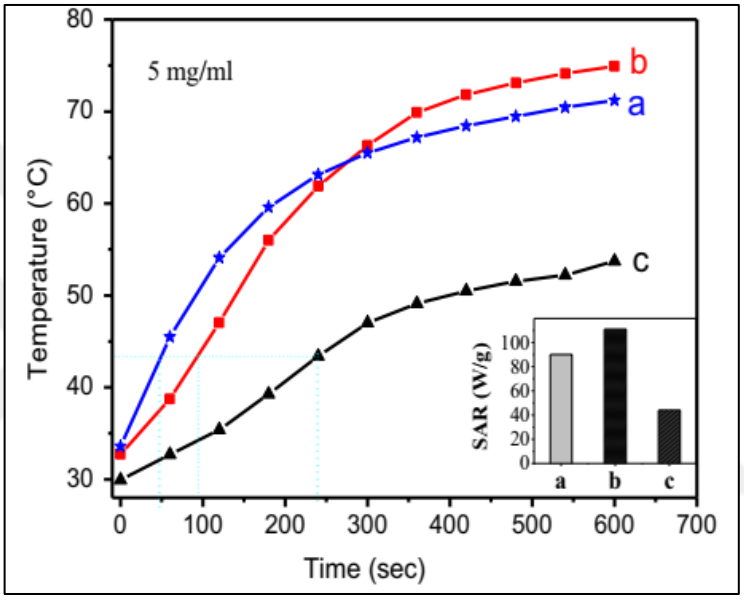

Figure 2.24. Temperature change over time for bare (a), magnetite-silica core-shell particles (b), Inset shows the corresponding SAR values [71]

3. MATERIALS

3.1. CHEMICALS

Table 3.1. Chemicals used for the synthesis of magnetite nanoparticles

Chemical Name	Formula	Structure	Provider
Iron (II) Sulfate Hepta Hydrate	$Fe(SO_4)_2 . 7H_2O$	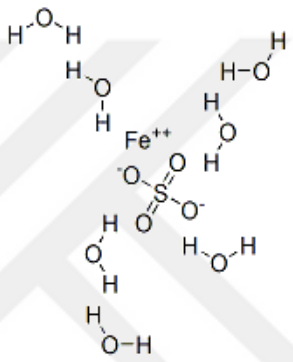	Riedel de Haën
Iron (III) Chloride	$FeCl_3$	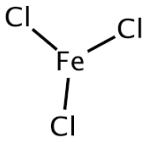	Riedel de Haën
Polyacrylic Acid (450kDa)	$(C_3H_4O_2)_n$	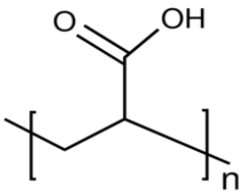	Sigma Aldrich
Polyacrylic Acid (250kDa)	$(C_3H_4O_2)_n$	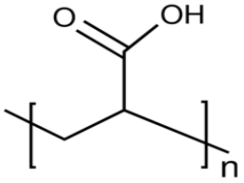	Sigma Aldrich
Potassium Nitrate	KNO_3	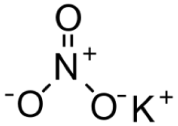	Sigma Aldrich

Table 3.1. (continued)

Potassium Hydroxide	KOH	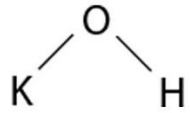	Emsure
Citric Acid	$C_6H_8O_7$	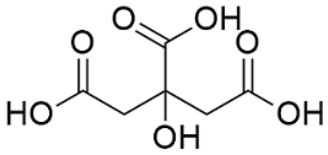	Sigma Aldrich
Polyethylenimine (25 kDa)	$H(NHCH_2CH_2)_nNH_2$	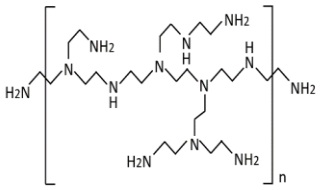	Sigma Aldrich
Polyethylene glycol (400 Da)	$(C_2H_4O)nH_2O$	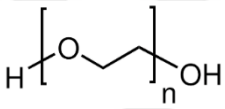	Sigma Aldrich
Ammonium Hydroxide	NH_4OH	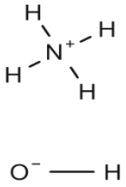	Sigma Aldrich

Table 3.2. Chemicals used for the Tiron chelation test

Chemical Name	Formula	Structure	Provider
Tiron	$C_6H_4Na_2O_8S_2$	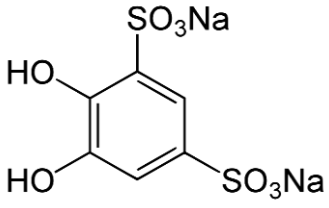	Fluka
Hydrochloric Acid (37%)	HCl	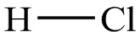	Sigma Aldrich
Sodium Hydroxide	NaOH	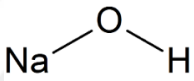	Riedel de Haën
Potassium Hydroxide	KOH	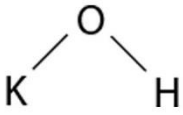	Emsure

3.2. INSTRUMENTS

Table 3.3. Instruments used for characterization of magnetic nanoparticles

Instrument	Manufacturer	Model
UV Visible Spectroscope (UV-VIS)	Inesa	L7 (Yeditepe University)
X-ray Diffraction (XRD)	Bruker	D8 Advance (Kastamonu University)
X-ray Diffraction (XRD)	Rigaku	D-Max 2200 PCI (Gebze Technical University)
Vibrating Sample Magnetometer (VSM)	Lake Shore	7407 (Kastamonu University)
Vibrating Sample Magnetometer (VSM)	Lake Shore	Quantum Design PMS9T (Gebze Technical University)
Transmission Electron Microscope (TEM)	JEOL	JEM 2100 PLUS (Yeditepe University)
Transmission Electron Microscope (TEM)	JEOL	JEOL JEM-ARM200F (Sabancı University)
Thermogravimetric Analysis (TGA)	PerkinElmer	Pyris1 (Yeditepe University)
Vacuum Oven	Memmert	V0-200 (Yeditepe University)

Table 3.3. (continued)

Hyperthermia Testing Device	nanoTherics	magneTherm
Fourier Transform Infrared Spectroscope (FTIR)	Thermo Scientific	Nicolet iS50
Water bath circulator	VWR	1146D (Yeditepe University)
Mechanical Stirrer	WiseStir	Feedback Control Digital (Yeditepe Üniversitesi)

4. EXPERIMENTAL PROCEDURE

4.1. SYNTHESIS OF MAGNETITE NANOPARTICLES

There are numerous chemical synthesis methods in the literature to synthesize of magnetite nanoparticles [52]. Considering the reaction kinetics of these synthesis methods, it is possible to obtain magnetic nanoparticles of different sizes and morphologies [46]. The variation in particle size depending on the synthesis method also directly affects the magnetic properties of the particles. In this study, since it is aimed to fully investigate the effects of particle size and associated magnetic properties of magnetite nanoparticles on SAR together with surface modification, co-precipitation (COP) method was selected for the synthesis of superparamagnetic nanoparticles and partial oxidation (POX) method was adopted for the synthesis of ferrimagnetic nanoparticles.

4.1.1. Co-Precipitation Method

The most employed method in the literature for the synthesis of magnetite nanoparticles is the precipitation method due to its simplicity, short reaction time and scalability. By using this method, superparamagnetic magnetite nanoparticles with narrow size distribution and approximately 5-20 nm in size can be synthesized [46]. Briefly, 80 ml of distilled water is taken into a jacketed glass reactor and the medium is brought to a temperature of 60 ^{o}C and kept constant at this temperature by means of an externally applied water bath. The reaction medium was purged of air with a continuous flow of nitrogen for 30 minutes to avoid the formation of any other iron oxide species, especially maghemite, due to oxidation. After half an hour, ferrous (0.242 g) and ferric (0.282 g) salts at 1:2 molar ratios, stoichiometrically required for magnetite formation were added to oxygen-free distilled water and allowed to dissolve completely for 5 minutes. Meanwhile, the reaction medium changes from transparent to orange color (Figure 4.1) and after complete dissolution, magnetite nanoparticles were precipitated with the rapid addition of sodium hydroxide solution (0.514 g / 10 ml distilled water). Following the addition of the base, the sudden pH increases in the reaction medium led to magnetite nucleation and the color of the medium instantly changed from orange to black indicating the successful formation of magnetite phase (Figure 4.1).

The reaction was continued under nitrogen gas for another 30 minutes and then the final product was centrifuged at 6000 RPM for 10 minutes to remove the salts and neutralize the pH. The magnetite nanoparticles obtained after centrifugation were then dried in vacuum (20 mBar) and at 60 ^{o}C for further characterization. Surfactants or polymers were dissolved in deoxygenated distilled water at the beginning of the reaction and the whole reaction was carried out identically in the presence of these surface agents to obtain surface-modified magnetite nanoparticles with colloidal stability in contrast to bare nanoparticles.

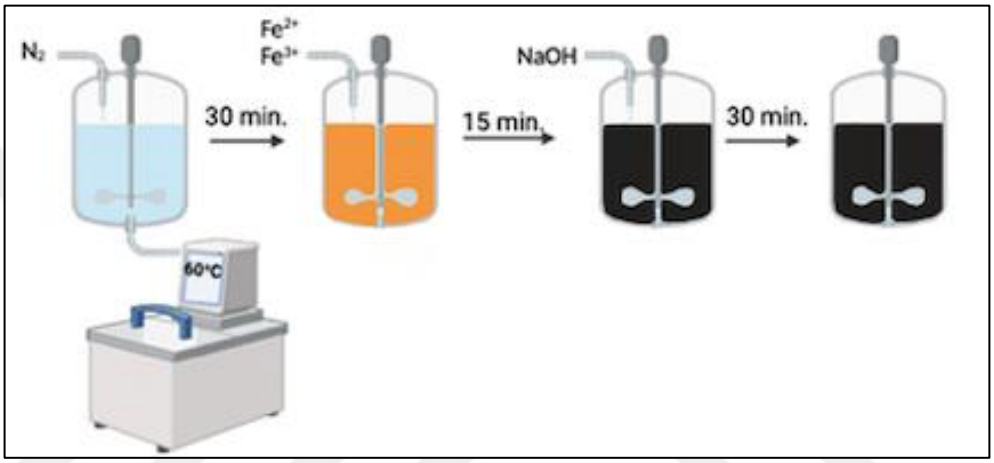

Figure 4.1. Schematic representation of the experimental pathway for chemical co-precipitation method

4.1.2. Partial Oxidation Method

Another relatively less commonly utilized water-based synthesis method for obtaining magnetite nanoparticles is the partial oxidation (POX) method. Using this method, relatively much larger (>20 nm) and most importantly ferrimagnetic nanoparticles can be obtained as a consequence of the corresponding reaction kinetics [48]. In this method, iron ions with dissimilar charges are not reacted in the stoichiometric ratio required for magnetite formation as in the co-precipitation method. Rather, the reaction starts only in the presence of iron (II) ions and then partially oxidized to iron (III) ions by a simple oxidant present in the medium. Thus, the nucleation and growth phases for magnetite formation are relatively slower, resulting in comparatively larger particles [49].

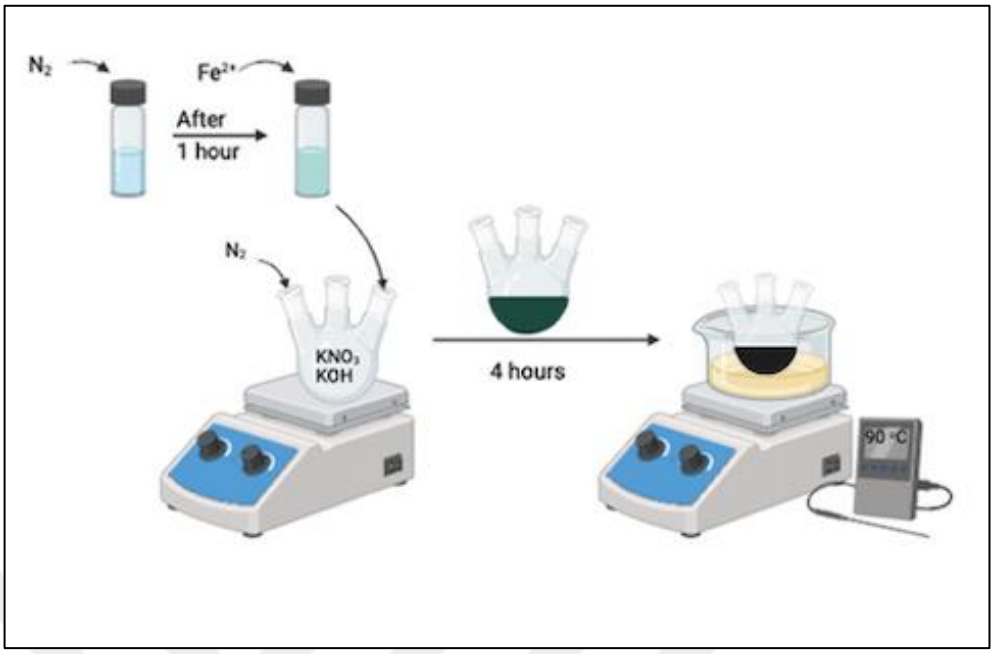

Figure 4.2. Schematic representation of the experimental pathway for partial oxidation method

Simply, 2.525 g of potassium nitrate and 0.974 g of potassium hydroxide were dissolved in 118.75 ml of distilled water and the solution was taken into a 3-neck round bottom flask. On the other hand, 6.25 ml of distilled water was also taken in a glass vial and both media were exposed to nitrogen gas for one hour to remove the ambient oxygen. Simultaneously, an oil bath was set to a constant temperature of 90 ^{o}C and the round bottom flask containing the base/oxidant solution was placed in the oil bath. Meanwhile, 0.8685 g of ferrous (II) sulfate heptahydrate was dissolved in 6.25 ml of previously de-aerated water and gently added to the base/oxidant solution using an injector. After 1 minute, the nitrogen gas supplied to the environment was cut off due to the system being sealed off and the reaction medium was continuously stirred and kept at constant temperature for an additional 4 hours. At this stage, the reaction medium turns green by the addition of iron (II) salt and then gradually turns black due to the formation of the magnetite phase with partially formed iron (III) ions. (Figure 4.2) Following the completion of the reaction, the magnetite nanoparticles obtained were separated from the medium and centrifuged at 6000 RPM for 10 minutes and then dried in vacuum at 60 ^{o}C for further characterization. Surfactants or polymers intended to be employed for surface functionalization and colloidal stabilization were introduced into the

base/oxidant solution at the beginning of the reaction and all nucleation and growth phases were ensured to take place in the presence of these agents.

4.2. CONCENTRATION DETERMINATION

The synthesis of magnetite nanoparticles was carried out by co-precipitation and partial oxidation methods for comparison in this study. Subsequently, Tiron test was carried out to determine the concentration of the obtained nanoparticles after they formed nanofluid with distilled water as the base liquid [72]. Tiron is a chemical substance that can form very strong complexes with iron and titanium. Since magnetite contains both iron (II) and iron (III) in its structure, this colorimetric method could be used to determine the concentration of nanofluids. Simply, concentrated hydrochloric acid (0.4 ml) was added to a suspension of magnetic nanofluid (0.1 ml) to liberate the iron ions contained within the structure of magnetite. This acidic environment also ensured that the shell around the particle, which provides colloidal stability, was eliminated. Following the addition of the Tiron solution (0.6 ml, 0.083 g/ml), the liberated iron ions and Tiron molecules formed a complex in a 1:3 ratio and the color of the solution changed instantly to dark maroon as the pH of the solution was enhanced by the addition of 4 M 3 ml of sodium hydroxide (Figure 4.3). Since this solution obtained as a result of the chelation between Tiron molecules and iron ions gives strong absorbance at 480 nm, absorbance measurements were performed using UV-Vis spectroscopy. The absorbance value obtained was then placed in Equation 5.1 to determine the concentration of magnetite nanoparticles. In order to determine the unknown concentration, the Tiron test was performed on 3 different samples with 3 replicates for each sample and the average of the absorbance value was then used in the equation.

$$Concentration\left(\frac{g}{ml}\right) = \frac{(abs@480\ nm) \times (Dilution\ Factor) \times 231.52 \times 25}{39986 \times 162.15 \times 3 \times 0.1} \quad (5.1)$$

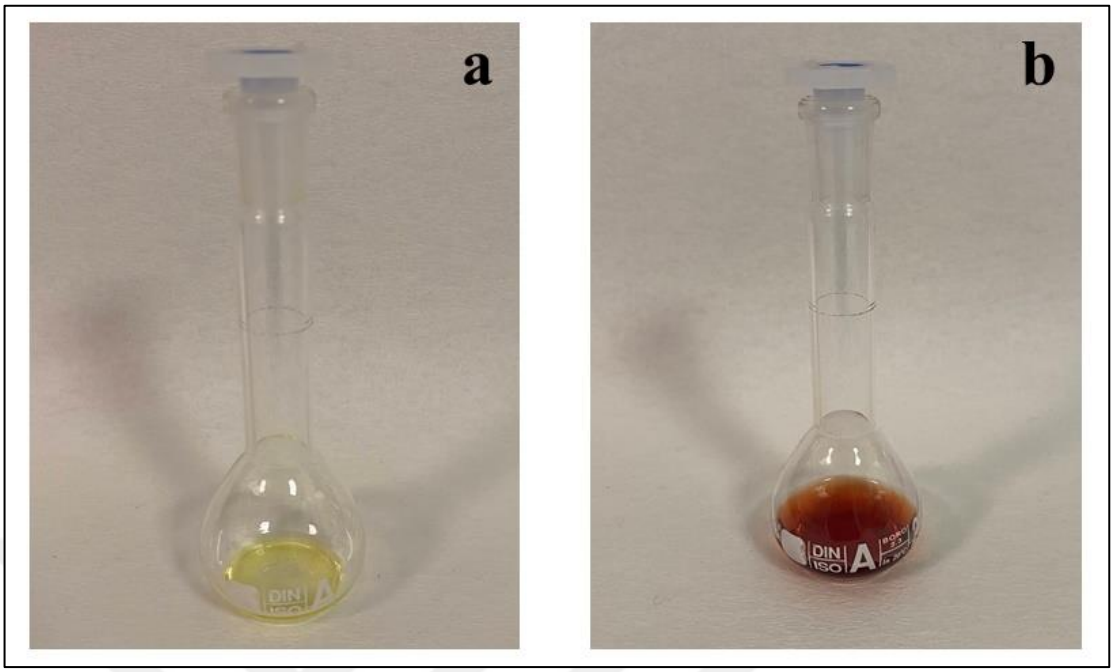

Figure 4.3. Color change during the concentration determination via Tiron test

4.3. MAGNETHERM

The essential objective of this study is to investigate the heating efficiency of magnetite nanoparticles prepared by different synthesis methods and thus having different average size and magnetic properties, after being modified with various and comparable surfactants, depending on the concentration, frequency and intensity of the externally applied alternating magnetic field, by considering SAR values. In order to evaluate the initial maximum slope of the heating curve (temperature vs time) required for the determination of SAR for a specific magnetic nanofluid, the variation of temperature as a function of time in the presence of an externally applied alternating magnetic field was acquired via the NanoTherics MagneTherm system which is composed of a coil assembly, function generator, DC power supply, and oscilloscope as shown in Figure 4.4.

Figure 4.4. NanoTherics- MagneTherm Instrument (a), Control units that adjust the magnetic field amplitudes and frequencies (function generator, DC Power supply and oscilloscope)(b)

The coil assembly of the system is capable of being fitted with two different coils bearing 9 and 17 turns, which allow measurements to be made using various frequencies ranging from 100 to 950 kHz and magnetic field amplitudes from 12 to 25 mT as illustrated in Table 4.1

Table 4.1. Magnetic field amplitude and frequency ranges for 17-turn coil

Coil turns	Capacitor type	Nominal frequency (kHz)	DC Power Supply Voltage	DC Power Supply Current	Maximum Current (mT)
17	200 nF	106.7	30	19.2	25
17	88 nF	160.2	25.8	13.5	17
17	26 nF	268.3	33.7	13.75	17
17	15 nF	378.8	37.3	12.8	16
17	6.2 nF	612.0	39.8	11.1	12

In order to regulate the current flowing through the coils to create a magnetic field within the MagneTherm system, the voltage input is provided by a DC power supply. In addition,

different capacitors are used to obtain the desired frequency while a function generator is used to generate the necessary waveform. Finally, temperature variation within the samples under the influence of an alternating magnetic field was measured by using a fiber optic temperature sensor and the data was digitized using the device-specific Osensa software. (Figure 4.5).

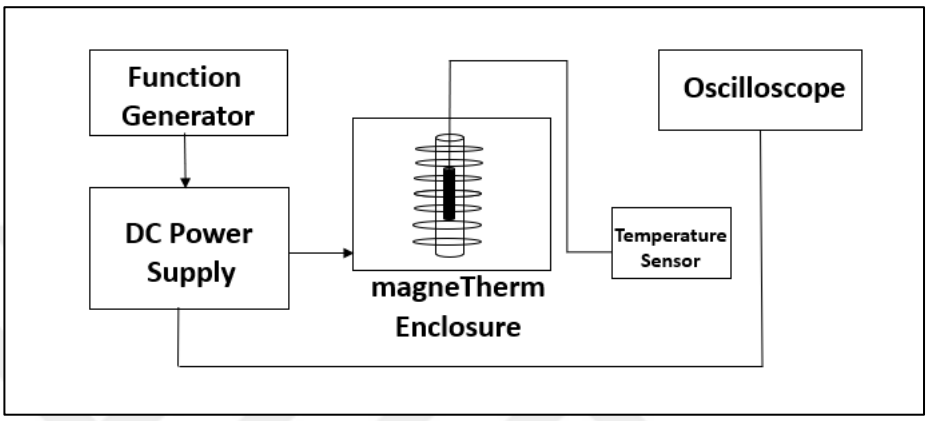

Figure 4.5. Representative diagram of the MagneTherm system

In order to obtain the heating curves of nanofluids containing MNP under the effect of an externally applied AMF briefly, 2 ml of suspensions with different concentrations were placed in a cryotube. The samples were then placed in styrofoam specially designed for the sample holder to minimize heat transfer to the surroundings. Subsequently, a fiber optic temperature sensor was placed at the center of the suspension to digitally monitor the temperature elevation occurring within the nanofluid at 1 second intervals, and finally, the sample holder was positioned at the center of the 17-turn coil which produces the AMF by the current provided via power supply (Figure 4.6). Tap water was used as a coolant to prevent the internal temperature rise in the system due to the magnetic field generated by the coils with the current flowing. Therefore, sufficient time was allowed for the temperature of the nanofluid to reach steady state before each measurement ensuring that the temperature variation was at most 0.1 ^{o}C. After reaching steady state, an alternating magnetic field was generated by applying voltage to the system and the temperature change in the medium was measured for at least 25 minutes. Since the system is not fully adiabatic, the measurements were also repeated for distilled water free of nanoparticles for each frequency and/or magnetic field strength utilized. All measurements were replicated at least a minimum of 3 times for both the nanofluid and control samples.

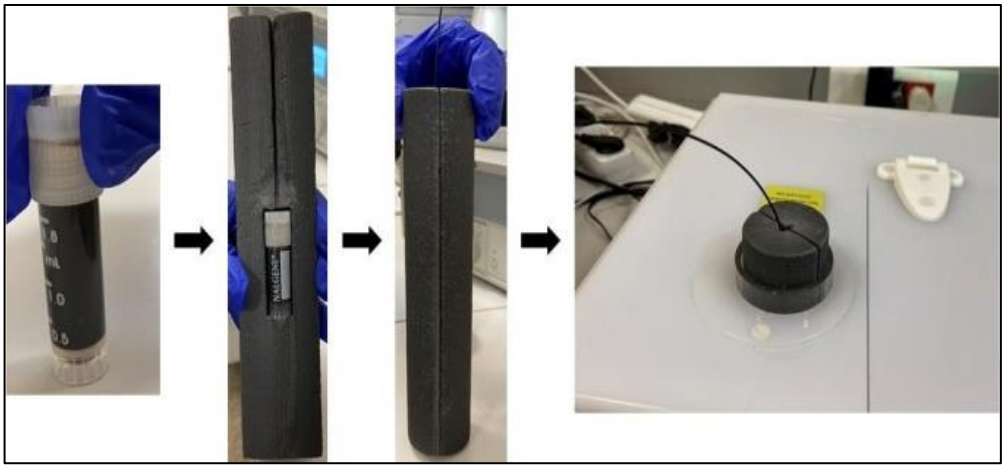

Figure 4.6. Sample preparation for heating curve measurements

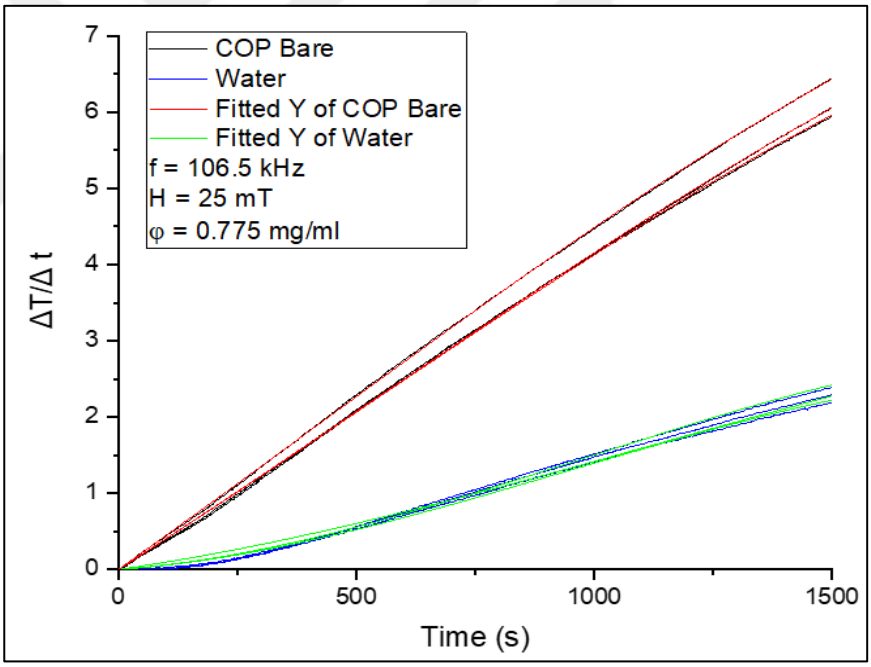

Figure 4.7. A representative heating curve for a magnetic nanofluid along with control measurement and their corresponding 3rd order polynomial fit

The temperature data of the nanofluid taken at 1 second intervals for each sample for a total of 25 minutes was then visualized using OriginLab. In order to determine the initial maximum slope required for the calculation of the SAR of the samples, the time-dependent temperature curves needed to be smoothed by eliminating noise. Therefore, a 3rd order polynomial regression was applied to the obtained curves and the calculations were carried

out through these curves (Figure 4.7). Although there is an insulating material surrounding the samples in the system, even for distilled water free of nanoparticles, a temperature rise occurs due to the heat generated by the alternating magnetic field applied. Consequently, this temperature variation obtained as a base was subtracted from the temperature differences observed in the samples after polynomial regression to obtain the resultant enhancement curves. These curves were then automatically divided into 50 second intervals and the maximum slope values in these segments were calculated with Slope Analyzer which is an add-on package for OriginLab (Figure 4.8). Finally, as multiple measurements were performed for each sample, SAR values were calculated using Equation 2.2 and presented with their standard deviations.

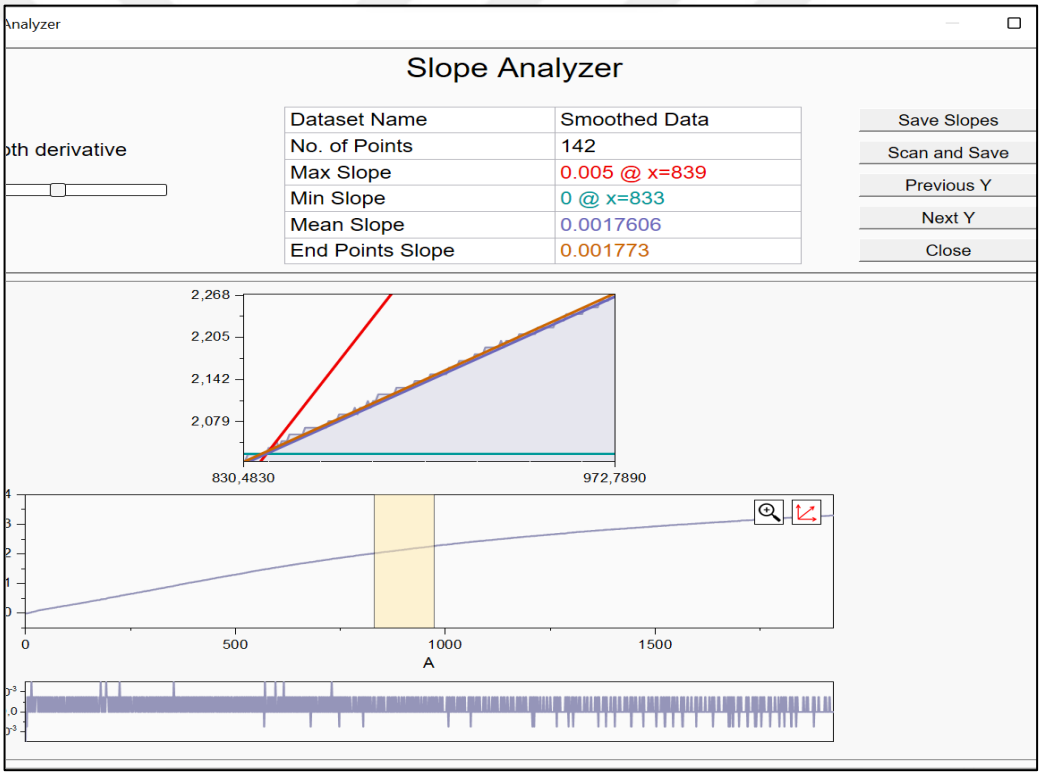

Figure 4.8. Maximum slope determination via Slope Analyzer add-on for OriginLab

4.4. CHARACTERIZATION OF MAGNETIC NANOPARTICLES

4.4.1. Transmission Electron Microscope (TEM)

The average size, size distribution, and morphology of bare nanoparticles were evaluated using JEOL JEM 2100 PLUS (200kV LaB6) transmission electron microscope (TEM) at Yeditepe University for nanoparticles synthesized via co-precipitation method. Additionally, the same properties of nanoparticles synthesized using the partial oxidation method were analyzed via 200keV JEOL JEM-ARM200F microscope at Sabancı University. For the measurements, sonicated suspensions were dropped onto 200 mesh Cu TEM grids and allowed to dry overnight. Representative average size of 100 individual nanoparticles were determined by measuring both the long and the short axes lengths using ImageJ. The corresponding size distribution for different samples were then plotted as histograms and related standard deviations were also calculated. In addition, high-resolution images of the samples were taken (HRTEM) in order to analyze the lattices which, exhibit the crystalline nature of the product.

4.4.2. X-Ray Diffraction (XRD)

X-ray diffraction (XRD) analysis for the phase identification of nanoparticles were carried out by Rigaku D-Max 2200 PCI diffractometer with Cu Kα radiation at Gebze Technical University and Bruker D8 Advance at Kastamonu University respectively. Diffraction patterns for dried powder form samples were acquired in between 20-70 2Θ values at room temperature. The intensities and positions of obtained diffraction peaks along with the ratios of the peak intensities were compared with JCPDS card for magnetite phase presented in the literature.

4.4.3. Vibrating Sample Magnetometer (VSM)

The magnetic properties of magnetite nanoparticles synthesized via both chemical co-precipitation method and partial oxidation method were examined by Lake Shore 7404 (Kastamonu University) and Quantum Design PMS9T (Gebze Technical University)

vibrating sample magnetometers (VSM). The hysteresis loops of powder form nanoparticles were acquired at room temperature and in a range of positive and negative externally applied magnetic field strengths. Subsequently, the corresponding saturation magnetization along with the coercivity and remanence of samples were calculated in order to reveal whether the particles exhibit superparamagnetic properties.

4.4.4. Fourier Transform Infrared Spectroscopy (FTIR)

Infrared spectra of bare and functionalized magnetite nanoparticles were obtained via Nicolet iS50 Fourier transform infrared spectroscope (FTIR) at Yeditepe University. For the measurements, spectrum of solid powder-form particles was acquired in the wavenumber range of 400 – 4000 cm^{-1} at room temperature and obtained bands and peaks were compared with the literature data to confirm the presence of surface modifying agents on the surface of magnetite nanoparticles synthesized via co-precipitation and partial oxidation methods.

5. RESULTS AND DISCUSSION

5.1. SYNTHESIS OF MAGNETITE NANOPARTICLES

In this study, the co-precipitation method, which is often preferred in the literature, and the water-based partial oxidation method, which is less commonly employed, were adopted for the synthesis of MNPs. The purpose of this approach is to measure the SAR values of bare and modified nanoparticles, which differ in both size and magnetic properties according to the applied synthesis method and to analyze the effect of different variables on this parameter. Nanoparticle synthesis was carried out primarily by co-precipitation method and during the course of the reaction, a sudden transformation from orange to black color was observed as described in the literature (Figure 5.1) [46]. It was expected that the orange color obtained by the dissolution of iron (II) and iron (III) salts in the medium would turn black as a result of magnetite nanoparticles precipitated by suddenly increasing the pH value of the medium with sodium hydroxide solution. This sudden color shift also indicated that the reaction rate and kinetics should also be taken into account during the analysis of the average size and morphology of the particles.

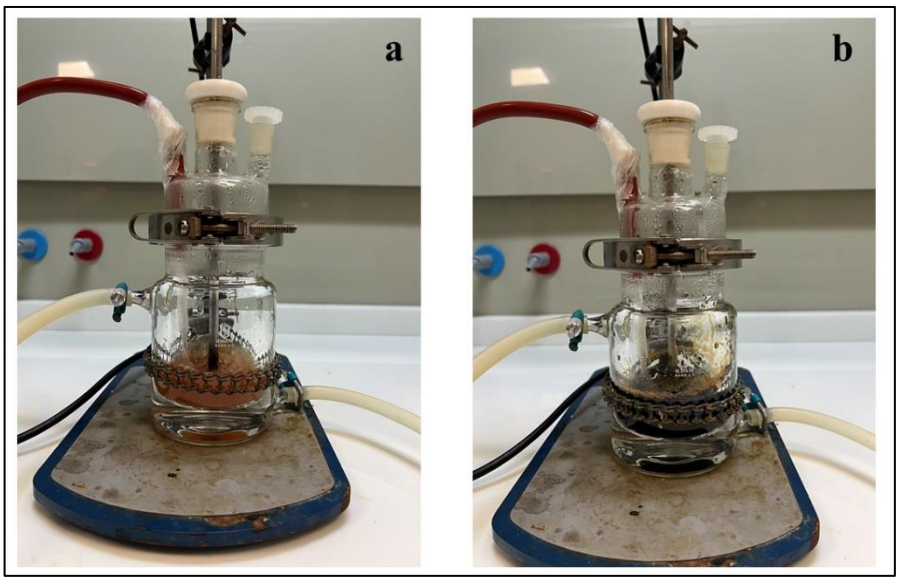

Figure 5.1. Color change during the formation of MNPs prepared by COP method

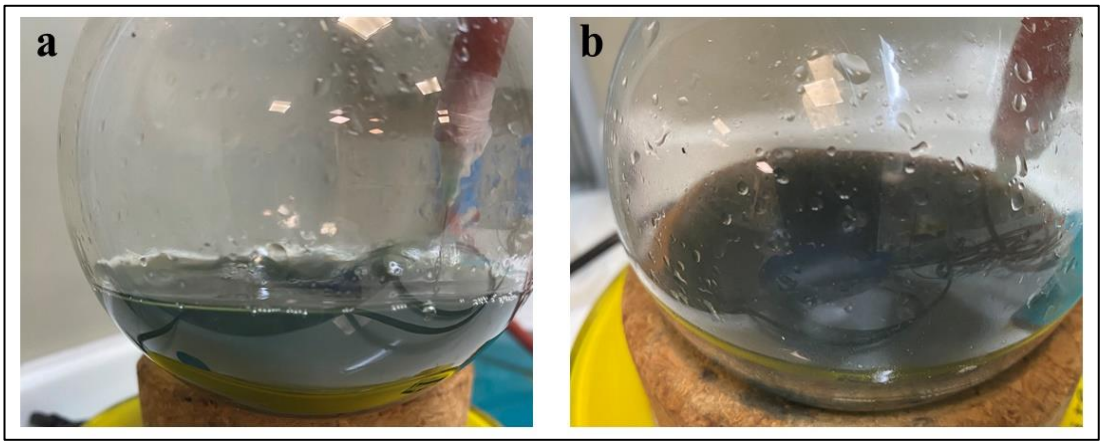

Figure 5.2. Color change during the formation of MNPs prepared by POX method

The other method employed in this study for the synthesis of magnetite nanoparticles is the partial oxidation method. The most important distinction of this method as compared to the co-precipitation method is that it allows the synthesis of larger nanoparticles with different magnetic properties. During the synthesis by following the method detailed in 4.1.2, it was observed that the color of the reaction medium turned light green upon addition of iron (II) salt. This is attributed to the formation of iron (II) oxide, the intermediate phase as shown in the literature [73]. Subsequently, the reaction medium gradually turned dark green and finally black, indicating the formation of magnetite nanoparticles. The fact that the abrupt color change obtained when the co-precipitation method was carried out but not in this method is due to the fact that the kinetics of the reactions are completely different from each other, as mentioned earlier.

Table 5.1. The characteristic colors of the iron oxide phases [74]

Chemical name	Mineral name	Chemical formula	Color
Iron oxide	Magnetite	Fe_3O_4	Black
Iron oxyhydroxide	Goethite	α-FeOOH	Yellow-brown
Iron oxyhydroxide	Akageneite	β-FeOOH	Red-brown
Iron oxyhydroxide	Lepidocrocite	γ-FeOOH	Orange
Iron sulphate tetrahydrate	Rozenite	$FeSO_4.4H_2O$	Green
Iron sulphate pentahydrate	Siderotil	$FeSO_4.5H_2O$	White
Iron sulphate heptahydrate	Melanterite	$FeSO_4.7H_2O$	Blue-green
Iron hydroxide sulphate dihydrate	Butlerite	$Fe(OH)SO_4.2H_2O$	Orange
Iron potassium hydroxide sulphate	Jarosite	$Fe_3K(OH)_6(SO_4)_2$	Yellow-brown

The preliminary phase identification of numerous iron oxide species, which are found in nature and prepared synthetically, can be carried out on the basis of color before any characterization method. Since magnetite is the only phase with black color among all these different iron oxide species (Table 5.1), the black colors observed in the samples synthesized and dried by co-precipitation and partial oxidation methods provide preliminary evidence that the magnetite phase has been successfully obtained as shown in Table 5.1 and Figure 5.3 [75].

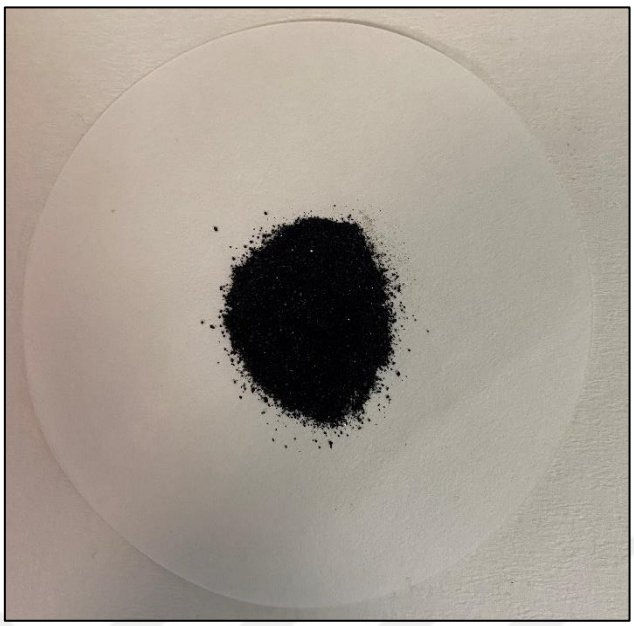

Figure 5.3. The color of the dried MNP synthesized by COP method

One of the most important distinctions that differentiate magnetite nanoparticles from other substances, although not from iron oxides, is that they possess magnetic properties. It can be seen from Figure 5.4 and Figure 5.5 that the particles synthesized by both co-precipitation and partial oxidation methods respond and migrate in the direction of the field under the influence of an externally applied magnetic force. In addition to this preliminary evaluation in terms of phase, a variation was also observed in the response of the particles synthesized by co-precipitation and partial oxidation to the externally applied magnetic field. It has been observed that the particles synthesized by COP method react to the magnetic field and drop to almost zero magnetization with the removal of the field, whereas for the particles synthesized by POX method, the magnetization persists after the removal of the field effect due to the ongoing interaction between the particles. This provides evidence that particles synthesized by different synthesis methods possess different magnetic properties as shown in the literature [73].

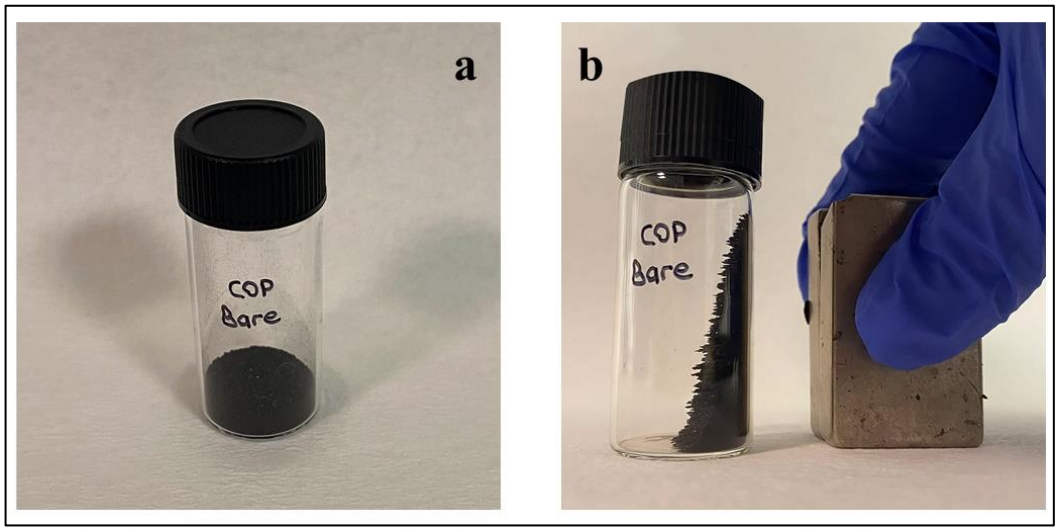

Figure 5.4. a) Powder-form MNPs synthesized via COP method b) The response of magnetite nanoparticles to an externally applied magnetic field

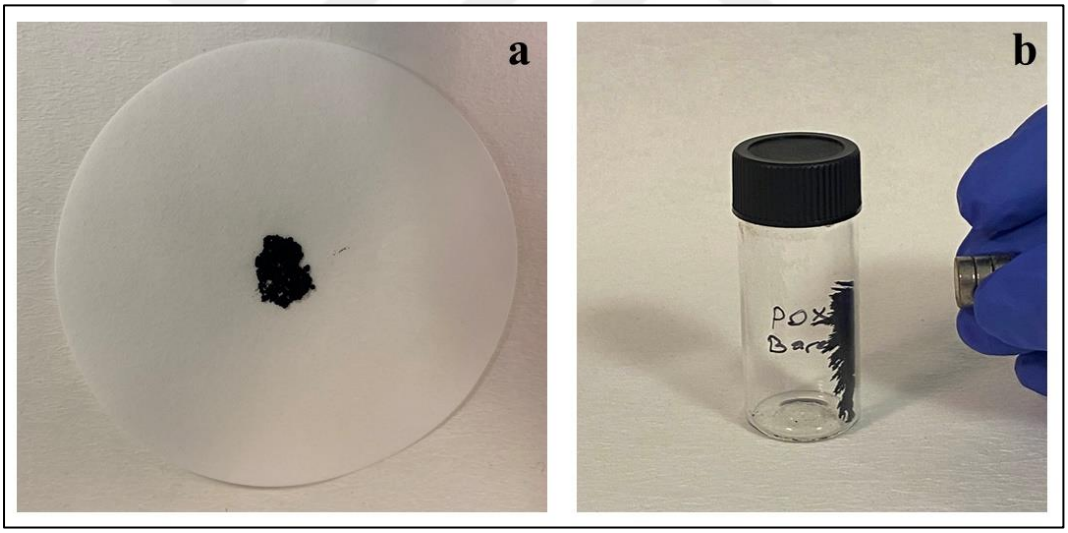

Figure 5.5. a) Powder-form MNPs synthesized via POX method b) The response of magnetite nanoparticles to an externally applied magnetic field

5.2. CHARACTERIZATION OF MAGNETITE NANOPARTICLES

The average size, size distribution and morphology of nanoparticles were analyzed via TEM. It has been clearly shown in the literature that particles synthesized via conventional chemical co-precipitation method yields comparably smaller nanoparticles (i.e., 6-20 nm) [46]. Whereas, partial oxidation method is capable of producing larger nanoparticles

depending on the reaction conditions [73]. The TEM images given in Figure 5.6a and Figure 5.6b clearly demonstrate that the particles synthesized by chemical precipitation method indeed yield considerably smaller nanoparticles as compared to counterparts synthesized by partial oxidation method as illustrated in Figure 5.7a and Figure 5.7b. The TEM analysis additionally indicated the formation of irregular morphologies (mostly spherical) for co-precipitation-based nanoparticles whereas the particles produced via partial oxidation method mostly exhibited well-defined octahedral and cubic nanoparticles as shown in the literature for the same type of nanoparticles [46] and [49].

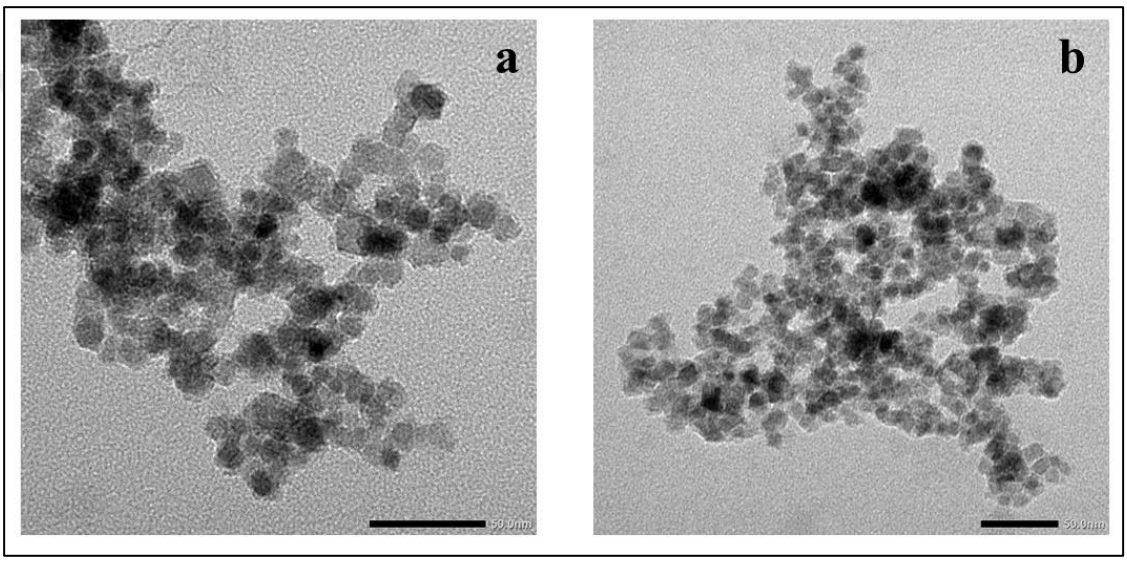

Figure 5.6. TEM images of bare magnetite nanoparticles synthesized via co-precipitation method at different magnifications a) Scale bar is 50 nm, b) Scale bar is 100 nm

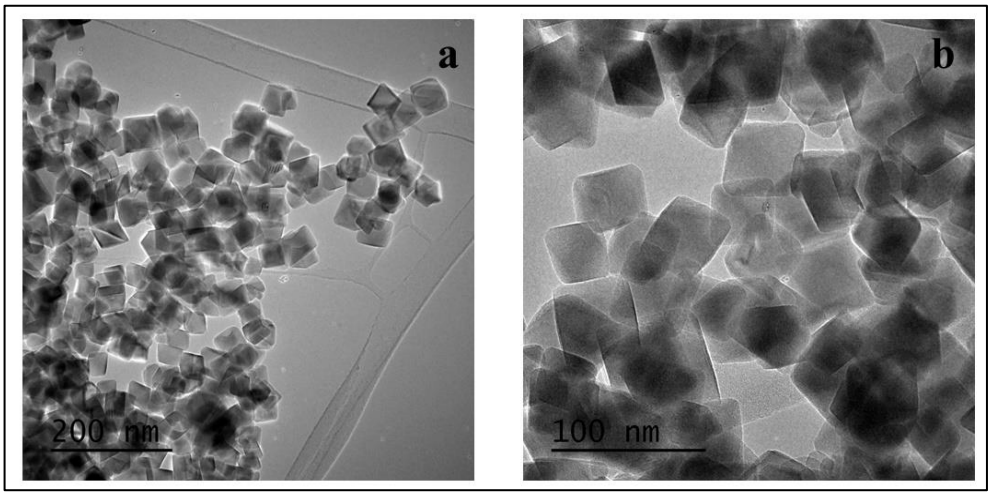

Figure 5.7. TEM images of bare magnetite nanoparticles synthesized via partial oxidation method at different magnifications a) Scale bar is 200 nm, b) Scale bar is 100 nm

The size analysis performed by measuring the short and long axis of at least 100 individual nanoparticles indicated that the superparamagnetic nanoparticles have an average size of 9.8 ± 2.5 nm while the nanoparticles synthesized via partial oxidation method possessed 41.6 ± 6.9 nm (Figure 5.8). The variation of average size in between different samples is solely due to the distinctive reaction kinetics of the corresponding synthesis method applied. It is well known that chemical COP method is performed at high supersaturation levels leading to rapid nucleation thus formation of smaller sized nanoparticles [47]. On the other hand, partial oxidation method possesses an extended growth phase as compared to nucleation stage yielding larger nanoparticles [46]. In addition to the imaging of the samples, the crystalline nature of nanoparticles was also analyzed via high resolution TEM imaging (HRTEM). The presence of lattices clearly demonstrates the crystalline nature rather than amorphous structures for magnetite nanoparticles regardless of the synthesis method employed as shown in Figure 5.9.

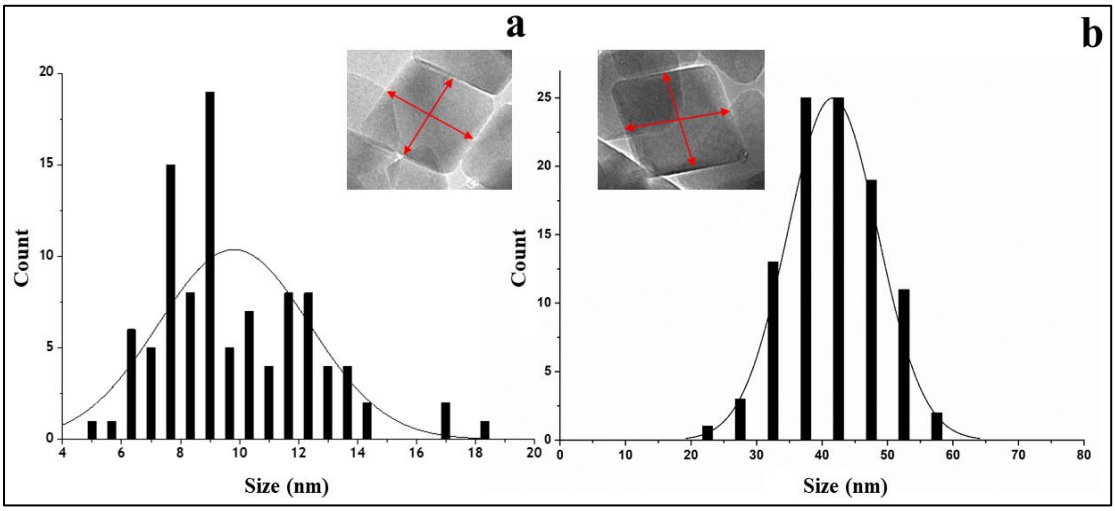

Figure 5.8. Size distributions obtained using TEM images of bare magnetite nanoparticles synthesized via a) co-precipitation method, b) partial oxidation method

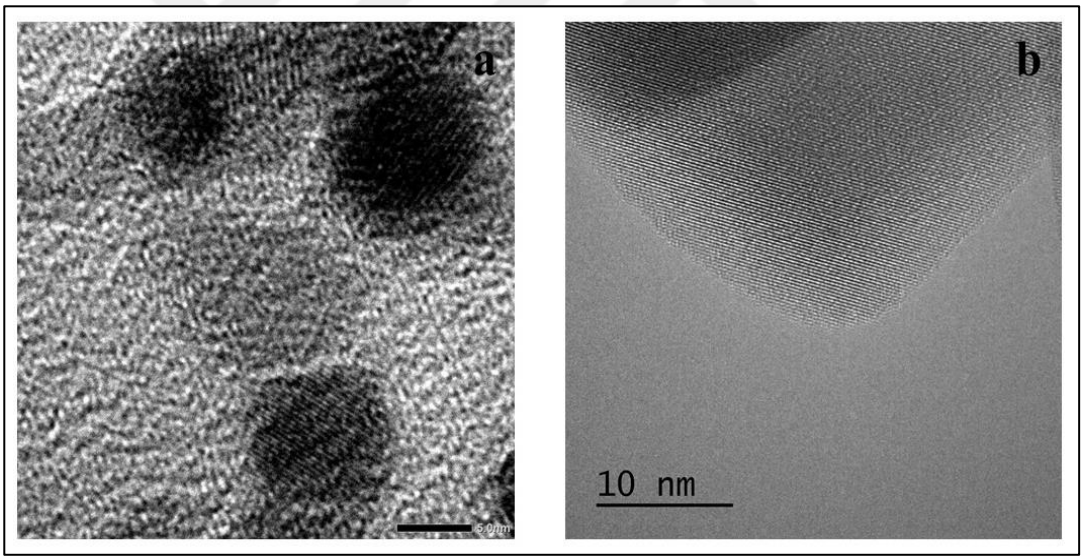

Figure 5.9. HRTEM images of bare magnetite nanoparticles synthesized by a) co-precipitation method (Scale bar = 5nm), b) partial oxidation method (Scale bar = 10 nm)

Afterwards, the phase identification of nanoparticles synthesized by two different aqueous chemical pathways was performed by X-ray diffraction (XRD). The diffraction patterns for both co-precipitation and partial oxidation originated nanoparticles exhibited 2Θ values mapped to the peak's positions and relative peak intensities which can be exactly matched with magnetite phase illustrated in the literature (Figure 5.10) [76]. Although, no other iron

oxide species are expected as a product of co-precipitation method due the presence of stoichiometric quantities required for magnetite phase, it is known that oxidative aging of ferrous ions may yield several iron oxide types if the reaction conditions are not sufficiently controlled [77]. As the diffraction analysis confirms the formation of phase pure magnetite nanoparticles, it can be concluded that POX method was performed effectively along with chemical precipitation method for the synthesis of MNPs in a controlled manner.

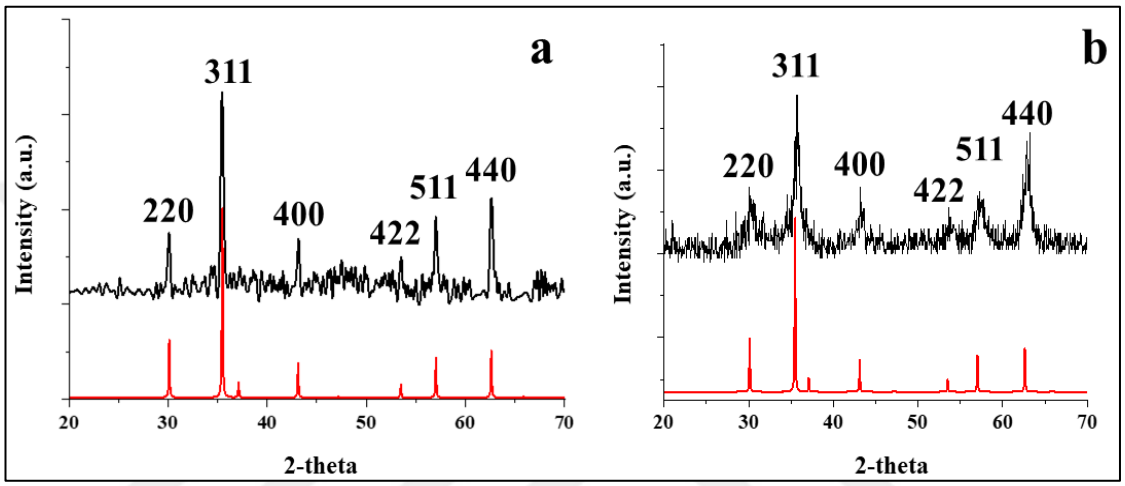

Figure 5.10. XRD patterns of bare magnetite nanoparticles synthesized via a) partial oxidation b) co-precipitation

Vibrating sample magnetometer (VSM) analysis was employed to determine the magnetic properties of magnetite nanoparticles synthesized by partial oxidation and co-precipitation methods. This analysis method can be used to determine the saturation magnetization at which the particles reach maximum magnetization. On the other hand, it is also possible to determine properties directly related to the magnetic behavior, such as coercivity and remanence. Basically, the magnetization of particles increases with increasing the intensity of the magnetic field strength in opposite directions. In addition, it is expected that the removal of the externally AMF will result in zero or negligible magnetization in superparamagnetic nanoparticles which is identified by the hysteresis curve to pass through origin but will conversely produce permanent magnetization in ferrimagnetic nanoparticles. The saturation magnetization of bare magnetite nanoparticles synthesized by the co-precipitation method and by the partial oxidation method were determined as 55.1 and 69.2 emu/g as illustrated in corresponding hysteresis curves shown in Figure 5.11. These relatively higher saturation magnetization values observed in nanoparticles synthesized by

partial oxidation method are also encountered in the literature which can be attributed to the larger average size of the corresponding particles as compared to superparamagnetic counterparts. In addition, nanoparticles obtained by the partial oxidation method exhibited significant coercivity and remanence as illustrated for the particles synthesized with the same procedure and regarded as ferrimagnetic in the literature (Figure 5.11) [48].

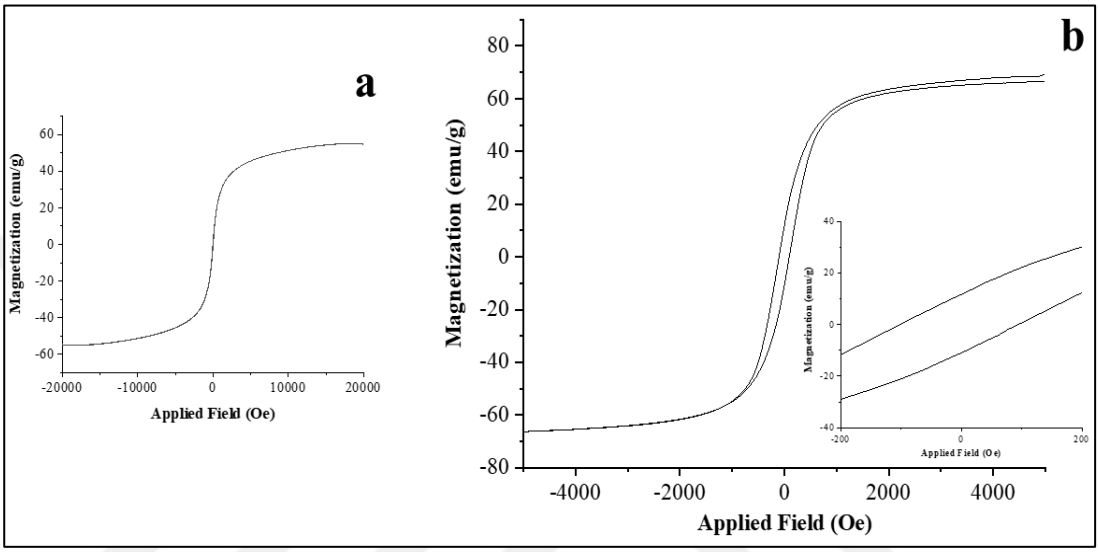

Figure 5.11. Hysteresis curve of bare magnetite nanoparticles synthesized by under varying magnetic field intensity a) partial oxidation method b) co-precipitation method

5.3. SURFACE MODIFICATION OF MAGNETITE NANOPARTICLES

In order to provide effective use of magnetite nanoparticles in any application, it is essential to ensure the colloidal stability of the particles. Regardless of the preferred method, surfactants or polymers should be used for surface functionalization, since the synthesized bare nanoparticles cannot remain suspended in suspension for a long time. In this study, magnetite nanoparticles synthesized by partial oxidation and co-precipitation methods were modified with PAA and for comparison superparamagnetic particles were modified with PEG and PEI in two layers to ensure colloidal stability and to examine the effect of surface functionalization on SAR. Since these polymers do not show toxic activity at sufficient concentrations and have a hydrophilic structure, they have been used together with magnetite nanoparticles in numerous studies in the literature for biomedical applications [49,78]. During the synthesis of magnetite nanoparticles, the entire synthesis was carried out in the

presence of polymers in order to ensure that surfactants were present at all stages of particle formation. In order to demonstrate that the surface modification of the nanoparticles was achieved, time-dependent stability analysis was initially performed. Considering the suspension pictures presented in Figure 5.12, it is evident that the bare nanoparticles prepared by partial oxidation method undergo complete precipitation within 1 hour. Since there is no stabilizing agent on the surface of these particles, such a rapid sedimentation is a highly expected result. In addition, only a partial phase separation appeared after 24 hours in the bare nanoparticles synthesized by co-precipitation. This contradictory situation in both bare particle systems was attributed to the different sizes of the nanoparticles. The much smaller size of the bare superparamagnetic nanoparticles synthesized by co-precipitation and their lack of permanent magnetization allowed them to remain suspended in suspension for a longer time. However, although a temporary colloidal stability can be achieved, time-dependent precipitation also occurs in these superparamagnetic nanoparticles.

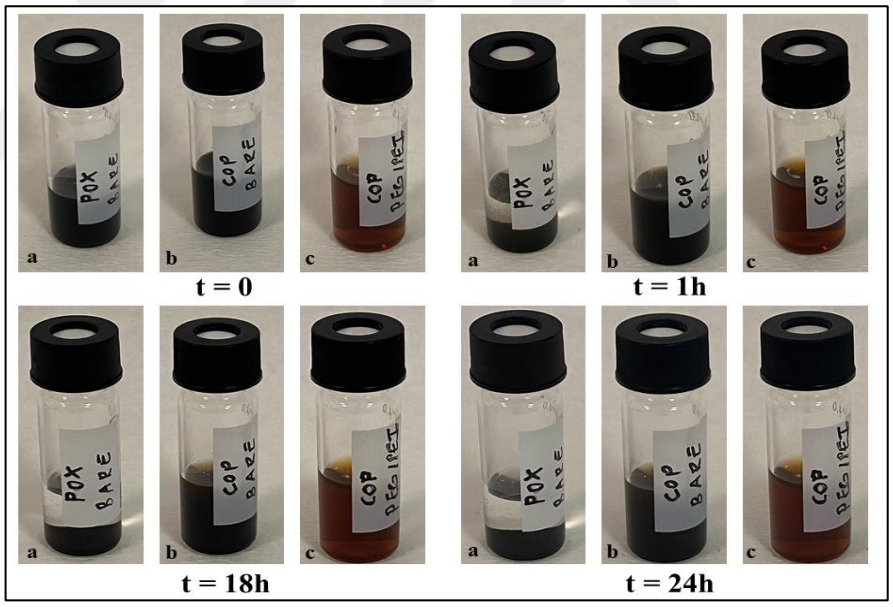

Figure 5.12. The colloidal stability of suspensions containing magnetite nanoparticles a) bare particles synthesized via partial oxidation b) bare particles synthesized via co-precipitation c) PEG-PEI modified particles synthesized via co-precipitation

Whereas, it was clearly seen that the polymers added to the medium during the synthesis increased the colloidal stability of the particles in water and no precipitation was observed after more than 24 hours. This indicates that the particles were successfully functionalized considering the relatively low time-dependent stability of the bare nanoparticles.

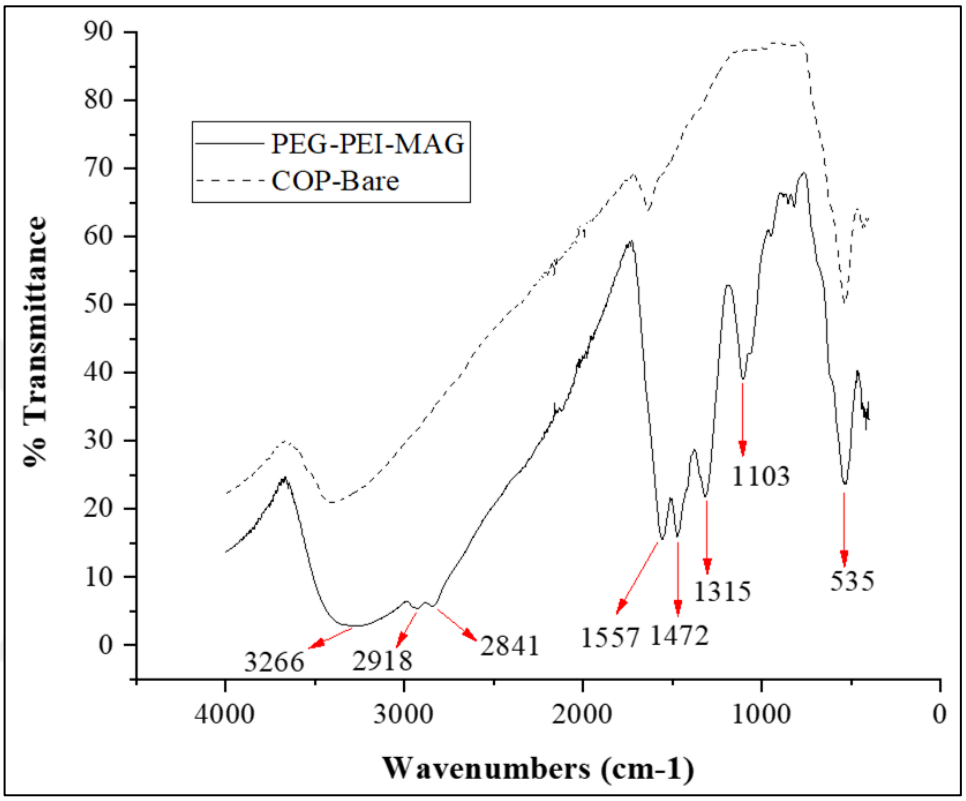

Figure 5.13. FTIR Spectra of bare and PEG-PEI modified magnetite nanoparticles synthesized via co-precipitation method [78]

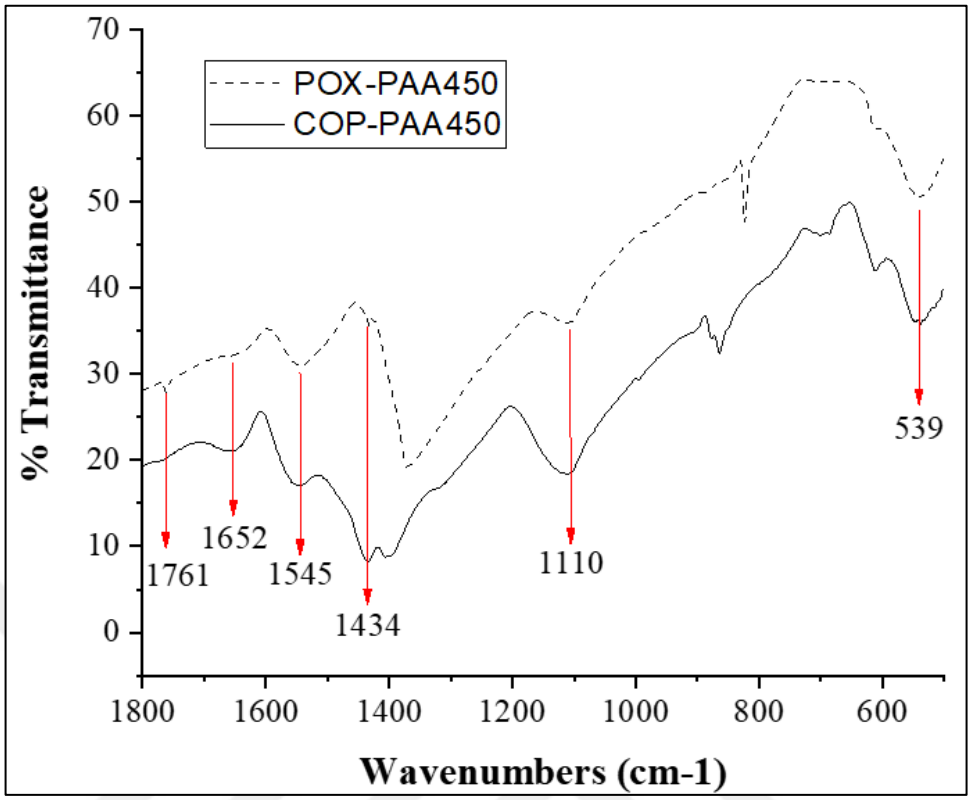

Figure 5.14. FTIR Spectra of bare and PAA modified magnetite nanoparticles synthesized via co-precipitation and partial oxidation methods

In addition to time-dependent colloidal stability tests, FTIR analysis was also performed to further demonstrate that magnetite nanoparticles synthesized by co-precipitation and partial oxidation methods were modified with PEG-PEI and PAA. This analysis was carried out with the Thermo Scientific Nicolet iS50 FT-IR device at Yeditepe University, in the wavelength range of 400-4000 cm^{-1}, and on powdered particles obtained at a pressure of 20 mBar and 60 ^{o}C using a vacuum oven. When the FTIR spectrum of the bare nanoparticles was examined, the characteristic absorption bands of the magnetite phase were observed at approximately 536 cm^{-1} and 1635 cm^{-1} and these bands can be attributed to Fe-O bond vibration and absorbed water molecules, respectively [79,80]. The presence of the same Fe-O mode (535 cm^{-1} and 539 cm^{-1}) in the modified nanoparticles suggests that the magnetite phase was successfully acquired for both samples and that the polymers introduced into the medium did not have a negative effect on the formation of the magnetite phase. The PEG-PEI functionalized particles additionally show absorption peaks at 1103 cm^{-1}, 1315 cm^{-1}, 1472 cm^{-1}, 1557 cm^{-1}, 2841 cm^{-1}, 2918 cm^{-1} and 3266 cm^{-1}, which can be indexed to C-O symmetrical stretching, C-N stretching, N-H stretching or C-H bending vibration, N-H

bending vibration, C-H stretching vibrations (for 2841 cm^{-1} and 2918 cm^{-1}) and N-H stretching modes respectively [78]. On the other hand, the PAA modified nanoparticles show absorption peaks at 1434 cm^{-1}, 1545 cm^{-1}, 1652 cm^{-1} and 1761 cm^{-1}, which may be assigned to CH_2 stretching, asymmetrical -COO stretching and -C=O stretching modes respectively. The bands near 1370 cm^{-1} and 1401 cm^{-1} may also be indexed to symmetrical -COO stretching modes [81–85]. These additional peaks obtained in the modified nanoparticles as compared to the bare nanoparticles further confirmed that the nanoparticles synthesized by both methods were successfully modified with surface active agents (Figure 5.13 and Figure 5.14).

5.4. SPECIFIC ABSORPTION RATE OF MAGNETITE NANOPARTICLES

SAR measurements are frequently performed in the literature to determine the efficiency of magnetite nanoparticles in magnetic hyperthermia applications [6]. Although there are numerous studies in this context, variations in nanoparticle preparation and the way SAR measurements are performed in each study can lead to quite different values. Whereas the SAR values of bare magnetite nanoparticles are generally not taken into account due to their inadequate application capabilities as a consequence of instability. While a high level of colloidal stabilization of magnetite nanoparticles is a requirement in applications such as hyperthermia, the temperature changes and subsequent SAR values of the bare nanoparticles under the influence of an externally applied magnetic field may also be examined in order to determine the limit and evaluate the efficiency. Since the partial oxidation method is rarely used in the literature, the aim of this study is to determine the heating efficiencies of both bare and modified magnetite nanoparticles synthesized by co-precipitation and partial oxidation methods concurrently. For this purpose, magnetite nanoparticles were prepared by two different methods and the heating efficiencies of the obtained nanoparticle systems were analyzed depending on the intensity and frequency of the externally applied magnetic field and as a function of nanoparticle concentration. In addition, the effect of polymers added to the nanoparticle surface to ensure colloidal stabilization was also investigated. Since the co-precipitation and partial oxidation methods used throughout the study produce magnetite nanoparticles that are completely different from each other in terms of size and magnetic properties, the effect of these variables on heating efficiencies was also investigated.

Initially, the heating efficiencies of bare magnetite nanoparticles synthesized by co-precipitation method were analyzed depending on the nanoparticle concentration, the intensity and frequency of the externally applied magnetic field. Essentially, the frequency and magnetic field pairs given in Table 5.2 were adopted for all samples, so that the effects of both frequency at comparable field strengths and magnetic field strength at fixed frequency could be examined.

Table 5.2. The frequency and the intensity pairs selected for the externally applied magnetic field

Coil turns	Capacitor type	Nominal frequency (kHz)	Field Strength (mT)
17	200 nF	106.5	24.0
17	200 nF	106.5	16.1
17	15 nF	378.2	15.4
17	6.2 nF	610.9	11.7

At the beginning of the analyses, control measurements were carried out at conditions specified in Table 1 with distilled water free from nanoparticles in order to prevent the temperature increase caused by the current supplied to the system to produce the magnetic field from affecting the further analysis and calculations. For distilled water free from nanoparticles, temperature measurements were taken with at least 3 repetitions, the temperature-time curve was regressed with a 3rd order polynomial as suggested in the literature (86) and finally the base was determined by averaging all measurements. Afterwards, the temperature-time curve of the nanofluids at that frequency and magnetic field strength was polynomially regressed with 3rd order (Figure 5.15a) and the base temperature increment was deduced from the data of each sample to determine the resulting temperature change (Figure 5.15b).

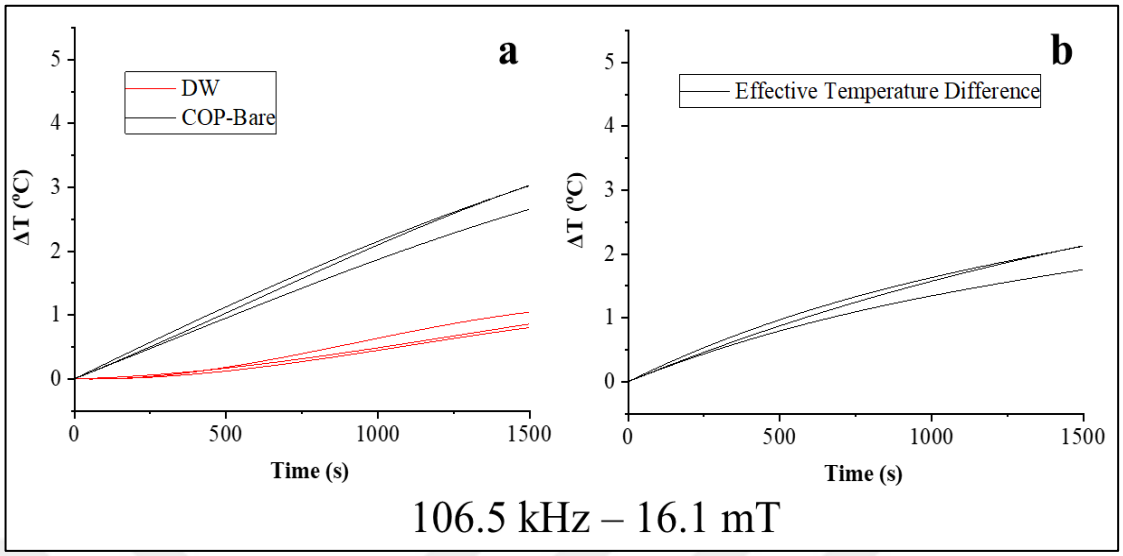

Figure 5.15. Regressed temperature vs. time data for distilled water and COP-Bare (a), Resultant heating curve for the sample (b)

Figure 5.15a shows that the heating curve of the suspension containing nanoparticles exhibits a temperature increase after a period of 1500 seconds. On the other hand, distilled water free of nanoparticles also heats up as a result of the electrical current and eventually presents minor a temperature variation in the range of 0-500 seconds. In the majority of the studies in the literature, this fact is either not taken into account when presenting the heating curves of magnetic nanofluids or, if a background subtraction is performed, it is not mentioned. This analysis reveals that since the calculation of SAR values of magnetic nanofluids uses the maximum slope due to the temperature change that occurs initially, a control measurement must be performed and extracted from the temperature change data of the sample as clearly stated in few studies [87].

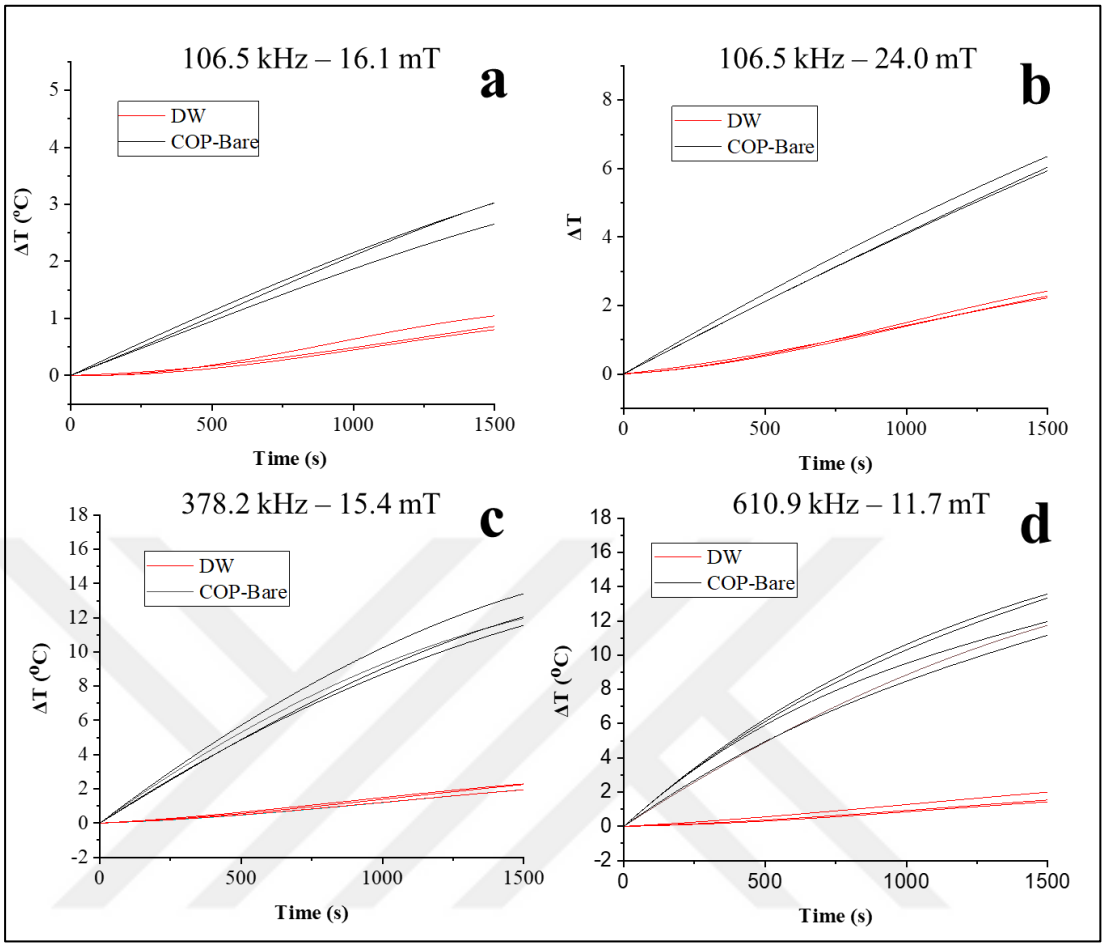

Figure 5.16. Temperature-time data for bare magnetite nanoparticles (0.775 mg/ml) a) 106.5 kHz – 16.1 mT, b) 106.5 kHz – 24.0 mT, c) 378.2 kHz – 15.4 mT, d) 610.9 kHz – 11.7 mT

The time-dependent temperature changes of bare magnetite nanoparticles synthesized by co-precipitation method under the effect of externally applied alternating magnetic field are given in Figure 5.16 together with the control group of distilled water and the resultant temperature changes are given in Figure 5.17 and Figure 5.18 for different concentrations. When the results are evaluated, it is seen that even at low concentrations, bare magnetite nanoparticles exhibit an extra temperature elevation as compared to distilled water at each magnetic field strength and frequency pairs applied (Figure 5.16). It is also observed that the resulting temperature differences increase with increasing the magnetic field strength from 16.1 mT to 24.0 mT at a fixed frequency value of 106.5 kHz. In addition, under approximately comparable magnetic field strengths (15.4 mT vs. 16.1 mT), it is observed that the temperature changes increase radically with increasing the frequency by more than

a factor of 3 (from 106.5 kHz to 378.2 kHz). Similar results for magnetic nanofluids have also been presented in the literature, showing a similar trend with the increase in magnetic field strength and frequency possibly due to Brownian and Néel relaxation losses as the relatively smaller average size of the nanoparticles are considered [88–92].

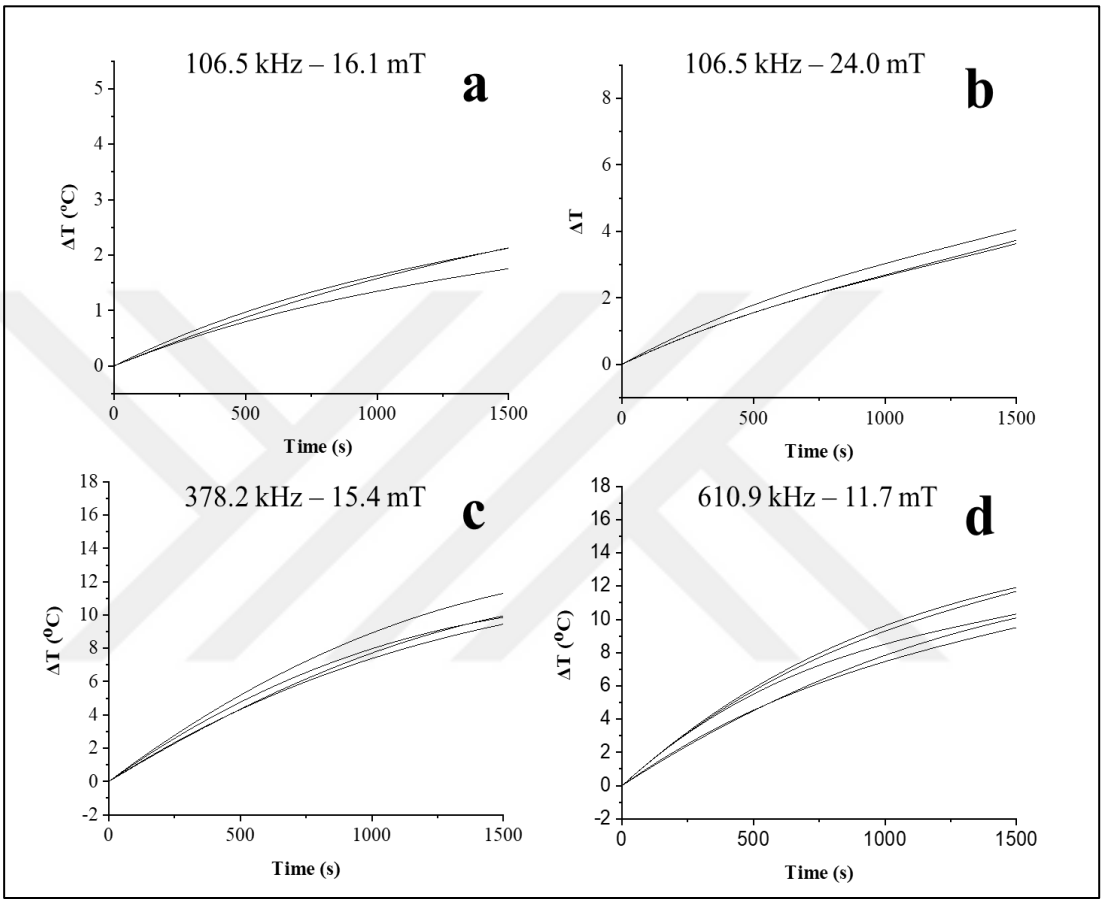

Figure 5.17. Resulting temperature-time data for bare (COP) magnetite nanoparticles (0.775 mg/ml) a) 106.5 kHz – 16.1 mT, b) 106.5 kHz – 24.0 mT, c) 378.2 kHz – 15.4 mT, d) 610.9 kHz – 11.7 mT

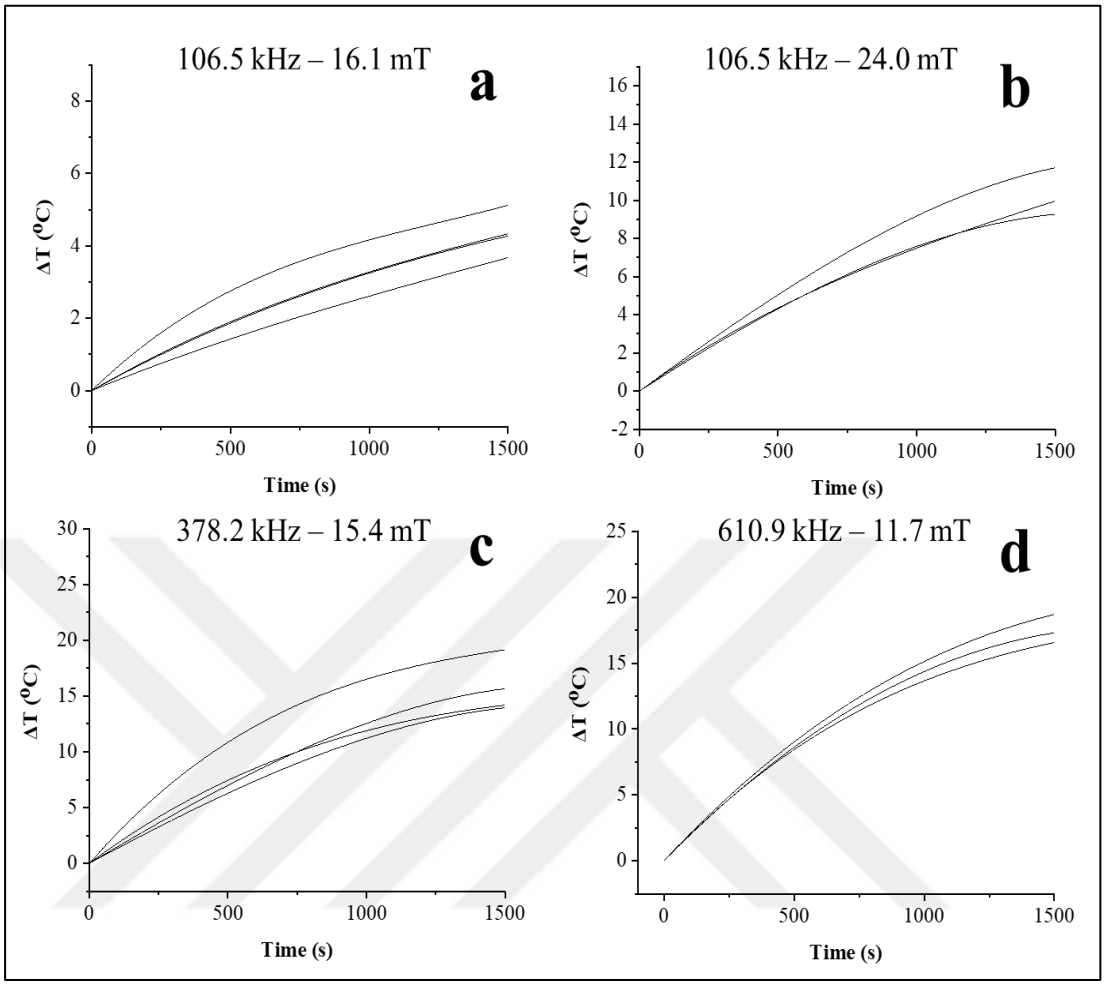

Figure 5.18. Resulting temperature-time data for bare (COP) magnetite nanoparticles (1.550 mg/ml) a) 106.5 kHz – 16.1 mT, b) 106.5 kHz – 24.0 mT, c) 378.2 kHz – 15.4 mT, d) 610.9 kHz – 11.7 mT

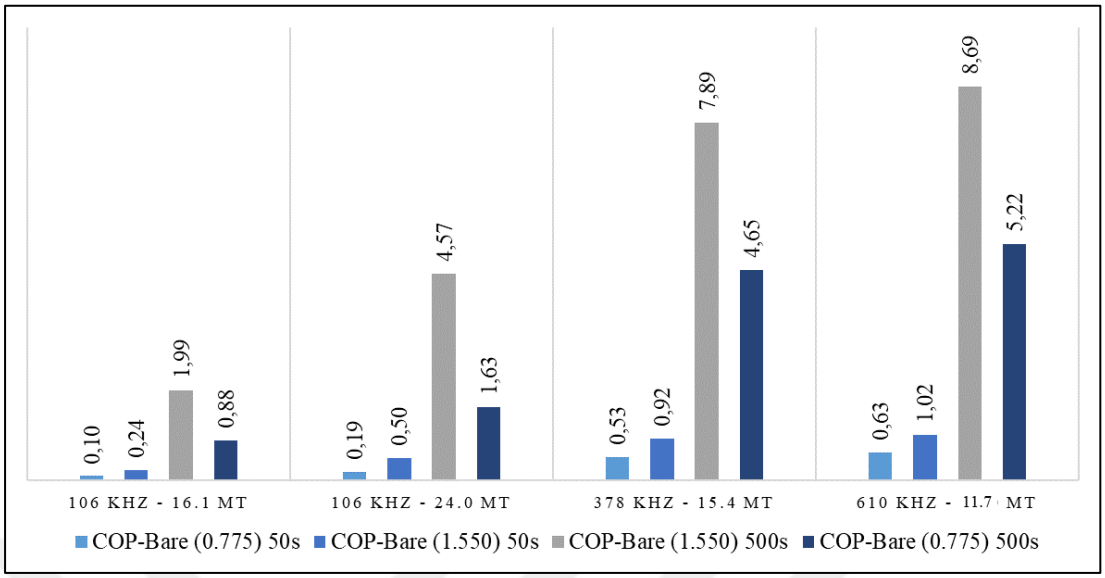

Figure 5.19. The variation of resultant temperature difference for bare magnetite nanoparticles synthesized via co-precipitation with respect to concentration

In order to demonstrate the effect of concentration on the heating curves regardless of the effect of colloidal stability, the analyses were also performed at higher concentrations, and it was observed that the temperature differences increased with increasing the magnetic field strength and frequency, in agreement with the results obtained at low concentrations (Figure 5.18). For example, at 106.5 kHz and 16.1 mT, an elevation of 1.99 ^{o}C was found at the end of 500 seconds, while an increase of 4.57 ^{o}C was achieved at the same frequency as the magnetic field strength was raised to 24.0 mT. When the frequency was increased to 378.2 kHz, this temperature increase was even higher and measured as 7.89 ^{o}C. The highest temperature elevation of 8.69 ^{o}C was obtained at a frequency of 610.9 kHz and a magnetic field strength of 12 mT. When the temperature increases obtained at the end of 500 seconds at both concentration values are compared, an 85% enhancement is observed by increasing the magnetic field strength from 16.1 mT to 24.0 mT at a frequency of 106.5 kHz for the low concentration, while this increase is determined as 2.3 times for the higher concentration. Under different frequencies and comparable magnetic field strengths, an enhancement of approximately 4 to 5 fold is also observed, indicating that the increase in frequency is more effective in temperature changes than the relative increase in magnetic field strength.

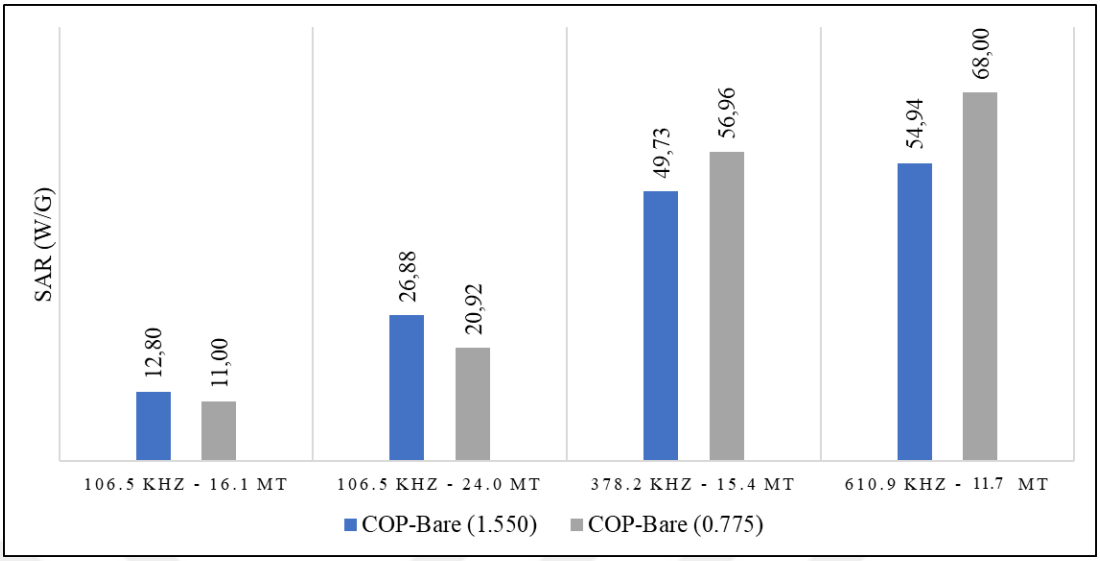

Figure 5.20. SAR of bare magnetite nanoparticles synthesized via co-precipitation at various magnetic field strengths and frequencies as a function of concentration

Finally, a comparison of the effect of concentration shows that the temperature changes clearly increase with increasing concentration, irrespective of the frequency and magnetic field strength. This is highly expected due to the higher number of magnetic nanoparticles per unit volume in the suspension, and similar results have been presented in the literature for modified nanoparticles [93].

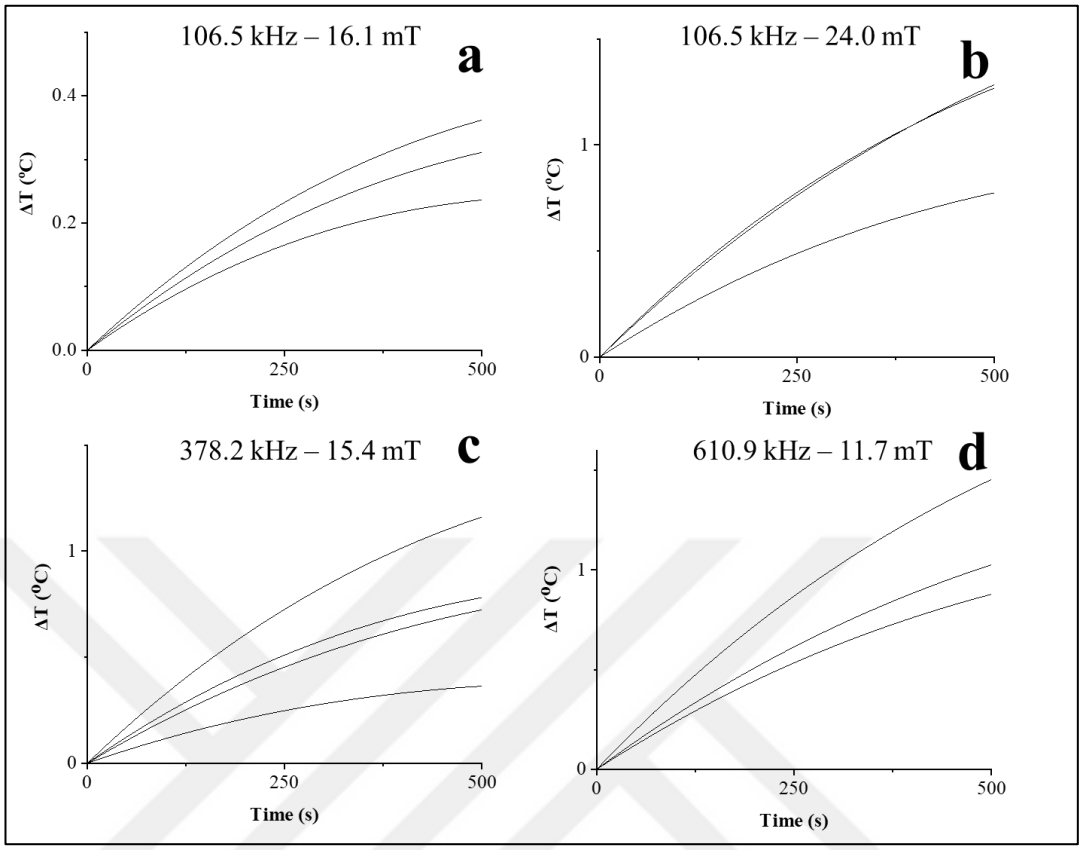

Figure 5.21. Resulting temperature-time data for bare (POX) magnetite nanoparticles (0.775 mg/ml) a) 106.5 kHz – 16.1 mT, b) 106.5 kHz – 24.0 mT, c) 378.2 kHz – 15.4 mT, d) 610.9 kHz – 11.7 mT

The SAR values calculated using the maximum slope values of the heating curves representing the time-dependent temperature changes of samples are also given in Figure 5.20. According to the results obtained, it was observed that when the magnetic field strength was increased from 16.1 mT to 24.0 mT at constant frequency (106.5 kHz), the SAR values increased from 11.00 W/g to 20.92 W/g for higher concentration and from 12.80 W/g to 26.88 W/g for lower concentration, respectively. Similar enhancements were also obtained by increasing the frequency from 106.5 kHz to 378.2 kHz (from 11.00 W/g to 56.96 W/g at high concentration) in combination with a comparable magnetic field strength. The highest SAR values for both concentrations were 54.94 W/g and 68.00 W/g at 610.9 kHz, which is the highest frequency measured. The increase in SAR values with increasing frequency and magnetic field has been shown in the literature for different nanofluids due to enhanced magnetic field properties leading to larger temperature variations [56,91]. Another significant aspect is the decrease in SAR values with increasing concentration, especially at

high frequencies, which has also been demonstrated in the literature and may be attributed to the higher dipolar interactions at increasing particle concentration [58,94].

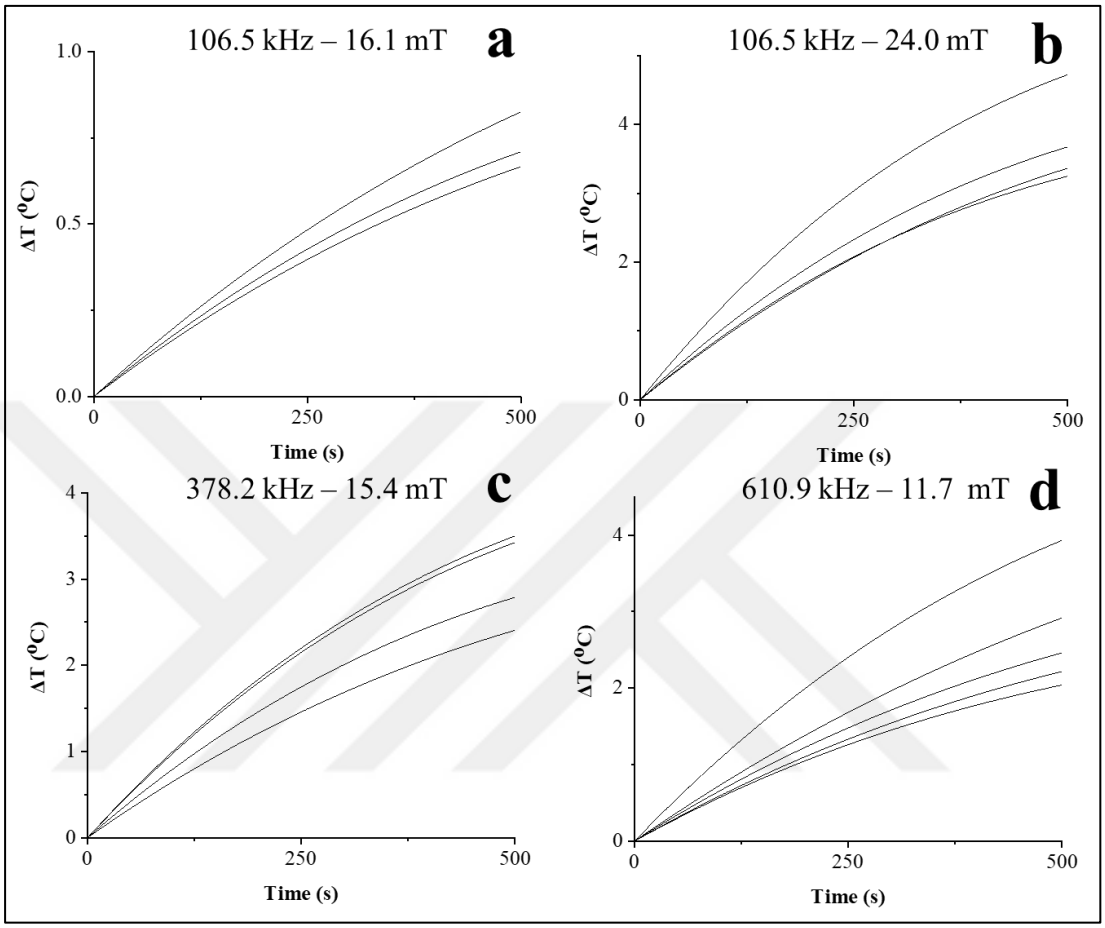

Figure 5.22. Resulting temperature-time data for bare (POX) magnetite nanoparticles (1.550 mg/ml) a) 106.5 kHz – 16.1 mT, b) 106.5 kHz – 24.0 mT, c) 378.2 kHz – 15.4 mT, d) 610.9 kHz – 11.7 mT

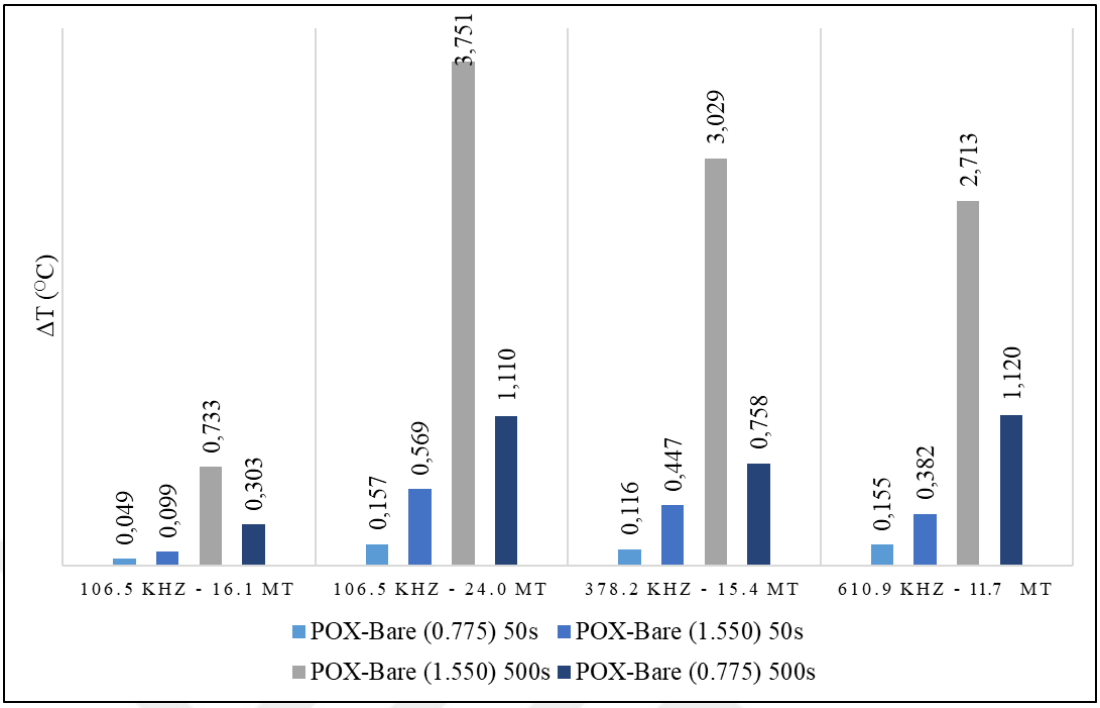

Figure 5.23. The variation of resultant temperature difference for bare (POX) MNPs synthesized via POX with respect to concentration

In order to make a direct comparison with the bare magnetite nanoparticles synthesized by co-precipitation (COP-Bare), bare magnetite nanoparticles were also synthesized by partial oxidation method (POX-Bare). As mentioned before, the nanoparticles prepared using this method are considered as a suitable candidate for comparison as they will exhibit different properties in terms of both size and magnetism. The heating curves of the suspensions prepared using POX-Bare nanoparticles at the same concentration values as COP-Bare nanoparticles under the same frequency and magnetic field strength are given in Figure 5.21 and Figure 5.22. Similar to the COP-Bare nanofluid, the temperature changes of the POX-Bare samples increased regardless of the concentration by increasing the frequency and magnetic field strength. For instance, Figure 5.23 shows that after 500 seconds, the temperature change increased from 0.73 ^{o}C to 3.75 ^{o}C by increasing the magnetic field strength from 16.1 mT to 24.0 mT at a frequency of 106.5 kHz for the higher concentration sample. Similarly, increasing the frequency from 106.5 kHz to 378.2 kHz at a comparable magnetic field strength increased the temperature change to 3.03 ^{o}C. In addition, increasing the concentration from 0.775 mg/ml to 1.550 mg/ml resulted in higher temperature differences at all frequency and magnetic field binaries. For example, at the end of 500

seconds, for 106.5 kHz and 24.0 mT, the temperature change for the higher concentration sample was 3.75 ºC, while for the lower concentration it was only 1.11 ºC. This variation can be attributed to the increase in the amount of magnetite nanoparticles in the suspension, which act as heating agents. Additionally, when Figure 5.23 is investigated, the increase in magnetic field strength is found to be more effective in temperature changes than the relative increase in frequency unlike superparamagnetic nanoparticles due to enhancement of hysteresis by the increase of applied magnetic field amplitude [95].

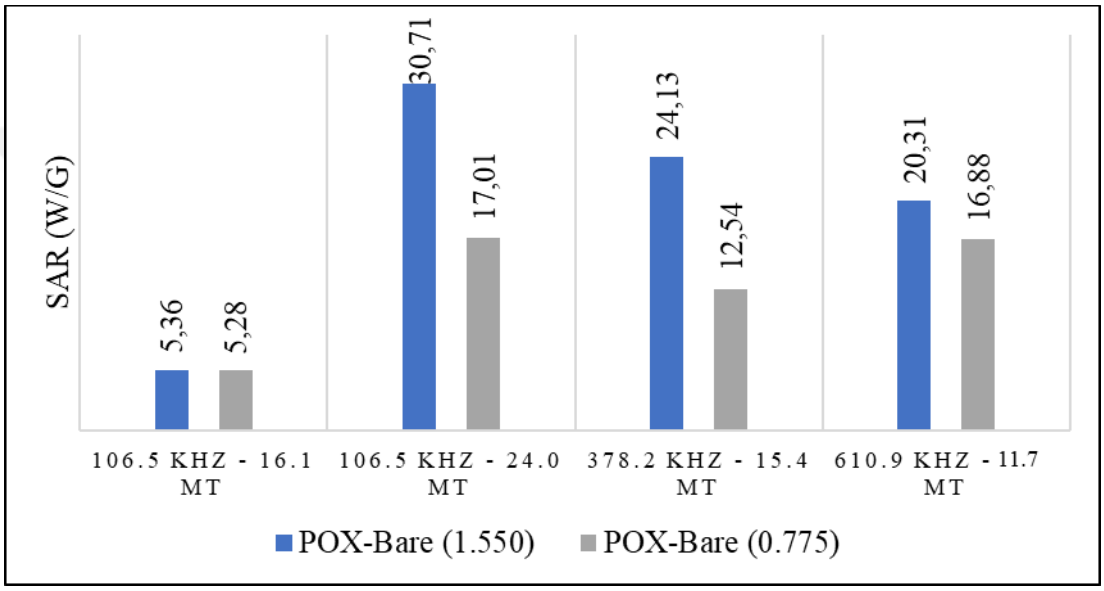

Figure 5.24. SAR of bare (POX) magnetite nanoparticles at various magnetic field strengths and frequencies as a function of concentration

SAR values calculated using the initial maximum slope of the heating curves obtained are also given in Figure 5.24. As in the case of superparamagnetic bare nanoparticles, it was observed that the SAR values increased with increasing magnetic field strength and frequency. For example, increasing the magnetic field strength from 16.1 mT to 24.0 mT at a fixed frequency of 106.5 kHz increased the SAR values from 5.28 W/g to 17.01 W/g at low concentration and from 5.36 W/g to 30.71 W/g at high concentration. When the variation of SAR values with concentration was analyzed, it was determined that SAR values of particles were generally higher at higher concentrations which has also been shown in the literature for nanoparticles with relatively larger sizes (~30 nm) where SAR increases up to a certain concentration and then decreases [96]. When the heating curves of POX-Bare nanoparticles are compared with COP-Bare nanoparticles, it is seen that COP-Bare

nanoparticles reach higher temperature changes in almost all frequency and magnetic field pairs (Figure 5.19 and Figure 5.23). For example, at the highest frequency of 610.9 kHz and 11.7 mT, COP-Bare and POX-Bare showed enhancements of 8.69 ^{o}C and 2.71 ^{o}C at the end of 500 seconds and at the highest concentration, respectively. This is considered as an anomaly, mainly due to the higher saturation magnetization of larger bare magnetite nanoparticles (POX-Bare) synthesized by partial oxidation compared to bare magnetite nanoparticles (COP-Bare) prepared by co-precipitation. However, the much higher colloidal stability achieved in suspensions containing COP-Bare nanoparticles due to their corresponding smaller size is worth noting. The time-dependent precipitation of POX-Bare nanoparticles, which occurs very rapidly, may become much more radical and rapid under the influence of an externally applied magnetic field. This indicates that a stable medium cannot be maintained within the suspension during the measurements. When both samples are evaluated, at the end of the analyzes performed to obtain the heating curves, no precipitation was observed in the COP-Bare samples despite the magnetic field interference, while a significant level of precipitation occurred in the POX-Bare samples. Thus, a homogeneous distribution could not be achieved within the suspension and the effective nanoparticle concentration was decreased. While the SAR values of POX-Bare nanoparticles were expected to be relatively higher as shown in the literature [96], the lower SAR values compared to COP-Bare nanoparticles, especially at high frequencies such as 378.2 kHz and 610.9 kHz, are attributed to this fact along with the relatively lower temperature enhancement. In the literature, there are various contradictory results in concentration-dependent studies examining the efficiency of magnetic nanoparticles in hyperthermia applications. While there are publications stating that the SAR value decreases with increasing concentration [94,97], there are also studies indicating that it remains constant [56,66] or increases up to a certain concentration and then decreases [96]. It is evident that an increase in concentration for different bare nanoparticles lead to opposite results as SAR increases for POX-Bare nanoparticles while decreases for COP-Bare nanoparticles with increasing concentration. This situation, especially when evaluated together with the results obtained for bare nanoparticles, reveals that the concentration effect should be examined in much more depth when determining the efficiency of any nanofluid in hyperthermia applications.

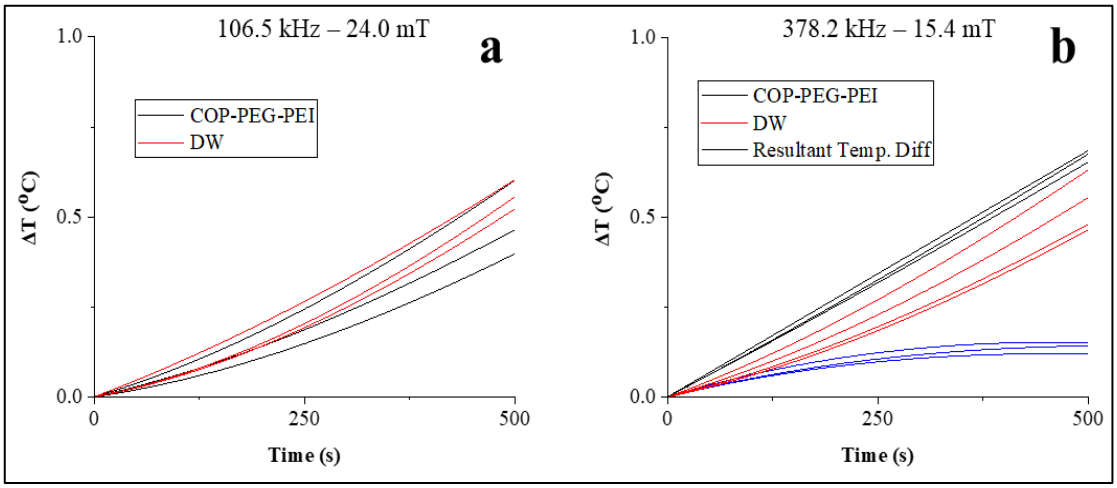

Figure 5.25. Temperature-time data for magnetite nanoparticles modified with PEG-PEI (0.775 mg/ml) a) 106.5 kHz – 24.0 mT, b) 378.2 kHz – 15.4 mT

Although the stability of bare nanoparticles may be relatively longer than each other, their efficiency in applications is very low due to their very limited colloidal stability. Therefore, surface modifications are required to increase the colloidal stability of nanoparticles. For this purpose, magnetite nanoparticles synthesized by co-precipitation method were modified with PEG-PEI (COP-PEG-PEI) and PAA (COP-PAA450(1:1)) in this study [78]. In this way, while their applicability was increased, their heating efficiency in comparison to bare nanoparticles could be examined. While the measurements were carried out exactly under the frequency and magnetic field strength applied to the bare nanoparticles, the concentration could only be attained at 0.775 mg/ml as higher concentrations could not be achieved due to insufficient stability. Measurements were initially performed under low frequency (106.5 kHz) and high magnetic field strength (24.0 mT).

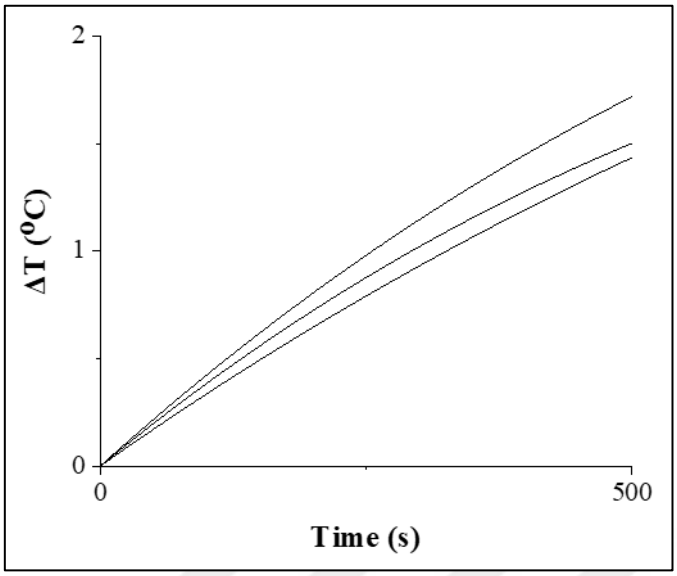

Figure 5.26. Resultant temperature-time data for magnetite nanoparticles modified with PEG-PEI (0.775 mg/ml) under the influence of an externally applied magnetic field of 610.9 kHz – 11.7 mT

According to the results presented in Figure 5.25a, it was realized that the nanofluids did not exhibit any enhancement as compared to distilled water under the influence of an externally applied alternating magnetic field. Measurements were then performed at 378 kHz and 15.4 mT by increasing the frequency, but no significant difference in resultant temperature difference was obtained (Figure 5.25b). Similar results were also obtained for COP-PAA nanofluids under the same conditions and at the same concentration (Figure 5.27a). Thus, the measurements were carried out at the highest frequency of 610.9 kHz and 11.7 mT and the temperature changes of the COP-PEG-PEI and COP-PAA450(1:1) nanofluids were calculated to be 1.55 ^{o}C and 0.50 ^{o}C on average after 500 seconds, respectively. The SAR values of the COP-PEG-PEI and COP-PAA450(1:1) nanofluids were also calculated as 21.08 W/g and 6.44 W/g based on the maximum slope obtained using the resultant heating curves given in Figure 5.26 and Figure 5.27b. When these obtained temperature increases and SAR values are compared with the bare nanoparticles (Figure 5.19 and Figure 5.20), it is evident that a decrease is present in both cases. This result is rational since surfactants or polymers applied to the surface of magnetic nanoparticles to increase their colloidal stability decrease the saturation magnetization [98].

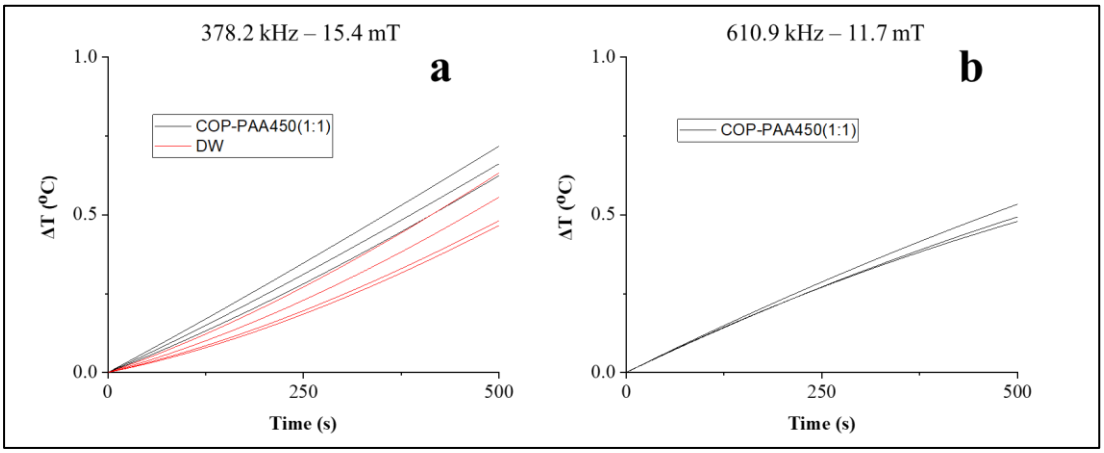

Figure 5.27. Temperature-time data for magnetite nanoparticles modified with PAA450(1:1) (0.775 mg/ml). a) 378.2 kHz – 15.4 mT, b) 610.9 kHz – 11.7 mT

On the other hand, when the effects of the polymers integrated on the surface of the nanoparticles prepared by co-precipitation method to increase their colloidal stability on temperature change and SAR were compared, it was determined that both temperature changes (1.55 ^{o}C vs. 0.50 ^{o}C) and SAR values (21.08 W/g vs. 6.44 W/g) were higher for COP-PEG-PEI at the same concentration value. This was attributed to the fact that the non-magnetic layer on the surface of COP-PEG-PEI (25 kDa) is estimated to be narrower than that of COP-PAA450(1:1) (450 kDa) considering its molecular weight and thus potentially being more magnetic.

For another comparison, the amount of polymer was doubled during the modification of magnetite nanoparticles synthesized by co-precipitation method with PAA (COP-PAA450(1:2)) and it was aimed to observe the effect of the polymer amount by this means. According to the results obtained, there was essentially no increase in temperature at 106.5 kHz – 16.1 mT, 106.5 kHz – 24.0 mT and 378.2 kHz – 15.4 mT magnetic field and frequency binaries, similar to other modified nanoparticles (Figure 5.28). However, at the lower concentration (0.775 mg/ml), an increase in medium temperature of approximately 0.73 ^{o}C was obtained at the end of 500 seconds by increasing the magnetic field to 610.9 kHz – 11.7 mT as shown in Figure 5.29.

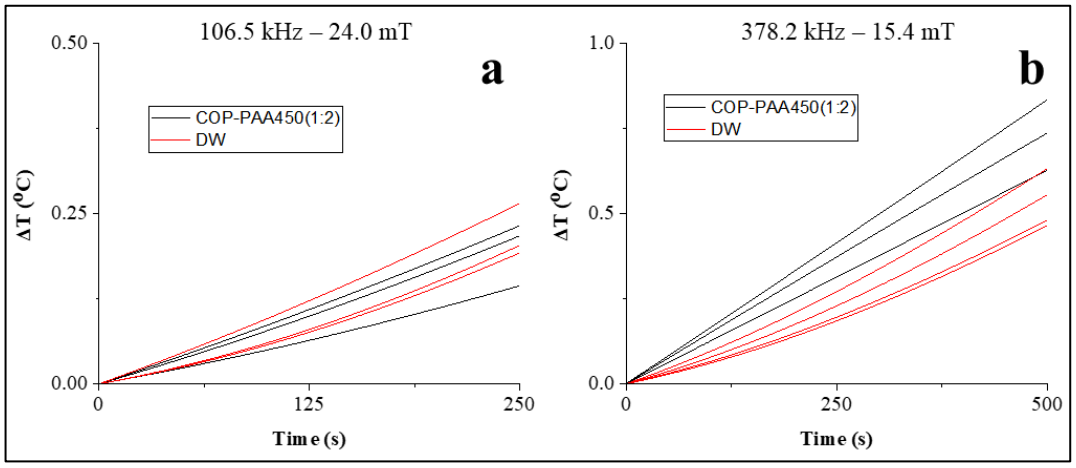

Figure 5.28. Temperature-time data for magnetite nanoparticles modified with PAA450(1:2) (0.775 mg/ml) a) 106.5 kHz – 24.0 mT, b) 378.2 kHz – 15.4 mT

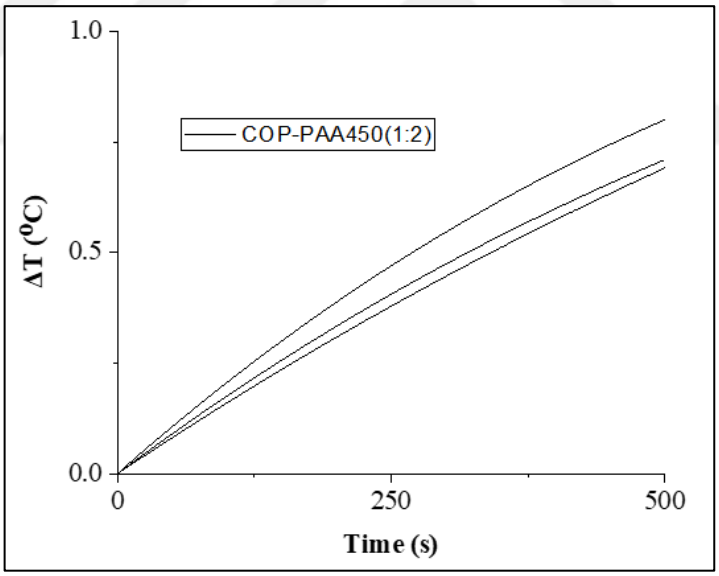

Figure 5.29. Resultant temperature-time data for magnetite nanoparticles modified with PAA450(1:2) (0.775 mg/ml) under the influence of an externally applied magnetic field of 610.9 kHz – 11.7 mT

In addition, by increasing the concentration (1.550 mg/ml), an enhancement of 0.60 ^{o}C was reached even at the lower frequency value (378.2 kHz – 15.4 mT) as shown in Figure 5.30, while 1.09 ^{o}C was attained at 610.9 kHz – 11.7 mT which once again illustrate that an increase in concentration also enhances the resulting temperature difference at comparable magnetic field properties. When these temperature changes and corresponding SAR values are evaluated together for all the particles prepared via co-precipitation method (Figure 5.31 and Figure 5.32), the lower recorded temperature changes, as well as SAR values, as compared to bare and COP-PEG-PEI nanoparticles are attributed to the relatively larger polymer layer on the surface, and the higher values as compared to COP-PAA450(1:1) is attributed to the potentially increased colloidal stabilization. It should be noted that when the amount of polymer was kept low, the nanofluid concentration could not be increased to 1.550 mg/ml, but with the doubling of the amount of polymer, the elevated concentration value could be reached. This led to a prejudgment that the COP-PAA450(1:2) nanofluid may be more colloidally stable which should be supported by zeta potential measurements in the subsequent future studies.

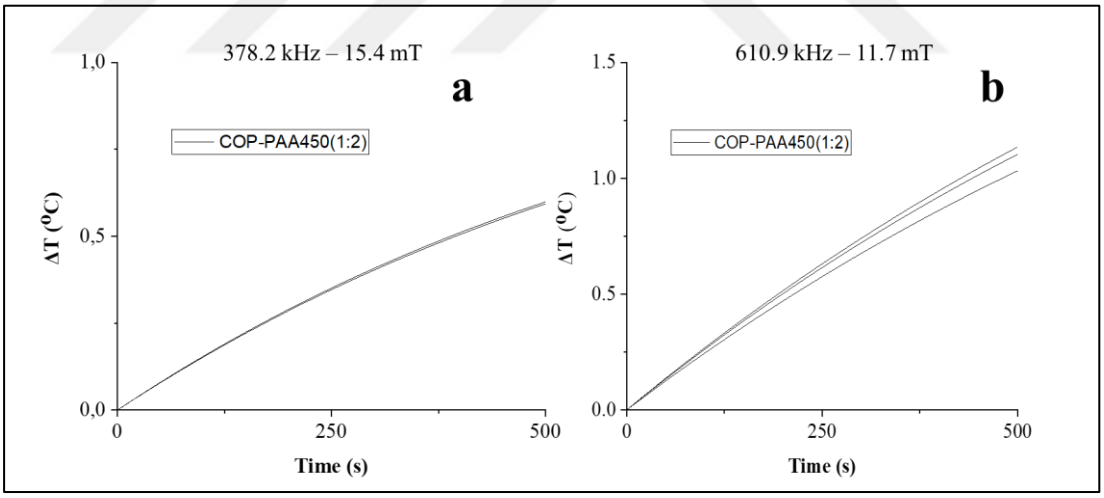

Figure 5.30. Resultant temperature-time data for magnetite nanoparticles modified with PAA450(1:2) (1.550 mg/ml) under the influence of an externally applied magnetic field of a) 378.2 kHz – 15.4 mT b) 610.9 kHz – 11.7 mT

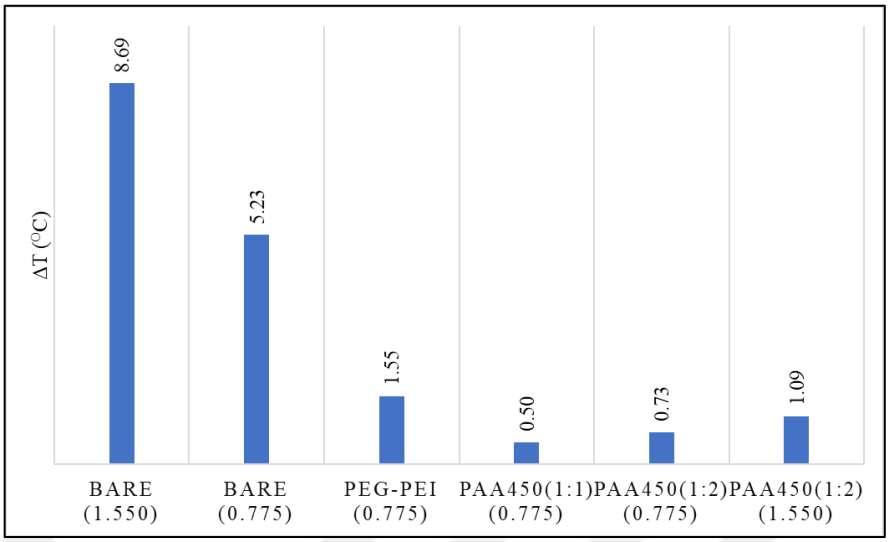

Figure 5.31. The variation of resultant temperature difference for modified magnetite nanoparticles synthesized via co-precipitation with respect to concentration under the influence of an externally AMF of 610.9 kHz – 11.7 mT

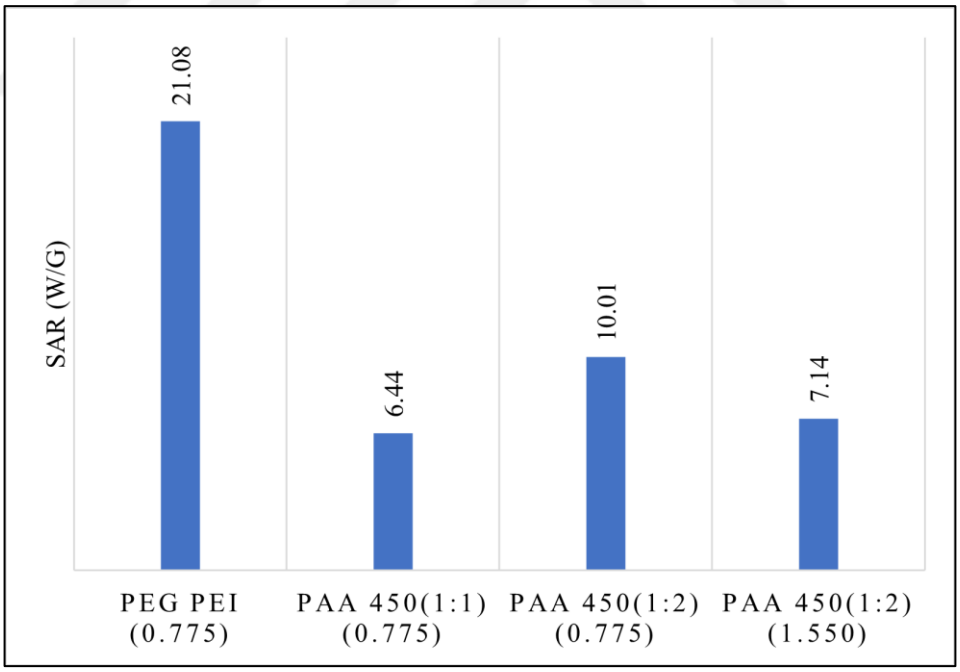

Figure 5.32. SAR of modified (COP) magnetite nanoparticles as a function of concentration under the influence of an externally AMF of 610.9 kHz – 11.7 mT

Finally, the surfaces of magnetite nanoparticles synthesized by partial oxidation method were modified with PAA (POX-PAA450(1:1)) in order to investigate the effects of surface

modification and nanoparticle concentration on temperature enhancement and SAR values for particles of relatively larger size. Since the nanoparticles synthesized by partial oxidation method are larger in size compared to the nanoparticles obtained by co-precipitation method, the effect of dimensional change could also be compared. According to the resultant heating curves presented in Figure 5.33, the time-dependent temperature enhancement could be obtained even for the lowest concentration (0.775 mg/ml) at the lowest possible frequency (106.5 kHz) for POX-PAA450(1:1) (Figure 5.33a and Figure 5.33b). The fact that no enhancement could be obtained in the nanoparticles prepared via co-precipitation method under the same conditions revealed that the magnetic field strength was much more effective in these modified particles, just as it was revealed in the comparison of bare nanoparticles. In addition, it was determined that the temperature enhancement increases by raising the magnetic field strength at the comparable frequency and by increasing the frequency at the comparable magnetic field strength, as expected and observed in bare nanoparticles. At a frequency of 106.5 kHz, the temperature changes at 500s with increasing the magnetic field strength from 16.1 mT to 24 mT were determined as 0.53 ^{o}C and 2.98 ^{o}C, respectively. Under comparable magnetic field strengths (16.1 mT vs. 15.4 mT), the temperature changes were measured as 0.53 ^{o}C and 0.79 ^{o}C, respectively, when the frequency was increased from 106.5 kHz to 378.2 kHz. Additionally, the temperature variation of 0.48 ^{o}C with increasing the frequency to 610.9 kHz, which is lower than that of obtained for 378.2 kHz - 15.4 mT, once again shows that magnetic field strength is more effective than frequency for larger-sized particles due to enhanced hysteresis loss (Figure 5.33d) [95].

In addition, increasing the concentration of magnetite nanoparticles synthesized by partial oxidation method to 1,550 mg/ml resulted in an increase in temperature enhancement at all frequency and magnetic field binaries as compared to the lower concentration (Figure 5.33 and Figure 5.34). As with all other nanofluids, the higher number of heating agents in the medium for systems possessing colloidal stability resulted in higher temperature changes as expected. Briefly, as the magnetic field strength was increased from 16.1 mT to 24.0 mT at a frequency of 106.5 kHz, the temperature changes were calculated as 0.80 ^{o}C and 6.02 ^{o}C, respectively (Figure 5.34a and Figure 5.34b). Whereas, under a magnetic field strength of 378.2 kHz - 15.4 mT, the temperature change was determined as 1.40 ^{o}C (Figure 5.34c). This confirms that the temperature variation is much more affected by increasing the magnetic field strength than by increasing the frequency, as in the case of low concentration.

When the nanoparticles with modified surfaces were compared with the bare nanoparticles, it was found that the modified nanoparticles showed higher temperature enhancement for low frequency and high magnetic field strength, which was attributed to the colloidal stability obtained in the modified nanoparticles, which was absent in the bare nanoparticles. In addition, contradictory results were observed at high frequency values and it was concluded that these two comparisons were not reliable, especially since the bare nanoparticles undergo rapid precipitation.

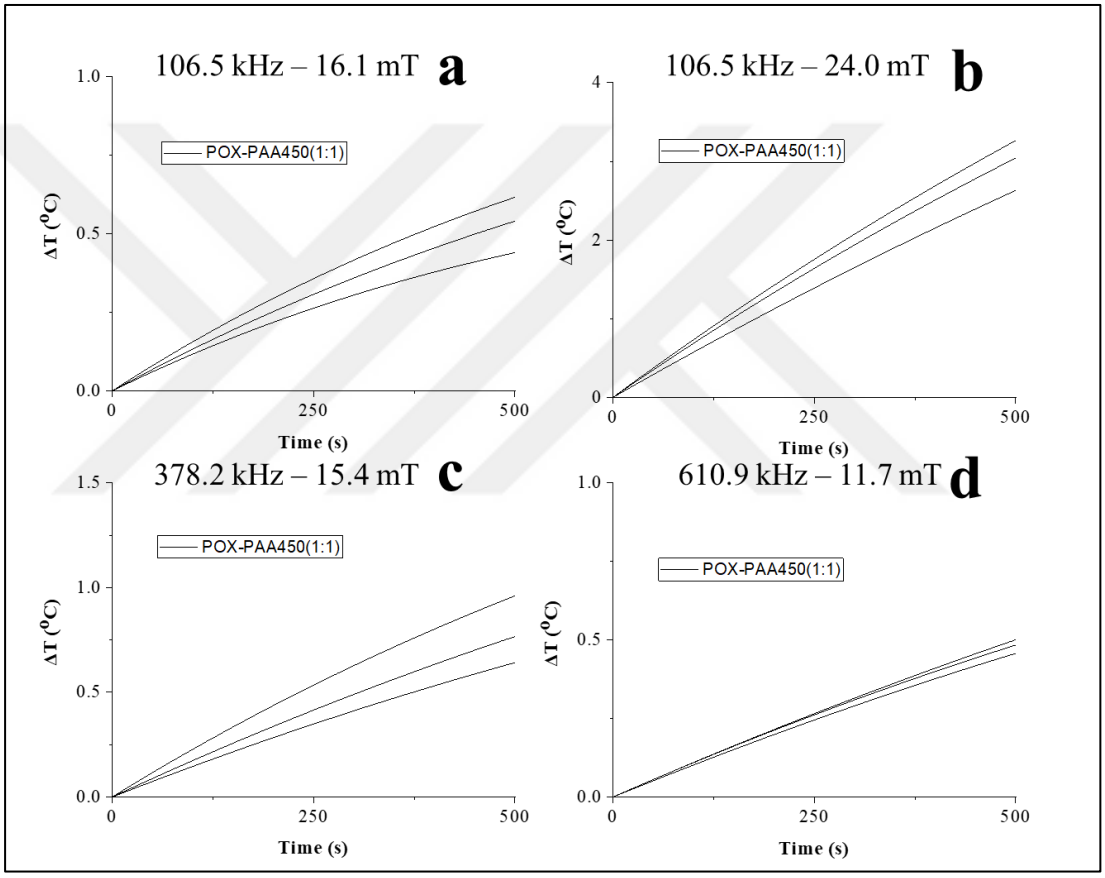

Figure 5.33. Resulting temperature-time data for (POX) magnetite nanoparticles modified with PAA450(1:1) (0.775 mg/ml) a) 106.5 kHz – 16.1 mT, b) 106.5 kHz – 24.0 mT, c) 378.2 kHz – 15.4 mT, d) 610.9 kHz – 11.7 mT

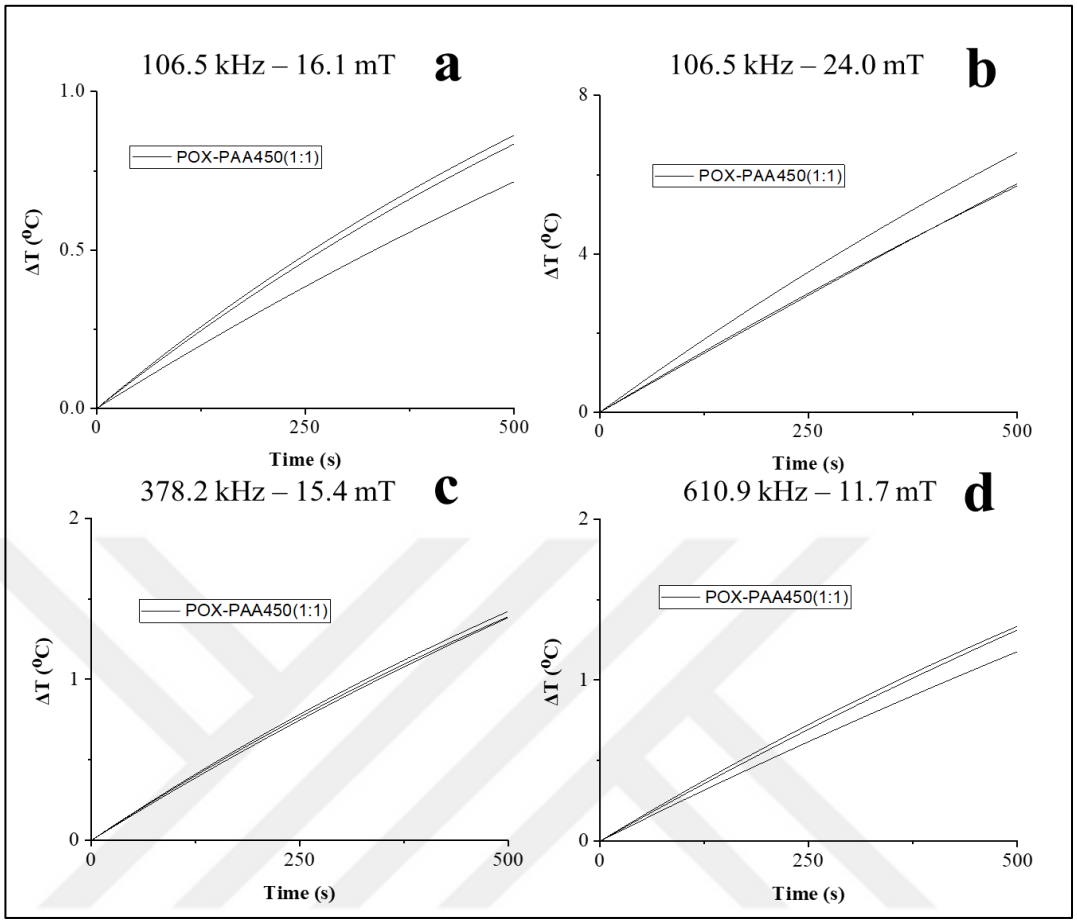

Figure 5.34. SAR for (POX) magnetite nanoparticles modified with PAA450(1:1) (1.550 mg/ml). a) 106.5 kHz – 16.1 mT, b) 106.5 kHz – 24.0 mT, c) 378.2 kHz – 15.4 mT, d) 610.9 kHz – 11.7 mT

Finally, nanofluids containing magnetite nanoparticles synthesized and modified by partial oxidation were compared with nanofluids containing nanoparticles synthesized and modified by co-precipitation at the same concentration (0.775 mg/ml). At the highest frequency of 610.9 kHz, POX-PAA450(1:1), COP-PAA450(1:1), COP-PAA450(1:2) and COP-PEG-PEI showed enhancements of 0.48, 0.50, 0.73 and 1.55 ^{o}C, respectively, indicating that partial oxidation based nanoparticles presented the lowest enhancement in heating performance at high frequency (Figure 5.33d, Figure 5.27b, Figure 5.29 and Figure 5.26). This result is expected considering that superparamagnetic nanoparticles were found to be much more affected by frequency. On the other hand, no comparison could be made at high magnetic field strength and low frequency since there was no enhancement in temperature for superparamagnetic nanoparticles at comparable magnetic field conditions.

However, with surface modification of the superparamagnetic nanoparticles, a lower temperature rise was obtained as compared to the bare nanoparticles (Figure 5.32). The fact that POX-PAA450(1:1) exhibits higher values than even COP-Bare nanoparticles at 106.5 kHz and 24.0 mT indicates that all potentially obtainable modified superparamagnetic nanoparticles may exhibit lower performances than larger nanoparticles under high magnetic field strengths (Figure 5.36 vs. Figure 5.20).

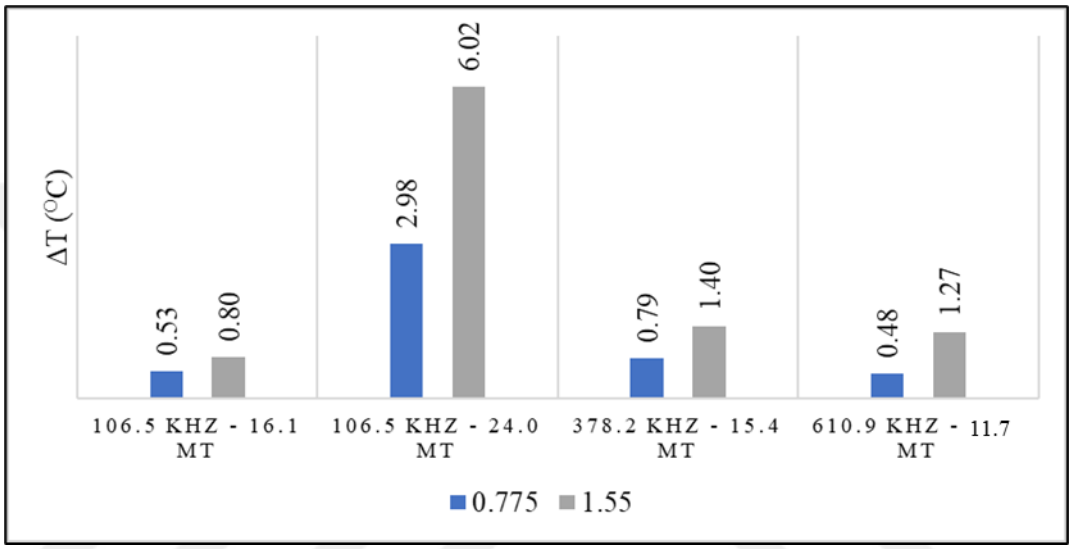

Figure 5.35. The variation of resultant temperature difference for (POX) magnetite nanoparticles modified with PAA450(1:1) with respect to concentration under the influence of an externally AMF

When SAR values for POX-PAA450(1:1) sample were analyzed, it was determined that there was a radical change in SAR values with increasing the magnetic field strength as in the case of temperature change, but the effect of frequency was found to be minimal (Figure 5.36). Compared to the bare nanoparticles, SAR values showed a clear increase at high magnetic field strengths (Figure 5.36 vs. Figure 5.24), while the SAR value obtained by increasing the frequency value to 610 kHz (5.85 W/g) was found to be lower than all modified superparamagnetic nanoparticles as frequency highly affects superparamagnetic nanoparticles. On the other hand, although SAR values generally decreased with increasing concentration, a different behavior was found especially at high frequency (610.9 kHz – 11.7 mT), indicating that concentration may have a very complicated effect and should be investigated in more depth, as frequently mentioned in the literature.

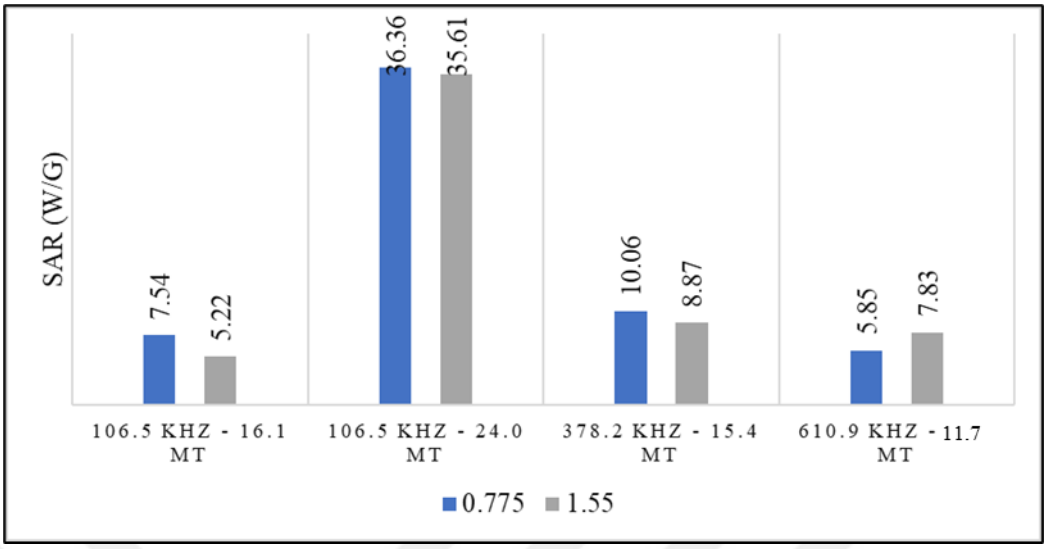

Figure 5.36. The variation of SAR for (POX) magnetite nanoparticles modified with PAA450(1:1) with respect to concentration under the influence of an externally AMF

6. CONCLUSION

Cancer is still the second leading cause of death worldwide. Traditional cancer treatment methods such as chemotherapy, radiotherapy and surgery, which are applied individually or in combination, fail to achieve the intended therapeutic effect due to their inefficiency and corresponding side effects. Therefore, alternative treatment methods based on different principles such as gene therapy, immunotherapy, stem cell therapy and hyperthermia have been studied for many years.

Hyperthermia is based on the principle of activating the response of the immune system and causing the death of cancer cells by disrupting the structures of membranes and proteins by increasing the local temperature between 39 ^{o}C and 44 ^{o}C at the tumor site. Furthermore, the utilization of magnetite nanoparticles exhibiting magnetic properties in hyperthermia applications is called as magnetic hyperthermia. The physical and magnetic properties of magnetite nanoparticles as well as their biocompatibility, which enables their use in biomedical applications, cause them to be especially preferred in hyperthermia applications. The application of magnetite nanoparticles as heating agents in magnetic hyperthermia is facilitated by their ability to convert electromagnetic energy into heat energy through different processes under the influence of an externally applied alternating magnetic field. The efficiency of magnetite and other magnetic nanoparticles in hyperthermia applications is quantified by specific absorption rate (SAR) and corresponding measurements are carried out by applying an alternating magnetic field of known frequency and intensity to the nanofluid containing magnetic nanoparticles in the absence of cancer cells and analyzing the subsequent temperature change in the medium. SAR generally depends on the concentration, size, magnetic properties and colloidal stability of the magnetic nanoparticles that constitute the nanofluid, as well as the frequency and intensity of the externally applied magnetic field. There are various synthesis methods for the synthesis of magnetic nanoparticles to enable their use in applications such as hyperthermia. The most commonly employed method is the co-precipitation method due to its simplicity which allows to obtain nanoparticles with superparamagnetic properties. On the other hand, the aqueous-based partial oxidation method, which allows the synthesis of ferrimagnetic magnetite nanoparticles, is not generally preferred due to the size and magnetic properties of the particles, which pose an obstacle to colloidal stability.

Therefore, the aim of this study is to synthesize both bare and modified superparamagnetic and ferrimagnetic nanoparticles by co-precipitation and partial oxidation methods, respectively, and to quantify and analyze subsequent temperature variations and SAR values under the influence of an externally applied alternating magnetic field. Hence, it is aimed to evaluate the effects of nanoparticle size, surface modification, concentration, magnetic field frequency and field strength on temperature variation and SAR in a wholistic manner.

In order to synthesize magnetite nanoparticles, co-precipitation and partial oxidation methods, which have different characteristics, were preferred for comparison in this study. The fact that the nanoparticles formed after the nucleation and growth phases during both synthesis methods possessed a black color indicated preliminary evidence that the targeted magnetite nanoparticles were successfully obtained. Following the syntheses, it was observed that the particles in the powder form obtained by drying reacted strongly to the externally applied magnetic field and their alignment in the direction of the magnetic field further supported the formation of magnetite nanoparticles.

The size and morphology of the nanoparticles obtained by both methods were analyzed by TEM and the results showed that nanoparticles with an average size of 9.8 nm were prepared by co-precipitation and 41.6 nm by partial oxidation as anticipated. Considering the reaction kinetics of both methods, such a variation in size is an expected result and has been demonstrated in our previous studies. Additionally, high-resolution TEM analysis revealed that both classes of nanoparticles have a crystalline structure rather than an amorphous state. XRD was also utilized to determine the crystal structures and phases of the nanoparticles. When the XRD patterns of the nanoparticles were evaluated, it was determined that all the peak positions and relative intensity ratios matched with the theoretical magnetite phase. Finally, the magnetic properties of the nanoparticles were determined by VSM and the results revealed that the nanoparticles synthesized by co-precipitation method displayed superparamagnetic properties and had a saturation magnetization of 55.1 emu/g while the nanoparticles synthesized by partial oxidation method were found to possess coercivity and remanence and attained relatively a higher saturation magnetization.

In order to make a comparison with the bare nanoparticles obtained in both methods, the surfaces of the nanoparticles synthesized by co-precipitation and partial oxidation methods were modified with polymers and when the peak and band positions revealed by the FTIR spectrum were evaluated, it was determined that the nanoparticles were successfully

functionalized. Moreover, in time-dependent colloidal stability tests, it was determined that bare nanoparticles prepared by partial oxidation method were subjected to rapid precipitation due to their high magnetization, whereas bare superparamagnetic nanoparticles remained suspended for a relatively longer time due to their size, but on the other hand, surface modified nanoparticles regardless of the synthesis method employed had colloidal stability for a much longer time as expected.

Finally, the heating capacities and SAR values of magnetite nanoparticles synthesized by different methods were measured depending on their concentration, frequency and intensity of the externally applied magnetic field. During the measurements, it was determined that although a certain level of insulation was provided by the hyperthermia system, the system was not fully adiabatic. Consequently, all measurements were repeated with distilled water free of nanoparticles under the designated frequencies and magnetic field strengths and a temperature increment was also obtained in this condition. Since these increases can directly affect the changes that nanoparticles can produce, the resulting temperature differences were calculated for each measurement and SAR values were calculated based on these resultant heating curves. Primarily, it was determined that superparamagnetic nanoparticles of relatively small size can only increase the temperature of the medium at very high frequencies, and with only increasing concentration they could achieve a temperature enhancement at lower values, whereas comparably larger sized nanoparticles caused an increase in local temperature of the medium at all concentration, frequency and magnetic field intensity values. It was also observed that higher temperature enhancements were attained with the increment of all these factors as the amount of magnetic nanoparticles in the medium increased and the properties of the magnetic field were intensified. For this reason, large-sized particles may be preferred for hyperthermia applications, especially when low magnetic field intensity is required, and if low-sized nanoparticles are to be preferred, high concentrations should be utilized. Otherwise, sufficient temperature increase can only be achieved by reaching high frequency values.

On the other hand, as in the case of temperature change, SAR values were found to increase with magnetic field strength and frequency for both nanoparticle types, but displayed different behaviors with variation in concentration as it can both positively and negatively affect SAR due to enhanced dipolar interactions.

In addition, on the basis of the comparison of nanoparticles of different sizes, it was determined that superparamagnetic nanoparticles were much more affected by frequency, while nanoparticles with coercivity and remanence were significantly influenced by magnetic field strength, which was attributed to the enhancement of hysteresis loss.

Although the modification of magnetite nanoparticles synthesized by co-precipitation method with different polymers in order to ensure colloidal stability, which has an extremely important role in terms of application, has a positive effect on stability, it has shown a contrary consequence in both temperature enhancement and SAR values possibly due to the reducing effects on magnetic properties. This argument may be supported by the fact that the highest temperature elevation was obtained with PEG-PEI, which has the lowest molecular weight in the modified nanoparticles. However, it may not be sufficient to consider only the polymer molecular weight as there may be a variety of interactions between the particle surface and functional groups.

This situation also reveals the potential for a decrease in heating efficiency as a consequence of the surface modification required by applications. However, in order to recover this reduction, the nanoparticle concentration might be increased. But in this case, the increase in nanoparticle concentration may cause toxic effects. High concentration and consequently a temperature enhancement could be achieved by increasing the amount of polymer as seen in the case of COP-PAA450(1:2). However, the higher amount of surfactant used to achieve a high nanoparticle concentration may also be toxic on its own or simultaneously decrease the magnetic properties. Finally, complications may also occur in obtaining concentrated nanofluid due to the kinetics and nature of the synthesis method employed. For all these reasons, the type of synthesis, hence the kinetics, the surface agent employed, and the nanoparticle concentration should be evaluated simultaneously for the design of nanofluids possessing colloidal stability, which are intended to be used in magnetic hyperthermia applications.

For future studies, in order to evaluate the optimum conditions to be used in hyperthermia applications, the properties of nanoparticle systems and the influencing factors, it is necessary to measure the magnetic properties of each nanoparticle in detail by means of VSM. In this case, the effect of coercivity and remanence values can be analyzed, especially for nanoparticles synthesized via partial oxidation. Moreover, since the colloidal stability of nanofluids is of great importance, long-term stability tests should be carried out for each

sample by zeta potential measurements. Since the concentration can cause toxic effects especially at high values, the highest concentrations that can be used in practice should be determined for each sample by cell viability tests. As shown in this study and in the literature, it is also a necessity to examine the effect of concentration on SAR in a much wider spectrum considering all parameters. On the other hand, for this study only, it is suggested that the Tiron method for determining the concentration of magnetic nanoparticles should be replaced with an instrumental analysis method since it consists of numerous error-prone steps, and that the hyperthermia device should be modified to set constant conditions by manipulating the voltage and current values to reduce the deviations in the measured samples at fixed frequency and magnetic field amplitude values.

REFERENCES

1. Nagai H, Kim YH. Cancer prevention from the perspective of global cancer burden patterns. Vol. 9, *Journal of Thoracic Disease*. AME Publishing Company; 2017. p. 448–51.

2. Garutti M, Foffano L, Mazzeo R, Michelotti A, Da Ros L, Viel A, et al. Hereditary Cancer Syndromes: A Comprehensive Review with a Visual Tool. Vol. 14, *Genes*. MDPI; 2023.

3. Fares J, Fares MY, Khachfe HH, Salhab HA, Fares Y. Molecular principles of metastasis: a hallmark of cancer revisited. Vol. 5, *Signal Transduction and Targeted Therapy*. Springer Nature; 2020.

4. Debela DT, Muzazu SGY, Heraro KD, Ndalama MT, Mesele BW, Haile DC, et al. New approaches and procedures for cancer treatment: Current perspectives. Vol. 9, *SAGE Open Medicine*. SAGE Publications Ltd; 2021.

5. Liebl CM, Kutschan S, Dörfler J, Käsmann L, Hübner J. Systematic review about complementary medical hyperthermia in oncology. Vol. 22, *Clinical and Experimental Medicine*. Springer Science and Business Media Deutschland GmbH; 2022. p. 519–65.

6. Liu X, Zhang Y, Wang Y, Zhu W, Li G, Ma X, et al. Comprehensive understanding of magnetic hyperthermia for improving antitumor therapeutic efficacy. *Theranostics*. 2020;10(8):3793–815.

7. Materón EM, Miyazaki CM, Carr O, Joshi N, Picciani PHS, Dalmaschio CJ, et al. Magnetic nanoparticles in biomedical applications: A review. *Applied Surface Science Advances*. 2021 Dec 1;6.

8. kianfar E. Magnetic Nanoparticles in Targeted Drug Delivery: a Review. Vol. 34, *Journal of Superconductivity and Novel Magnetism*. Springer; 2021. p. 1709–35.

9. Niculescu AG, Chircov C, Grumezescu AM. Magnetite nanoparticles: Synthesis methods – A comparative review. *Methods*. 2022 Mar 1;199:16–27.

10. Vereda F, de Vicente J, Hidalgo-Alvarez R. Oxidation of ferrous hydroxides with nitrate: A versatile method for the preparation of magnetic colloidal particles. *J Colloid Interface Sci*. 2013 Feb 15;392(1):50–6.

11. Włodarczyk A, Gorgoń S, Radoń A, Bajdak-Rusinek K. Magnetite Nanoparticles in Magnetic Hyperthermia and Cancer Therapies: Challenges and Perspectives. Vol. 12, *Nanomaterials*. MDPI; 2022.

12. Cancer. [cited 2022 3 February]. Available from: https://www.who.int/news-room/fact-sheets/detail/cancer

13. Cooper G. *The Cell: A Molecular Approach*. 2nd edition Sinauer Associates Inc; 2000.

14. Benign vs Malignant Tumors. [cited 2022 Augst 16] Available from: https://www.technologynetworks.com/cancer-research/articles/benign-vs-malignant-tumors-364765

15. Sinha T. Tumors: Benign and Malignant. *Cancer Ther Oncol Int J*. 2018 May 1;10(3).

16. Abbas Z, Rehman S. An Overview of Cancer Treatment Modalities. *Neoplasm*. InTech; 2018.

17. How can cancer kill you? [cited 2022 Apr 8]. Available from: https://www.cancerresearchuk.org/about-cancer/coping/dying-with-cancer/how-can-cancer-kill-you

18. Arruebo M, Vilaboa N, Sáez-Gutierrez B, Lambea J, Tres A, Valladares M, et al. Assessment of the evolution of cancer treatment therapies. Vol. 3, *Cancers*. 2011. p. 3279–330.

19. Mondal J, Panigrahi AK, Khuda-Bukhsh AR. Conventional Chemotherapy: Problems and Scope for Combined Therapies with Certain Herbal Products and Dietary Supplements. Available from: www.austinpublishinggroup.com

20. Farhan Atyaf Sarhan. The modern X-ray imaging manners for diagnosis of the dental diseases. *Eurasian Journal of Physics, Chemistry and Mathematics*. 2022;7:138–48.

21. Baskar R, Lee KA, Yeo R, Yeoh KW. Cancer and radiation therapy: Current advances and future directions. Vol. 9, *International Journal of Medical Sciences*. 2012. p. 193–9.

22. Breasted JH. The Edwin Smith Surgical Papyrus, Volume 2: Facsimile Plates and Line for Line Hieroglyphic Transliteration. *The University of Chicago Press*. 1930.

23. Lebrun A, Zhu L. Magnetic Nanoparticle Hyperthermia in Cancer Treatment: History, Mechanism, Imaging-Assisted Protocol Design, and Challenges. *Theory and Applications of Heat Transfer in Humans.* 2018. p. 631-667

24. Borghaei H, Smith MR, Campbell KS. Immunotherapy of cancer. Vol. 625, *European Journal of Pharmacology*. 2009. p. 41–54.

25. Immunotherapy to Treat Cancer [cited 2019 Sep 24]. Available from: //www.cancer.gov/about-cancer/treatment/types/immunotherapy

26. Side Effects of Immunotherapy [cited 2022 May 1]. Available from: https://www.cancer.net/navigating-cancer-care/how-cancer-treated/immunotherapy-and-vaccines/side-effects-immunotherapy

27. Immunology 101: What is cancer immunotherapy? [cited 2020 Jan 1]. Available from: https://www.ucir.org/immunology-101/what_is_cancer_immunotherapy

28. Cancer gene therapy: Understanding the basics. [cited 2022 Apr 14]. Available from: https://acgtfoundation.org/news/gene-therapy-for-cancer/

29. HOW DOES GENE THERAPY WORK? [cited 2021 Sep 4]. Available from: https://www.thegenehome.com/how-does-gene-therapy-work/techniques

30. What Is Gene Therapy? [cited 2022 Feb 7]. Available from: https://www.verywellhealth.com/gene-therapy-5214362#toc-risks-of-gene-therapy

31. Li H, Yang Y, Hong W, Huang M, Wu M, Zhao X. Applications of genome editing technology in the targeted therapy of human diseases: mechanisms, advances and prospects. Vol. 5, *Signal Transduction and Targeted Therapy*. Springer Nature; 2020.

32. Misra R, Acharya S, Sahoo SK. Cancer nanotechnology: Application of nanotechnology in cancer therapy. Vol. 15, *Drug Discovery Today*. 2010. p. 842–50.

33. Alexis F, Rhee JW, Richie JP, Radovic-Moreno AF, Langer R, Farokhzad OC. New frontiers in nanotechnology for cancer treatment. Vol. 26, *Urologic Oncology: Seminars and Original Investigations*. 2008. p. 74–85.

34. Patra JK, Das G, Fraceto LF, Campos EVR, Rodriguez-Torres MDP, Acosta-Torres LS, et al. Nano based drug delivery systems: Recent developments and future prospects. Vol. 16, *Journal of Nanobiotechnology*. BioMed Central Ltd; 2018.

35. Deshpande GA. Cancer Nanotechnology: The Recent Developments in the Cancer Therapy. *Global Journal of Nanomedicine*. 2016 May 19;1(1).

36. Bucak S, Altan CL. Magnetic nanoparticles and cancer. *Nanotechnology in Cancer*. Elsevier Inc.; 2017. p. 105–37.

37. Salahpour Anarjan F. Active targeting drug delivery nanocarriers: Ligands. *Nano-Structures and Nano-Objects*. 2019 Jul 1;19.

38. Chaubey P, Momin M, Sawarkar S. Significance of Ligand-Anchored Polymers for Drug Targeting in the Treatment of Colonic Disorders. Vol. 10, *Frontiers in Pharmacology*. Frontiers Media S.A.; 2020.

39. Johannsen M, Thiesen B, Wust P, Jordan A. Magnetic nanoparticle hyperthermia for prostate cancer. *International Journal of Hyperthermia*. 2010 Dec;26(8):790–5.

40. Cheng Y, Weng S, Yu L, Zhu N, Yang M, Yuan Y. The Role of Hyperthermia in the Multidisciplinary Treatment of Malignant Tumors. Vol. 18, *Integrative Cancer Therapies*. SAGE Publications Inc.; 2019.

41. Behrouzkia Z, Joveini Z, Keshavarzi B, Eyvazzadeh N, Aghdam RZ. Hyperthermia: How can it be used? Vol. 31, *Oman Medical Journal*. Oman Medical Specialty Board; 2016. p. 89–97.

42. Wu W, Wu Z, Yu T, Jiang C, Kim WS. Recent progress on magnetic iron oxide nanoparticles: Synthesis, surface functional strategies and biomedical applications. Vol. 16, *Science and Technology of Advanced Materials. Institute of Physics Publishing.* 2015.

43. MAGNETITE CRYSTAL CLUSTER [cited 2023 Jan 8]. Available from: https://sydneycrystalshow.com/for-sale/magnetite-crystal-cluster/

44. Nawaz M, Sliman Y, Ercan I, Lima-Tenório MK, Tenório-Neto ET, Kaewsaneha C, et al. Magnetic and pH-responsive magnetic nanocarriers. In: Stimuli Responsive Polymeric Nanocarriers for Drug Delivery Applications: *Volume 2: Advanced Nanocarriers for Therapeutics*. Elsevier; 2018. p. 37–85.

45. Nee Koo K, Fauzi Ismail A, Hafiz Dzarfan Othman M, Rahman MA, Zhong Sheng T. Preparation and characterization of superparamagnetic magnetite (Fe3O4) nanoparticles: A short review. Vol. 15, *Malaysian Journal of Fundamental and Applied Sciences*. 2019.

46. Altan CL. Biomimetic synthesis, magnetic properties and applications of magnetite nanoparticles. Phd Thesis. Eindhoven University of Technology, 2014.

47. Soltani N, Saion E, Erfani M, Rezaee K, Bahmanrokh G, Drummen GPC, et al. Influence of the polyvinyl pyrrolidone concentration on particle size and dispersion of ZnS nanoparticles synthesized by microwave irradiation. *Int J Mol Sci.* 2012;13(10):12412–27.

48. Vereda F, De Vicente J, Del Puerto Morales M, Rull F, Hidalgo-Álvarez R. Synthesis and characterization of single-domain monocrystalline magnetite particles by oxidative aging of Fe(OH)2. Journal of Physical Chemistry C. 2008 Apr 17;112(15):5843–9.

49. Altan CL, Gurten B, Sadza R, Yenigul E, Sommerdijk NAJM, Bucak S. Poly(acrylic acid)-directed synthesis of colloidally stable single domain magnetite nanoparticles via partial oxidation. *J Magn Magn Mater*. 2016 Oct 15;416:366–72.

50. Maity D, Choo SG, Yi J, Ding J, Xue JM. Synthesis of magnetite nanoparticles via a solvent-free thermal decomposition route. J Magn Magn Mater. 2009 May;321(9):1256–9.

51. Vargas-Ortiz JR, Gonzalez C, Esquivel K. Magnetic Iron Nanoparticles: Synthesis, Surface Enhancements, and Biological Challenges. Vol. 10, *Processes.* MDPI; 2022.

52. Lu AH, Salabas EL, Schüth F. Magnetic nanoparticles: Synthesis, protection, functionalization, and application. Vol. 46, *Angewandte Chemie - International Edition*. 2007. p. 1222–44.

53. Peiravi M, Eslami H, Ansari M, Zare-Zardini H. Magnetic hyperthermia: Potentials and limitations. *Journal of the Indian Chemical Society*. 2022 Jan 1;99(1):100269.

54. Gilchrist RK;, Medal R, Shorey WD, Hanselman RC, Parrott JC, Taylor CB. Selective inductive heating of lymph nodes. *Ann Surg*. 1957;146:596–606.

55. Ashikbayeva Z, Tosi D, Balmassov D, Schena E, Saccomandi P, Inglezakis V. Application of nanoparticles and nanomaterials in thermal ablation therapy of cancer. Vol. 9, *Nanomaterials*. MDPI AG; 2019.

56. Shah RR, Davis TP, Glover AL, Nikles DE, Brazel CS. Impact of magnetic field parameters and iron oxide nanoparticle properties on heat generation for use in magnetic hyperthermia. *J Magn Magn Mater*. 2015 Aug 1;387:96–106.

57. Wildeboer RR, Southern P, Pankhurst QA. On the reliable measurement of specific absorption rates and intrinsic loss parameters in magnetic hyperthermia materials. *J Phys D Appl Phys*. 2014 Dec 10;47(49).

58. Narayanaswamy V, Sambasivam S, Saj A, Alaabed S, Issa B, Al-Omari IA, et al. Role of magnetite nanoparticles size and concentration on hyperthermia under various field frequencies and strengths. *Molecules*. 2021 Feb 2;26(4).

59. Xu H, Pan Y. Experimental evaluation on the heating efficiency of magnetoferritin nanoparticles in an alternating magnetic field. *Nanomaterials*. 2019 Oct 1;9(10).

60. Linh PH, Thach P Van, Tuan NA, Thuan NC, Manh DH, Phuc NX, et al. Magnetic fluid based on Fe3O4 nanoparticles: Preparation and hyperthermia application. *Journal of Physics: Conference Series*. Institute of Physics Publishing; 2009.

61. Herrero de la Parte B, Rodrigo I, Gutiérrez-Basoa J, Correcher SI, Medina CM, Echevarría-Uraga JJ, et al. Proposal of New Safety Limits for In Vivo Experiments of Magnetic Hyperthermia Antitumor Therapy. *Cancers (Basel)*. 2022 Jul 1;14(13).

62. Xu H, Pan Y. Experimental evaluation on the heating efficiency of magnetoferritin nanoparticles in an alternating magnetic field. *Nanomaterials*. 2019 Oct 1;9(10).

63. Rajan A, Sharma M, Sahu NK. Assessing magnetic and inductive thermal properties of various surfactants functionalised Fe3O4 nanoparticles for hyperthermia. *Sci Rep.* 2020 Dec 1;10(1).

64. Nemati Z, Salili SM, Alonso J, Ataie A, Das R, Phan MH, et al. Superparamagnetic iron oxide nanodiscs for hyperthermia therapy: Does size matter? *J Alloys Compd.* 2017;714:709–14.

65. Ma M, Wu Y, Zhou J, Sun Y, Zhang Y, Gu N. Size dependence of specific power absorption of Fe3O 4 particles in AC magnetic field. *J Magn Magn Mater*. 2004 Jan;268(1–2):33–9.

66. De La Presa P, Luengo Y, Multigner M, Costo R, Morales MP, Rivero G, et al. Study of heating efficiency as a function of concentration, size, and applied field in γ-Fe2O3 nanoparticles. *Journal of Physical Chemistry C*. 2012 Dec 6;116(48):25602–10.

67. Gonzalez-Fernandez MA, Torres T, Andrés-Vergés M, Costo R, de la Presa P, Serna CJ, et al. Magnetic Nanoparticles for Power Absorption: optimizing size, shape and magnetic properties.

68. Khurshid H, Alonso J, Nemati Z, Phan MH, Mukherjee P, Fdez-Gubieda ML, et al. Anisotropy effects in magnetic hyperthermia: A comparison between spherical and cubic exchange-coupled FeO/Fe3O4 nanoparticles. *J Appl Phys*. 2015 May 7;117(17).

69. Mohapatra J, Xing M, Beatty J, Elkins J, Seda T, Mishra SR, et al. Enhancing the magnetic and inductive heating properties of Fe3O4 nanoparticles via morphology control. *Nanotechnology*. 2020 Apr 17;31(27).

70. Jamir M, Islam R, Pandey LM, Borah JP. Effect of surface functionalization on the heating efficiency of magnetite nanoclusters for hyperthermia application. *J Alloys Compd*. 2021 Feb 15;854.

71. Majeed J, Pradhan L, Ningthoujam RS, Vatsa RK, Bahadur D, Tyagi AK. Enhanced specific absorption rate in silanol functionalized Fe3O4 core-shell nanoparticles: Study

of Fe leaching in Fe3O4 and hyperthermia in L929 and HeLa cells. *Colloids Surf B Biointerfaces*. 2014 Oct 1;122:396–403.

72. Yoe JH, Jones' AL. Colorimetric Determination of Iron with Disodium 1,2-dihydroxybenzene-3,5-disulfonate.

73. Altan CL, Lenders JJM, Bomans PHH, De With G, Friedrich H, Bucak S, et al. Partial oxidation as a rational approach to kinetic control in bioinspired magnetite synthesis. *Chemistry - A European Journal*. 2015 Apr 13;21(16):6150–6.

74. Jegdić B, Polić-Radovanović S, Ristić S, Alil A. CORROSION OF ARCHAEOLOGICAL ARTEFACT MADE OF FORGED IRON.

75. Schwertmann U, Cornell RM. Iron Oxides in the Laboratory: Preparation and Characterization. 2nd ed. *Wiley-VCH*; 2008.

76. Kim W, Suh CY, Cho SW, Roh KM, Kwon H, Song K, et al. A new method for the identification and quantification of magnetite-maghemite mixture using conventional X-ray diffraction technique. *Talanta*. 2012 May 30;94:348–52.

77. Gareev KG. Diversity of Iron Oxides: Mechanisms of Formation, Physical Properties and Applications. Vol. 9, *Magnetochemistry*. MDPI; 2023.

78. Verimli N, Goralı Sİ, Abisoglu B, Altan CL, Sucu BO, Karatas E, et al. Development of light and pH-dual responsive self-quenching theranostic SPION to make EGFR overexpressing micro tumors glow and destroy. *J Photochem Photobiol B*. 2023 Nov 1;248:112797.

79. Puvvada N, Mandal D, Panigrahi PK, Pathak A. Aqueous route for the synthesis of magnetite nanoparticles under atmospheric air: Functionalization of surface with fluorescence marker. *Toxicol Res (Camb)*. 2012;1(3):196–200.

80. Choquehuanca A, Ruiz-Montoya JG, La Rosa-Toro Gómez A. Discoloration of methylene blue at neutral pH by heterogeneous photo-Fenton-like reactions using crystalline and amorphous iron oxides. *Open Chem*. 2021 Jan 1;19(1):1009–20.

81. Sanchez LM, Martin DA, Alvarez VA, Gonzalez JS. Polyacrylic acid-coated iron oxide magnetic nanoparticles: The polymer molecular weight influence. Colloids Surf A Physicochem Eng Asp. 2018 Apr 20;543:28–37.

82. Zhou C, Zhang W, Xia M, Zhou W, Wan Q, Peng K, et al. Synthesis of poly(acrylic acid) coated-Fe3O4 superparamagnetic nano-composites and their fast removal of dye from aqueous solution. *J Nanosci Nanotechnol*. 2013 Jul;13(7):4627–33.

83. Guo L, Liu G, Hong RY, Li HZ. Preparation and characterization of chitosan poly(acrylic acid) magnetic microspheres. *Mar Drugs*. 2010;8(7):2212–22.

84. Shin JR, An GS, Choi SC. Influence of carboxylic modification using polyacrylic acid on characteristics of Fe_3O_4 nanoparticles with cluster structure. *Processes.* 2021 Oct 1;9(10).

85. Hosny NM, Abbass M, Ismail F, El-Din HMN. Radiation synthesis and anticancer drug delivery of poly(acrylic acid/acrylamide) magnetite hydrogel. *Polymer Bulletin.* 2023 Apr 1;80(4):4573–88.

86. Gu Y, Yoshikiyo M, Namai A, Bonvin D, Martinez A, Piñol R, et al. Magnetic hyperthermia with ϵ-Fe2O3nanoparticles. *RSC Adv*. 2020 Aug 4;10(48):28786–97.

87. Simeonidis K, Morales MP, Marciello M, Angelakeris M, De La Presa P, Lazaro-Carrillo A, et al. In-situ particles reorientation during magnetic hyperthermia application: Shape matters twice. *Sci Rep*. 2016 Dec 6;6.

88. Iglesias GR, Jabalera Y, Peigneux A, Fernández BLC, Delgado Á V., Jimenez-Lopez C. Enhancement of magnetic hyperthermia by mixing synthetic inorganic and biomimetic magnetic nanoparticles. *Pharmaceutics*. 2019;11(6).

89. Bonvin D, Arakcheeva A, Millán A, Piñol R, Hofmann H, Mionić Ebersold M. Controlling structural and magnetic properties of IONPs by aqueous synthesis for improved hyperthermia. *RSC Adv.* 2017;7(22):13159–70.

90. Tao C, Zhu Y. Magnetic mesoporous silica nanoparticles for potential delivery of chemotherapeutic drugs and hyperthermia. *Dalton Transactions*. 2014 Nov 7;43(41):15482–90.

91. Deatsch AE, Evans BA. Heating efficiency in magnetic nanoparticle hyperthermia. Vol. 354, *Journal of Magnetism and Magnetic Materials*. 2014. p. 163–72.

92. Torres-Lugo M, Rinaldi C. Thermal potentiation of chemotherapy by magnetic nanoparticles. Vol. 8, *Nanomedicine.* Future Medicine Ltd.; 2013. p. 1689–707.

93. Maity D, Chandrasekharan P, Yang CT, Chuang KH, Shuter B, Xue JM, et al. Facile synthesis of water-stable magnetite nanoparticles for clinical MRI and magnetic hyperthermia applications. *Nanomedicine.* 2010 Dec;5(10):1571–84.

94. Piñeiro-Redondo Y, Bañobre-López M, Pardiñas-Blanco I, Goya G, López-Quintela MA, Rivas J. The influence of colloidal parameters on the specific power absorption of PAA-coated magnetite nanoparticles. *Nanoscale Res Lett.* 2011;6:1–7.

95. Mohapatra J, Zeng F, Elkins K, Xing M, Ghimire M, Yoon S, et al. Size-dependent magnetic and inductive heating properties of Fe3O4 nanoparticles: Scaling laws across the superparamagnetic size. *Physical Chemistry Chemical Physics*. 2018;20(18):12879–87.

96. Salas G, Veintemillas-Verdaguer S, Morales MDP. Relationship between physico-chemical properties of magnetic fluids and their heating capacity. Vol. 29, *International Journal of Hyperthermia. Informa Healthcare*; 2013. p. 768–76.

97. Tompkins J, Huitink D. Induction heating response of iron oxide nanoparticles in varyingly viscous mediums with prediction of brownian heating contribution. *Nanoscale and Microscale Thermophysical Engineering.* 2020;24(3–4):123–37.

98. Yuan Y, Rende D, Altan CL, Bucak S, Ozisik R, Borca-Tasciuc DA. Effect of surface modification on magnetization of iron oxide nanoparticle colloids. *Langmuir*. 2012 Sep 11;28(36):13051–9.